THE INNATE REGULATORY PROTEIN NLRP12 MAINTAINS COMMENSAL BACTERIAL SYMBIOSIS, AND MITIGATES INTESTINAL INFLAMMATION AND OBESITY

Liang Chen

A dissertation submitted to the faculty of the University of North Carolina at Chapel Hill in partial fulfillment of the requirements of the degree Doctor of Philosophy in the Department of Microbiology and Immunology in the School of Medicine

Chapel Hill
2018

Directed by:

Jenny P.Y. Ting

Jonathan Hansen

Ian Carroll

Blossom A. Damania

Glenn K. Matsushima

ABSTRACT

Liang Chen: The Innate regulatory protein NLRP12 maintains commensal bacterial symbiosis, and mitigates intestinal inflammation and obesity
(Under the direction of Jenny P.Y. Ting)

The nucleotide-binding domain, leucine-rich repeat containing proteins (NLRs), are pattern recognition receptors that play important roles in innate immunity (Bertin, Nir et al. 1999, Inohara, Koseki et al. 1999, Hoffman, Mueller et al. 2001, Aganna, Martinon et al. 2002, Harton, Linhoff et al. 2002, Manji, Wang et al. 2002, Ting and Davis 2005).

NLR family can be categorized into two groups, the inflammasome-forming and non-inflammasome-forming NLRs. Inflammasomes-forming NLRs have been extensively studied due to their pro-inflammatory and anti-pathogen functions. However, mutations of non-inflammasome-forming NLRs, have been reported to cause auto-inflammatory diseases (Borghini, Tassi et al. 2011, Allen 2014, Karki, Man et al. 2016, Abe, Lee et al. 2017).

NLRP12, a negative regulator of innate immunity, suppresses colon inflammation and colorectal cancer (Zaki, Vogel et al. 2011, Allen, Wilson et al. 2012). Here, we identified that NLRP12 expression in mucosal tissue negatively correlates with colitis severity. We also showed that exposure to commensal bacteria was required to

differentiate colitis severity between WT and *Nlrp12*$^{-/-}$ mice, and commensal bacteria caused more basal inflammation attributed to the NLRP12-deficient hematopoietic cell components (such as CD11c^{+} macrophages and DCs). Meanwhile, this elevated basal inflammation promoted a dysbiotic microbiota in the *Nlrp12*$^{-/-}$ mice. Both the genetic defects of NLRP12 and the consequent dysbiotic microbiota worked together to achieve cumulative pathology. Finally, we found reconstitution of the absent beneficial bacteria in the *Nlrp12*$^{-/-}$ mice by cohousing with WT mice or inoculation of Lachnospiraceae can attenuate colitis severity.

We also found *NLRP12* expression was lower in patients with higher body mass index (BMI), and *Nlrp12*$^{-/-}$ mice were more susceptible to high-fat-diet (HFD) induced obesity. These observations coincided with excessive systemic inflammation fueled by HFD, the NLRP12 mutation, and a skewed gut microbiota composition. We identified that the gut microbiota was required to accelerate the weight gain in the *Nlrp12*$^{-/-}$ mice, and restoration of the decreased beneficial strains by cohousing with WT mice or Lachnospiraceae inoculation can attenuate the obesity and improve insulin sensitivity. We found Lachnospiraceae, which were reduced by HFD-feeding and *Nlrp12*-deficiency, might produce anti-inflammatory short-chain-fatty-acid (SCFA) to promote IL10 secretion. Lachnospiraceae treatment restricts obesity and improves insulin sensitivity by suppressing the systemic inflammation caused by HFD and *Nlrp12*-deficiency.

To my family whose love, support, and joy they brought to my life kept me going throughout this demanding journey.

ACKNOWLEDGEMENTS

I would like to thank my mentor, Dr. Jenny P.-Y. Ting, for providing her thoughtful guidance and solid support, which greatly inspired my research interests and expanded my knowledge during the time in her laboratory. In addition, she shared me with her secrets about how she succeeds in manuscripts and grants writing, which demonstrates an important truth - a successful scientist should know your audience. After I started my thesis project, I feel fortunate to work in Dr. Ting's laboratory, which provides me the great resources and opportunities to collaborate with others to pursue the scientific hypotheses.

I would also like to thank the members of my committee, Drs. Jonathan Hansen, Ian Carroll, Blossom A. Damania, and Glenn K. Matsushima. Throughout the time of my graduate studies, they have always provided great insight and helpful suggestions. Importantly, there are also many lab members and collaborators that I want to thank, who participated in this research project and provided valuable comments and suggestions. I also want to give my thanks specifically to Drs. Justin E. Wilson and Jason Tam for their kind help in proofreading my dissertation.

TABLE OF CONTENTS

LIST OF FIGURES

LIST OF ABBREVIATIONS

Ab: antibody

ATM: adipose tissue macrophage

BHI: brain heart infusion medium

BMT: bone marrow transplant

BMDM: bone marrow derived macrophage

CC: cecal content

CD: Crohn disease

ChIP: chromatin immunoprecipitation

cLP: colonic lamina propria

CLS: crown like structure

CoHo: cohousing

CRC: colorectal cancer

CV: conventional raised

DAI: disease associated index

DAMPs: disease associated molecular patterns

DC: dendritic cell

DSS: dextran sodium sulfate

FM: fecal microbiota

GF: germ free

GWAT: gonadal white adipose tissue

HDAC: histone de-acetylation

HFD: high fat diet

IBD: inflammatory bowel disease

ITT: insulin tolerance test

InWAT: inguinal white adipose tissue

ICE: interleukin-1 beta converting enzyme

IKK: The IκB kinase

LC-MS: Liquid chromatography–mass spectrometry

MAC: macrophage

NLRs: nucleotide-binding oligomerization domain-like receptors

NLS: nuclear localization sequence

OGTT: oral glucose tolerance test

OTU: operational taxonomy unit

PAMPs: pathogen associated molecular patterns

ROS: Reactive oxygen species

SiHo: single housing

SCFA: short chain fatty acid

T2D: type 2 diabetes

UC: ulcerative coliti

CHAPTER 1: INTRODUCTION

1.1 NBD-LRR containing proteins/NOD-like receptor (NLR).

Pattern Recognition Receptors (PRRs) are important host immune receptors and sensors that recognize PAMPs (Pathogen-associated Molecular Patterns) or DAMPs (Damage-associated Molecular Patterns) and mediate downstream immunity (Kis-Toth, Szanto et al. 2011). The intracellular nucleotide-binding domain leucine repeat containing proteins (also known as NOD-like receptors) (NLR) belong to this group of receptors and sensors, which play important roles in host innate immunity (Hoffman, Mueller et al. 2001, Feldmann, Prieur et al. 2002, Ting, Lovering et al. 2008, Corridoni, Arseneau et al. 2014). NLRs have a conserved domain configuration and are composed of a nucleotide-binding domain (NBD), a leucine-rich-repeat domain (LRR) and a specific effector domain (Kanneganti, Ozoren et al. 2006). Generally, NLR family members can be further categorized based on their specific effector domains. The NLR family includes NLRC proteins (e.g. NLRC3, NLRC4 and NLRC5) which contain the caspase recruitment domains (CARD); NLRP proteins (e.g. NLRP3, NLRP6 and NLRP12) which contain a pyrin domain (PYR); and NLRs with other effector domains including the baculovirus inhibitor of apoptosis protein repeat (BIR), the transactivation

domain (AD), and uncharacterized domain (X) (e.g. NLRX1) (Ting, Lovering et al. 2008). Alternatively, NLR proteins can also be classified into two groups by function: inflammasome-forming and non-inflammasome-forming NLRs based on their ability to form an inflammasome complex.

Inflammasome-forming NLRs: NLRP3 is one of the most extensively studied inflammasome-forming NLRs (Hoffman, Mueller et al. 2001, Feldmann, Prieur et al. 2002, Kanneganti, Ozoren et al. 2006, Lich, Arthur et al. 2006, Mariathasan, Weiss et al. 2006). The typical function of the NLRP3 inflammasome complex is to sense intracellular PAMPs and DAMPs leading to caspase 1 activation and IL-1β and IL-18 secretion, which mediate downstream innate and adaptive immunity. The NLRP3 inflammasome complex usually contains a NLRP3 protein, the adaptor protein ASC (apoptosis-associated speck-like protein containing a CARD), and the enzyme caspase-1. The activation of NLRP3 inflammasome involves a 2-steps mechanism: 1) increased transcriptional induction of the inflammasome components, and 2) assembly of the inflammasome component for IL-1β and IL-18 production. After activation, these components can assemble to form a wheel-like complex with polymeric filaments (Cai, Chen et al. 2014, Lu, Magupalli et al. 2014), which can cleave and activate caspase-1 to further process pro-IL-1β and pro-IL-18 and allow for secretion of mature IL-1β and IL-18 (Hoffman, Mueller et al. 2001, Sutterwala, Ogura et al. 2006).

Although identifying ligands that are recognized by NLRP3 remains a major

challenge in the field (Leemans, Cassel et al. 2011), multiple ligands have been identified to selectively activate other inflammasome-forming NLRs (e.g., NOD1, NOD2 and NLRC4), which uniformly trigger inflammasome assembly and leads to IL-1β secretion (Harton, Linhoff et al. 2002, Amer, Franchi et al. 2006, Franchi, Amer et al. 2006, Kis-Toth, Szanto et al. 2011). For example, bacterial flagellins, needles or rods can be recognized by NAIPs (NLR family apoptosis inhibitory proteins), the partner proteins of NLRC4. Mouse NAIP1 and NAIP2 are able to bind the bacterial needle and rod proteins (Kofoed and Vance 2011, Zhao, Yang et al. 2011, Rayamajhi, Zak et al. 2013, Yang, Zhao et al. 2013, Rauch, Tenthorey et al. 2016), and NAIP5 and NAIP6 can bind flagellins (Lightfield, Persson et al. 2008, Zhao, Yang et al. 2011, Rauch, Tenthorey et al. 2016). After binding to their microbial ligands, NAIP proteins interact with NLRC4 to trigger inflammasome assembly and activation (Inohara and Nunez 2003, Ting and Davis 2005). Also, bacterial peptidoglycans (sugar components of the bacterial cell wall) are recognized by NOD1 and NOD2 and can induce IL-1β secretion (Kofoed and Vance 2011, Zhao, Yang et al. 2011, Halff, Diebolder et al. 2012, Qu, Misaghi et al. 2012).

Non-inflammasome-forming NLRs: Mutations in NLRP3 are the genetic basis for cold-induced autoinflammatory disease (CIAS) and Muckle-Wells syndrome (MWS) (Hoffman, Mueller et al. 2001, Neven, Callebaut et al. 2004). A gain of function NLRP3 mutation with elevated IL-1β secretion has been linked to the MWS and implicates the

role of the NLRP3 inflammasome in promoting these autoinflammatory diseases (Agostini, Martinon et al. 2004). Similarly, mutations in NLRP12 have been clinically reported to associate with cold-induced autoinflammatory disease (Borghini, Tassi et al. 2011). In this study, one missense nucleotide change (882C>G) was identified in a Caucasian family afflicted with increased sensitivity to cold exposure causing arthralgia and myalgia but not always with a rash or fever. However, the patients in this study refused to take the test of cold exposure, and therefore it is still unclear if this mutation of NLRP12 causes other autoinflammatory phenotypes. This genetic mutation is caused by an amino acid substitution, Asp294Glu, and the monocytes carrying this mutation displayed an accelerated secretion of IL-1β and high production of reactive oxygen species (ROS), which correlated with symptom severity. However, the regulation of NF-κB activity and production of TNF were not affected by this mutation in NLRP12. In another study, a truncated p.Arg284X and a frameshift Val635ThrfsX12 mutation were identified in two families with periodic fever syndrome associated with increased NF-κB signaling (Jeru, Duquesnoy et al. 2008). In this study, transfecting plasmids containing the mutant NLRP12 sequences into the HEK293T cell resulted in an increased NF-κB activation compared to the wild type NLRP12-expressing plasmid in response to TNF stimulation. Later, the same group showed the peripheral blood mononuclear cells isolated from two patients carrying this *NLRP12* (p.Arg284X) mutation displayed an increased spontaneous secretion of IL-1β. Although treatment of IL-1 receptor

antagonist (Anakinra) normalized the IL-1β at the beginning, secondarily relapse accompanied by increased IL-6 and TNF secretion occurred after 14 months treatment, which suggests the elevation of other proinflammatory cytokines might contribute to the inconsistent response to the anti-IL-1-receptor treatment (Jeru, Hentgen et al. 2011). In addition, more cases report patients with *NLRP12* mutations have been found to develop various autoinflammatory disorders including periodic fevers, rash, joint and muscle pains (Jeru, Duquesnoy et al. 2008, Borghini, Tassi et al. 2011, Vitale, Rigante et al. 2013, Xia, Dai et al. 2016, Shen, Tang et al. 2017). Even though most of the *NLRP12* mutations are located in the same exon 3, however, not all patients carrying the *NLRP12* mutation develop same autoinflammatory disorders described above. In addition, not all patients display an increased NF-κB activity and are responsive to the same clinical manifestation (such as anti-IL-1-receptor treatment), which demonstrates the heterogeneous nature of FCAS with NLRP12 mutations. At least, these evidences implicate that non-inflammasome NLRs also play an important role in regulating autoinflammatory disorders, and potentially other diseases including infectious diseases, type 2 diabetes, and tumorigenesis (Allen 2014). We will discuss the functions of several negative-regulatory NLRs in this section.

We and other groups have shown that NLRX1, NLRC3 and NLRP12 can serve as negative regulator of immunity (Fiorentino, Stehlik et al. 2002, Jounai, Kobiyama et al. 2011, Zaki, Vogel et al. 2011, Allen, Wilson et al. 2012, Anand, Malireddi et al. 2012,

Cui, Li et al. 2012). Specifically, NLRP12 can attenuate the NF-κB signaling via inhibition of IRAK phosphorylation (Williams, Lich et al. 2005) and proteasomal degradation of NIK (Lich, Williams et al. 2007). Although others have suggested that NLRX1 might induce ROS production to activate NF-κB and JNK pathway (Tattoli, Carneiro et al. 2008, Xia, Cui et al. 2011, Yin, Sun et al. 2017), the tumor suppressor role of NLRX1 in preventing tumorogenesis is consistently reported by multiple groups showing NLRX1 limits the activation of NF-κB and STAT3 signaling (Koblansky, Truax et al. 2016) or inhibits the TNF signaling (Tattoli, Killackey et al. 2016). In the context of antiviral signaling, we and others found that NLRX1 is a mitochondrial protein that can inhibit the antiviral innate immune response (Moore, Bergstralh et al. 2008, Allen, Moore et al. 2011, Lei, Wen et al. 2012, Lei, Wen et al. 2013, Guo, Konig et al. 2016, Ma, Hopcraft et al. 2017) but another group reported this not to be the case (Soares, Tattoli et al. 2013). These controversial findings might be due to complicated functions of NLRX1 in different tissues or cells, as NLRX1 can suppress IRF3 but activate IRF1 to promote stronger anti-viral response in the human hepatocytes (Feng, Lenarcic et al. 2017). NLRP14 promotes fertilization by preventing inappropriate responses to the exogenous nucleic acids of the fertilized oocyte, where NLRP14 is involved in the ubiquitination and degradation of TBK1 (TANK binding kinase 1) to inhibit the DNA and RNA-induced inflammatory response (Abe, Lee et al. 2017). NLRC3 has been reported to inhibit NF-κB signaling by binding and inducing degradation of TRAF6 (TNF receptor-

associated factor 6) after LPS stimulation (Schneider, Zimmermann et al. 2012). Recently, NLRC3 was also reported to inhibit the STING (Stimulator of interferon genes)-dependent immune response to cytosolic DNA by interfering with STING-TBK1 binding and preventing the trafficking of STING to the perinuclear area, which is important for its anti-viral function (Zhang, Mo et al. 2014). In addition to its function in immunity, NLRC3 was recently reported to negatively regulate the mTOR pathway and limit intestinal stem cell proliferation (Karki, Man et al. 2016). NLRP2 was reported to function as a NF-κB inhibitor protein where overexpression of human *NLRP2* in THP1 cells attenuated the activation of IκB kinases in response to IL-1β and TNF stimulation, and knockdown of *NLRP2* increased the production of ICAM-1 (intercellular adhesion molecule 1) (Bruey, Bruey-Sedano et al. 2004). Another study found the expression of *NLRP2* was regulated by NF-κB, which indicated that NLRP2 may control NF-κB activation through a feed-back regulatory loop (Fontalba, Gutierrez et al. 2007). NLRP4 has been shown to interact with Beclin-1, an important protein to initiate autophagy (Jounai, Kobiyama et al. 2011). Knocking down the expression of NLRP4 enhanced autophagy after stimulation with various bacteria, which suggests that NLRP4 acts as a negatively regulator of autophagy. Furthermore, NLRP4 was demonstrated to inhibit type I interferon signaling by targeting TBK1 for ubiquitination (Charoenthongtrakul, Gao et al. 2012, Cui, Li et al. 2012, Lin, Zhao et al. 2016). NLRC5 can inhibit NF-κB dependent cytokine (TNF and IL6) production and type I interferon signaling by blocking

the phosphorylation of IKKα/β and the activation of IRF3, respectively (Benko, Magalhaes et al. 2010, Cui, Zhu et al. 2010, Tong, Cui et al. 2012, Hu 2015, Meng, Cai et al. 2015, Ma and Xie 2017). Interestingly, it has been reported that NLRC5 can interact with ASC to promote IL-1β, and knockdown of NLRC5 nearly eliminated IL-1β, and IL-18 production, which suggests that NLRC5 has a more comprehensive mechanism in regulating its pro- and anti-inflammatory role (Davis, Roberts et al. 2011). In agreement, rhinovirus ion channel protein 2B can trigger IL-1β secretion in human bronchial cells depending on collaborative activation of NLRC5 and NLRP3 inflammasome (Triantafilou, Kar et al. 2013). Recently, two reports identified NLRP11 as a novel negative regulator for NF-κB, MAPK and type I interferon signaling activation. These groups found that NLRP11 can target TRAF6 for proteasomal degradation and thus inhibit the inflammatory response after LPS and viral RNA stimulation (Qin, Su et al. 2017, Wu, Su et al. 2017). NLRP6 has been described as an inflammasome-forming NLR, because co-transfection of NLRP6 and ASC led to a co-localization of NLRP6 and ASC and a formation of inflammasome punctate structures in the cytoplasm. This resulted in the synergistic increase of NF-κB and MAPK signaling, and the activated pro-caspase-1 for mature IL-1β production, which suggests that NLRP6 is proinflammatory (Grenier, Wang et al. 2002). In addition, NLRP6 was found to couple with the RNA helicase DHX15 to sense enteric viral RNA and promote antiviral signaling for type I/III interferon production (Wang, Zhu et al. 2015). In other animal models,

NLRP6 is critical for preventing excessive inflammatory response. *Nlrp6*$^{-/-}$ mice were more susceptible to DSS/AOM induced inflammation-driven colorectal cancer manifested by elevated proinflammatory cytokines (MIP-2, TNF, IL-1β, IL-6 and IFNγ), which illustrates the tumor suppressor role of NLRP6 (Chen, Liu et al. 2011). Similarly, *Nlrp6*-deficient mice were also shown to be highly resistant to infection with the bacterial pathogens *Listeria monocytogenes*, *Salmonella* Typhimurium and *Escherichia coli*, characterized by increased NF-κB and MAPK signaling. In the same study, *Nlrp6*$^{-/-}$ bone-marrow-derived macrophages also displayed amplified NF-κB and MAPK signaling after *L. monocytogenes*, Pam3CSK4 or LPS stimulation (Anand, Malireddi et al. 2012). Another group showed that *Nlrp6*$^{-/-}$ mice were more prone to DSS-induced colitis, as loss of *Nlrp6* attenuated the production of IL-18 leading to an increased overgrowth of transmissible colitogenic bacteria (Elinav, Strowig et al. 2011). In summary, dissecting the mechanisms of how regulatory NLRs interfere with immune signaling remains understudied and is still a huge challenge in the NLR field.

NLRP12 as an inhibitory NLR protein. In contrast to proinflammatory NLRs such as NLRP3, NLRP12 reduces the inflammatory response. Our previous reports and public dataset (data source: www.biogps.com) have shown that NLRP12 is primarily expressed by myeloid-monocytes in both human and mice (Williams, Lich et al. 2005, Lich, Williams et al. 2007). In activated human monocyte, Blimp-1 binds to the promoter of *NLRP12* and suppresses its transcription, which suggests a potential suppressor role

of NLRP12 for inflammatory pathway activation (Lord, Savitsky et al. 2009). NLRP12 targets NIK (NF-κB inducing kinase) and IRAK (Interleukin-1 receptor-associated kinase) for proteasomal degradation and thus suppresses the non-canonical and canonical NF-κB pathway, respectively (Williams, Lich et al. 2005, Lich, Williams et al. 2007). NLRP12 also suppresses expression of inflammatory cytokines and chemokines in the inflamed colon tissue, such as TNF, IL6, IL-1, CXCL12 and CXCL13. Loss of the *Nlrp12* gene in mice leads to severe DSS-induced colitis and increased intestinal polyp formation in the AOM/DSS model of colitis-associated colon cancer (Zaki, Vogel et al. 2011, Allen, Wilson et al. 2012). In addition, patients with NLRP12 mutations have been found to develop autoinflammatory disorders including periodic fevers, rash, joint and muscle pains (Jeru, Duquesnoy et al. 2008, Borghini, Tassi et al. 2011, Vitale, Rigante et al. 2013, Xia, Dai et al. 2016, Shen, Tang et al. 2017). Others have observed that NLRP12 ameliorates neuronal inflammation in EAE, a model of multiple sclerosis, by limiting proinflammatory cytokines released from the microglia cells and CD4+ T cells (Gharagozloo, Mahvelati et al. 2015, Lukens, Gurung et al. 2015). Recently, we have found that the expression of NLRP12 negatively correlates to inflammatory genes (e.g., IL-6, TNF, and IL-1B) in human CD14+ monocytes.

1.2 The role of non-inflammasome-forming NLRs in immune disease

Inflammasome complexes recognize various inflammation-inducing PAMPs and

DAMPs. Therefore, inflammasome-forming NLRs have pivotal roles in the pathogenesis of multiple immune diseases, which includes obesity and other metabolic syndromes, atherosclerosis, colitis and other intestinal inflammatory diseases, colorectal cancer, and multiple sclerosis (MS) and other neurological disorders. These have been comprehensively reviewed by others (Davis, Wen et al. 2011, Strowig, Henao-Mejia et al. 2012, Guo, Callaway et al. 2015, Gharagozloo, Gris et al. 2017, Kanneganti 2017, Patel, Carroll et al. 2017, Song, Pei et al. 2017). Here we provide a short synopsis of inflammasome NLRs while emphasis is placed on the contribution of non-inflammasome-forming NLRs to the development of immune diseases.

Intestinal inflammation and tumorigenesis. *In vivo* and *in vitro,* NLRP3 and NLRP6 are classic inflammasome-forming NLRs and mediate proinflammatory responses. In multiple gene profiling studies, IL-1β is elevated in colorectal cancers and invasive breast cancers, which suggests that the inflammasome and IL-1β are pro-tumorigenic (Lewis, Varghese et al. 2006, Liu, Truax et al. 2015, Jeon, Han et al. 2016). However, compared to the WT mice, mice deficient in components of the inflammasome display increased colitis disease severity in the murine DSS (dextran sodium sulfate) model of colitis (Agostini, Martinon et al. 2004, Mariathasan, Newton et al. 2004, Meylan, Tschopp et al. 2006, Miao, Alpuche-Aranda et al. 2006, Sutterwala, Ogura et al. 2006). Moreover, in a colitis-associated colorectal cancer model where mice are treated with a carcinogen, AOM (azoxymethane), together with DSS induces more tumorigenesis in

mice lacking the inflammasome NLRs and IL-1β, which suggests that the inflammasome protects mice from tumorigenesis. The controversial observations maybe because of the nature of DSS in inducing colitis and colorectal cancer where DSS causes intestinal barrier destruction and allows bacteria to infiltrate into the lamina propria and lumen. In this model, inflammasome components are important for bacterial clearance and barrier function (Zaki, Boyd et al. 2010), and therefore loss of the inflammasome leads to an amplified inflammatory response triggered by commensal microbes and promotes colitis and tumorigenesis.

For the non-inflammasome NLRs, NLRP12 can suppress tumorigenesis in colon by attenuating the non-canonical NF-κB pathway (Lich, Williams et al. 2007, Allen, Wilson et al. 2012) and canonical NF-κB pathway (Zaki, Vogel et al. 2011), and inhibiting the expression of proinflammatory cytokines and chemokines (e.g. TNF, IL6, CXCL12, CXCL13, COX2 and MIP2) from the colon tissue. We and others then showed that the loss of NLRP12 promotes the formation of intestinal polyps in the murine AOM-DSS colorectal cancer model (Zaki, Vogel et al. 2011, Allen, Wilson et al. 2012). Similarly, NLRX1 is also reported to suppress the inflammatory pathways including NF-κB, MAPK, STAT3 and IL-6 secretion, which leads to an attenuated tumorigenesis in both AOM-DSS and *Apc*$^{+/min}$ colorectal cancer mouse models (Koblansky, Truax et al. 2016). In addition, another non-inflammasome protein, NLRC3, has been reported to suppress activation of the mTOR signaling pathways to inhibit intestinal stem-cell-derived

organoid proliferation, and mediate protection against colorectal cancer (Karki, Man et al. 2016).

Obesity and type 2 diabetes. In this dissertation, our data indicates that NLRP12 mitigates the severity of diet induced obesity and insulin tolerance by suppressing HFD-induced systemic inflammation, such as IL6, TNF and IL-1β secretion. In the HFD-fed *Nlrp12*$^{-/-}$ mice, we found there was increased activation of the NF-κB pathway and maturation of IL-1β in both fat and intestinal tissues. The mechanism of how NLRP12 attenuates the secretion of IL-1β remains unclear. We found that cohousing with WT mice or antibiotic treatment can normalize the production of IL-1β from HFD-fed *Nlrp12*$^{-/-}$ mice to a similar level as WT mice, which implicates the role of microbiota in promoting inflammasome activation in *Nlrp12*$^{-/-}$ mice. Accordingly, transferring the fecal contents from HFD-fed *Nlrp12*$^{-/-}$ mice induced elevated phosphorylation of p65 and maturation of IL-1β as compared to transferring the fecal contents from WT mice. Inflammasome signaling is a critical driving force for obesity and insulin tolerance. Except for one study (Henao-Mejia, Elinav et al. 2012), others report that mice missing inflammasome components (e.g. NLRP3, ASC and IL1b) are less vulnerable to HFD-related obesity and insulin tolerance (Stienstra, Joosten et al. 2010, Stienstra, van Diepen et al. 2011, Vandanmagsar, Youm et al. 2011, Wen, Gris et al. 2011, Youm, Adijiang et al. 2011, Stienstra, Tack et al. 2012). Palmitic acid, the most abundant saturated fatty acid in the HFD, can induce IL-1β secretion via the NLRP3

inflammasome. Furthermore, injection of IL-1β into mice dramatically reduces insulin signaling (Wen, Gris et al. 2011). This agrees with the finding that expression of NLRP3 inflammasome components and IL-1β is increased in the adipose and liver tissue of obese humans with type 2 diabetes (Vandanmagsar, Youm et al. 2011), suggesting that IL-1β has a critical role in promoting the accelerated weight gain in the *Nlrp12*$^{-/-}$ mice. This is further confirmed by our preliminary data showing *Nlrp12*$^{-/-}$ *IL1β*$^{-/-}$ mice displayed an attenuated obesity compared to the *Nlrp12*$^{-/-}$ mice.

Multiple sclerosis disease model and other models of neurological disorders.

Multiple sclerosis (MS), is one of the most common autoimmune diseases, afflicting approximately 400,000 people in the US and 2.5 million worldwide (data source: http://www.clevelandclinicmeded.com/), The pathogenesis of this disease features the loss of axons, destruction of oligodendrocytes and myelin sheaths, and formation of plaques that are caused by infiltrating auto-reactive CD4+ T cells and other immune cells of the central nervous systems. Experimental autoimmune encephalomyelitis (EAE) is a well-established experimental animal model that has features that mimic the autoimmune and demyelination processes that occurs in MS. To induce EAE, mice are immunized with myelin oligodendrocytes glycoprotein (MOG) and pertussis toxin to initiate MOG-specific CD4+T cells and other inflammatory immune cells that infiltrate into the CNS (e.g., spinal cord). Although there are controversial observations of whether *NLRP3*$^{-/-}$ mice are protected from EAE (Gris, Ye et al. 2010, Shaw, Lukens et

al. 2010, Inoue, Williams et al. 2012), mice lacking other inflammasome components (e.g., IL-1β, IL-18, ASC and Casp1) are uniformly less susceptible to EAE (Furlan, Martino et al. 1999, Shi, Takeda et al. 2000, Matsuki, Nakae et al. 2006, Gris, Ye et al. 2010, Jha, Srivastava et al. 2010, Shaw, Lukens et al. 2010, Inoue, Williams et al. 2012), which implicates that the inflammasome has a critical role in promoting EAE. In contrast to NLRP3, two independent groups showed that NLRP12 was able to attenuate the progression of EAE (Gharagozloo, Mahvelati et al. 2015, Lukens, Gurung et al. 2015). Gharagozloo et al. showed a significant increase in the expression of pro-inflammatory genes *Ccr5, Cox2* and *Il1β* in the spinal cords of the *Nlrp12*$^{-/-}$ mice compared to WT mice during EAE. In addition, they also found that the primary *Nlrp12*$^{-/-}$ microglia cells produce more inducible nitric oxide (iNOS), TNF and IL-6. On the other hand, Lukens et al. did not find an increased paralysis in the *Nlrp12*$^{-/-}$ mice during EAE; instead, they found *Nlrp12*$^{-/-}$ mice developed an atypical EAE featured by ataxia and loss of balance. They focused on the function of NLRP12 in the CD4+ T cells and found NLRP12 suppressed the activation of NF-κB and the production of IL4 in those T cells.

1.3 Introduction to commensal microbiota and microbiome

It is estimated that there are 10 trillion commensal microbes which reside in our bodies, which is approximately the same number of eukaryotic cells (Sender, Fuchs et al. 2016). The majority of commensal bacteria inhabit the gastrointestinal tract, and can

influence energy harvest from food and impact bowel disease and obesity. Thus, a better understanding of the function of commensal bacteria might improve the treatment of multiple diseases. Before the invention of next generation sequencing (NGS), the study of commensal community was impeded due to the difficulty of isolating and culturing commensal microbes after isolation from their host. The advent of deep sequencing allows us to perform culture-free detection of an unlimited number of environmental commensal bacteria in parallel (Sabat, van Zanten et al. 2017), and introduces a new term “microbiome” to describe the collective microbial genomes of the entire bacterial community.

Bacterial 16S ribosomal RNA (rRNA) gene sequencing is one of the most commonly used method for studying phylogeny and taxonomy of bacteria (https://www.illumina.com), which are difficult for the traditional low throughput sequencing or PCR-based approaches (Janda and Abbott 2007). As the sequence of the bacterial 16S rRNA gene are relatively unique in each species, the 16S rRNA sequencing has provided invaluable information for robustly identifying bacterial diversity and family-level abundance changes in the tissue environment in response to different perturbations. However, information on bacterial gene regulation is not determined by 16S rRNA sequencing. Recent studies aim to bridge the commensal microbiome changes to metabolite changes and connect the microbiome to metabolic

diseases. Therefore, there is an urgent need to develop methods that are able to investigate the gene and pathway regulation of the microbial community.

Beyond the 16S rRNA gene sequencing, metagenomics shot-gun sequencing has become a powerful alternative for analyzing the environmental microbial community (Qin, Li et al. 2010). Unlike the 16s rRNA microbiome sequencing, which only targets the region of DNA coding the 16s ribosomal RNA, metagenomics shot-gun sequencing surveys the whole genome of the microorganism. Therefore, the metagenomics shot-gun sequencing can provide both taxonomic and functional information of the environmental microbiota. In other words, the metagenomics shot-gun sequencing can address two questions at once: what species are present and what are metabolites they capable of producing (Sharpton 2014)? In addition, the 16s rRNA microbiome sequencing targets the genomic locus coding 16s rRNA, which is often not amplified consistently and evenly across different species and will produce systematic bias when performing quantification analysis. For metagenomics shot-gun sequencing, the microbial DNA is fragmented into tiny pieces and sequenced independently, which limits the unappreciated amplification bias in certain species during the 16s rRNA microbiome sequencing (Kennedy, Hall et al. 2014). However, similar to the gene regulation in host cells, the transcription of commensal microbial genes can vary widely in response to distinct perturbations (Maurice, Haiser et al. 2013), Therefore, the 16S and metagenomics sequencing both fail to capture the expression information of the

microbial gene that contributing to the functional pathway. To resolve this dilemma, ultra-high throughput microbial RNA sequencing, “metatranscriptome”, has rapidly become the method of choice for revealing altered bacterial gene expression and pathway activation in various environments (McNulty, Yatsunenko et al. 2011). However, the existing databases to annotate and determine the function of the bacterial genes are still under-developed.

1.4 Commensal microbiota in inflammatory diseases

Microbiome in IBD patients. Because our gut holds a huge amount of commensal microbes, the relation between gut microbiota and inflammatory bowel disease (IBD) has been intensely studied. Crohn’s disease (CD) and ulcerative colitis (UC) are the most common IBD and together affect more than 3.6 million people (Loftus 2004). Several twin studies have shown that the concordance rate for UC between monozygotic twins is dramatically and unexpectedly less than 50% (Halme, Paavola-Sakki et al. 2006). Therefore, other environmental factors, such as gut microbial composition, can play an important role in the pathogenesis of IBD.

Many studies consistently report a decrease in bacterial diversity, also known as α-diversity or species richness, which is a standard to measure the total number of different species in a community. Several studies comparing CD patients and healthy controls, and pairs of monozygotic twins with or without CD, reveal a consistent reduced

α-diversity in CD patients (Manichanh, Rigottier-Gois et al. 2006, Dicksved, Halfvarson et al. 2008). Furthermore, this reduction of diversity is attributed to species extinction particularly within the Firmicutes phylum (Kang, Denman et al. 2010). Although, there is a consistent reduction of microbial diversity in the inflamed versus non-inflamed tissues, the total load of bacterial abundance was not affected (Sepehri, Kotlowski et al. 2007).

It is difficult to collect fecal samples from IBD patients without any prior treatment in the clinic, but there is a study that includes 447 treatment-naïve pediatric CD patients collected as new-onset cases with 221 healthy control subjects. This study identifies a unique gut microbiome signature in the CD patients manifested by an increased relative abundance in the bacterial groups of Enterobacteriaceae, Pasteurellacaea, Veillonellaceae, and Fusobacteriaceae, but a decreased proportion of Erysipelotrichales, Bacteroidales, and Clostridiales in the IBD group compared to the healthy group. Also, this microbiome signature has been suggested to correlate strongly with disease status (Gevers, Kugathasan et al. 2014).

In the steady state, our intestine is a reservoir for commensal bacteria which control inflammation induced by pathogenic organisms and intestinal cells. The small intestine has a single layer of mucus and the colon has two layers of mucus to prevent intense inflammatory responses induced by infiltrating bacteria (Johansson, Larsson et al. 2011). The mucus contains mucin, IgA, anti-microbial peptides and various defensins that help to control bacterial overgrowth, and permits commensal bacteria to perform

their probiotic functions but not stimulate inflammatory responses. In the disease stage, it has been found that the secretion of mucin is altered (Wlodarska, Thaiss et al. 2014), and there is an increase in active IgA (Fransen, Zagato et al. 2015, Viladomiu, Kivolowitz et al. 2017), anti-microbial peptides and defensins which control the infiltration of bacteria (Zilbauer, Dorrell et al. 2005, Schauber, Rieger et al. 2006). Hence, this anti-microbial machinery is frequently increased in ulcerative colitis and might cause a dysbiotic intestinal microbiome. Since the interaction between the microbiome and host immunity can be bidirectional, the dysbiotic microbiome might further exaggerate the host inflammatory response. Sequencing analysis based on bacterial 16S RNA has revealed that the Clostridia bacterial groups are decreased in IBD patient (Gevers, Kugathasan et al. 2014). Clostridia bacterial groups are linked to the production of short chain fatty acids (SCFA) (Duncan, Barcenilla et al. 2002), which include acetate, propionate and butyrate. These molecules were first described as a primary energy source for colonic epithelial cells (Ahmad, Krishnan et al. 2000), and were recently demonstrated to induce the expansion of colonic anti-inflammatory regulatory T cells (Atarashi, Tanoue et al. 2013, Smith, Howitt et al. 2013). However, 16S sequencing misses the transcriptional information of SCFA-related genes in the gut microbiota. Thus, shot-gun metatranscriptome sequencing and metabolome analysis might provide more detailed insights into the function of the microbiota in these diseases.

Microbiome in obese patients. IBD and obese patients share a number of similar changes in the microbiome. For instance, there is an overall decrease of diversity in both IBD and obesity (Turnbaugh, Hamady et al. 2009, Le Chatelier, Nielsen et al. 2013) and a major shift of the microbiome characterized by a reduction of Clostridia bacterial groups (Larsen, Vogensen et al. 2010). Therefore, many of the same changes in the gut microbial community, even in specific taxa, are observed across these two diseases, which indicates that the increased intestinal inflammation caused by the western diet might function in a similar way to IBD that results in the elimination of certain strains while promoting other strains to thrive in this inflammatory gut environment. Analysis of the microbiome from IBD and obese individuals by metagenomic sequencing revealed a similar increase in abundance of microbial genes for bacterial membrane transport (Turnbaugh, Hamady et al. 2009, Greenblum, Turnbaugh et al. 2012). In the context of microbial gene function in type 2 diabetes, metagenomics sequencing identified that there is an enrichment of genes in sulfate reduction and oxidative stress resistance but a reduction of genes in the pathways of vitamin metabolism and SCFA production (Qin, Li et al. 2012). Furthermore, feces isolated from obese twins were found to show increased energy harvest and induced expedited obesity in germ-free recipient mice, compared to the feces transplanted from lean twins (Turnbaugh, Hamady et al. 2009). These results suggest that commensal

microbiota has a critical role in regulating the progress of nutrition metabolism and obesity.

As discussed in our previous publication (Chen, Wilson et al. 2017), the reduction of biodiversity and Clostridiales groups and increased Erysipelotrichaceae bacterial groups are consistently reported in the microbiome from both obese human and mouse models of obesity. Erysipelotrichaceae has been reported to correlate with increased TNF levels, resulting in chronic intestinal inflammation (Dinh, Volpe et al. 2015). Additionally, the abundance of Erysipelotrichaceae was found to be enhanced in patients with IBD or in animal models of IBD (Chen, Liu et al. 2012, Dey, Soergel et al. 2013). The immunogenic role of Erysipelotrichaceae in IBD has been systematically reviewed (Kaakoush 2015). However, one study has found an opposite association between Erysipelotrichaceae and colitis (Gevers, Kugathasan et al. 2014). In contrast, Erysipelotrichaceae has been consistently reported to associate with obesity (Ley, Backhed et al. 2005, Turnbaugh, Backhed et al. 2008, Zhang, DiBaise et al. 2009, Fleissner, Huebel et al. 2010, Zhang, Zhang et al. 2010), which is supported by our finding that there is a strong correlation between the high abundance of Erysipelotrichaceae and exacerbated weight gain.

1.5 Concluding remarks

In this section, a sub-group of non-inflammasome forming NLRs are discussed as negative regulators of immune signaling. Our group has provided substantial evidence suggesting that these negative regulatory NLRs are important components to keep inflammatory responses in check and prevent autoinflammatory disorders. Among the negative regulatory NLRs, NLRP12, has been reported to ameliorate experimental colitis and inflammation-driven colorectal cancer in mice (Lich, Williams et al. 2007, Zaki, Vogel et al. 2011, Allen, Wilson et al. 2012). However, the clinical relevance of NLRP12 in IBD is still unknown. In addition, increased intestinal inflammation in IBD was reported by multiple studies to affect the gut microbiome (Le Chatelier, Nielsen et al. 2013, Gevers, Kugathasan et al. 2014, Kostic, Xavier et al. 2014), and emerging studies report a dysbiotic microbiome in multiple inflammasome-forming-NLR deficient mice (Petnicki-Ocwieja, Hrncir et al. 2009, Elinav, Strowig et al. 2011, Henao-Mejia, Elinav et al. 2012, Couturier-Maillard, Secher et al. 2013). Loss of Nlrp12, a classical negative regulatory NLR, has not been comprehensively studied for its function in regulating the colonic microbiome composition.

In addition to colitis, obesity is another inflammation-driven disorder, which involves multiple inflammatory signaling pathways (Greenberg and Obin 2006, Monteiro and Azevedo 2010, Lumeng and Saltiel 2011, Saltiel and Olefsky 2017). The NLRP3 inflammasome was demonstrated by multiple groups to promote obesity and insulin

resistance (Stienstra, Joosten et al. 2010, Stienstra, van Diepen et al. 2011, Vandanmagsar, Youm et al. 2011, Wen, Gris et al. 2011, Youm, Adijiang et al. 2011, Stienstra, Tack et al. 2012). TNF and IL-6 were also demonstrated to be critical promoters for obesity development (Kirchgessner, Uysal et al. 1997, Khosravi, Ka et al. 2013). In contrast, our and other's previous studies have shown that Nlrp12 attenuated the activation of NF-κB and the expression of TNF and IL-6 in the inflamed colon tissue (Lich, Williams et al. 2007, Zaki, Vogel et al. 2011, Allen, Wilson et al. 2012), which provides evidence to hypothesize that NLRP12 might reduce inflammation-driven obesity during HFD.

Based on the previous publications discussed above, this dissertation aims to dissect the role of NLRP12 in the intestinal inflammation-obesity-dysbiosis axis. We identified correlations between NLRP12 expression in mucosal tissue with colitis severity in IBD patients. We elucidated the role of elevated basal inflammation in *Nlrp12*$^{-/-}$ mice to promote the formation of a dysbiotic colonic microbiome. For the obesity study, we collaborated with others to survey *NLRP12* expression in the adipose tissue from obese and lean individuals to determine the connection between *NLRP12* expression with adipogenesis. We also proposed to test if HFD induced more obesity with increased insulin tolerance in *Nlrp12*$^{-/-}$ mice and if this is fueled by excessive systemic inflammation and a skewed gut microbiome composition.

CHAPTER 2: NLRP12 ATTENUATES COLON INFLAMMATION BY MAINTAINING COLONIC MICROBIAL DIVERSITY AND PROMOTING PROTECTIVE COMMENSAL EXPANSION[1]

2.1 INTRODUCTION

Colitis is a multi-factorial disease thought to involve the dynamic interplay of host genetics, microbiome and inflammatory response. In this chapter, we found that *NLRP12*, a negative regulator of innate immunity, is reduced in human colitis by comparing monozygotic twins and other patient cohorts. In parallel, Nlrp12-deficiency in mice caused increased colonic basal inflammation, leading to a less-diverse microbiome, loss of protective gut commensal strains (*Lachnospiraceae*) and increased colitogenic strains (*Erysipelotrichaceae*). Dysbiosis and colitis susceptibility associated with Nlrp12-deficency were ameliorated by treatment with antibodies targeting inflammatory cytokines or by administration of beneficial commensal *Lachnospiraceae* isolates. Fecal transplant in gnotobiotic Nlrp12-deficient mice shows that NLRP12 and the microbiome each contribute to immune signaling that culminate in colon inflammation. These findings reveal a feed-forward loop where NLRP12 promotes

[1] This chapter is part of a manuscript published on the *Nature Immunology* on 13 March 2017: Chen et al, NLRP12 attenuates colon inflammation by maintaining colonic microbial diversity and promoting protective commensal bacterial growth.

specific commensals that can mitigate gut inflammation, while cytokine blockade during NLRP12-deficiency can reverse dysbiosis.

The healthy intestine is inhabited by trillions of resident bacteria and has evolved a fine-tuned balance between pathogen recognition and commensal tolerance (Kau, Ahern et al. 2011). In contrast, microbial imbalance, referred to as dysbiosis, is highly associated with inflammatory bowel diseases (IBD), including ulcerative colitis (UC) and Crohn's disease (CD), which have limited treatment options. Hence, understanding the host gene-microbiota interaction that contributes to colitis holds promise in unveiling novel microbiome-based therapeutic options.

A hallmark of IBD is the dysregulated activation of inflammatory cytokines and signaling pathways such as the NF-KB, MAPK or STAT family members (Karrasch and Jobin 2008). Several innate immune receptors/sensors known as NLRs (nucleotide-binding domain, leucine-rich repeat proteins or NOD-like receptors) regulate these pathways. NLRs are a family of intracellular innate immune sensors that exert either pro- or anti-inflammatory functions. The NLR family member NOD2 activates NF-KB, and mutations in *NOD2* represent the first genetic association with CD susceptibility (Hugot, Chamaillard et al. 2001, Ogura, Bonen et al. 2001). Despite of a contradicting report (Shanahan, Carroll et al. 2014), *Nod2*-deficient mice display gut dysbiosis and an expansion of colitogenic bacteria, which may contribute to exacerbated colitis symptoms in these animals (Couturier-Maillard, Secher et al. 2013, Jiang, Wang et al.

2013, Ramanan, Tang et al. 2014). Similarly, loss of the inflammasome-forming protein NLRP6 is associated with the expansion of pathogenic microbes, including *Prevotella*, resulting in exacerbated experimental colitis (Elinav, Strowig et al. 2011). Although the NLRP12 inflammasome has been implicated in the recognition of specific infections (Vladimer, Weng et al. 2012), NLRP12 has clear non-inflammasome and anti-inflammatory functions by restricting both the canonical NF-KB pathway via inhibition of IRAK phosphorylation (Williams, Lich et al. 2005) and the non-canonical NF-KB pathway via promoting NIK (NF-KB-inducing kinase) degradation (Lich, Williams et al. 2007, Allen, Wilson et al. 2012). Colons from *Nlrp12*$^{-/-}$ mice contain elevated non-canonical and canonical NF-KB signaling molecules during experimental colitis (Zaki, Vogel et al. 2011, Allen, Wilson et al. 2012). Although NLRP12 and other family members serve as negative regulators of inflammatory signaling in experimental colitis in mice, their impact on the colonic bacterial ecology and translational relevance to humans are completely unknown.

2.2 RESULTS

Commensal microbiota is required for the differential colitis severity between WT and *Nlrp12*$^{-/-}$ mice

Our group and others have demonstrated an anti-inflammatory role for NLRP12 during experimental colitis (Zaki, Vogel et al. 2011, Allen, Wilson et al. 2012). To

determine how NLRP12 is regulated in human colitis, we analyzed an ulcerative colitis (UC) study including 10 pairs of monozygotic twins and seven additional UC gene-profiling studies (**Fig. 2.1, a-h**), and found that *NLRP12* was significantly down-regulated in active UC cohorts compared to healthy controls. Conversely, *NLRP12* expression was indistinguishable between samples from healthy participants and inactive UC patients after various treatments. Except for *NLRP6*, inflammasome forming *NLRP3 and NOD2* expressions were increased in the active UC stage compared to healthy and inactive UC groups (**Fig. 2.1, i-l**). In animals, conventionally-raised (CV) *Nlrp12*$^{-/-}$ mice displayed more severe colitis compared to wild type mice following the oral administration of 3% dextran sodium sulfate (DSS), which induces experimental colitis. These differences include significantly increased weight loss, mortality, histology score and clinical disease symptoms measured as disease-associated index (DAI), and *Nlrp12*$^{-/-}$ mice exhibited reduced colon length (indication of increased colonic inflammation) compared to WT animals as reported (**Fig. 2.2, a-e**) (Zaki, Vogel et al. 2011, Allen, Wilson et al. 2012). Additionally, the loss of Nlrp12 resulted in increased immune signaling marked by heightened NF-KB, ERK and STAT3 activation (**Fig. 2.2, f-h**). These findings establish a link between reduced *NLRP12* expression and human IBD and consolidate NLRP12's protective role in limiting colon inflammation via suppressing excessive immune responses.

In addition to the association between genetic susceptibility and colon inflammation, mounting evidence supports a role for the microbiota during IBD pathogenesis (Gevers, Kugathasan et al. 2014). Moreover, NLRP12 limits inflammation induced by microbial components (Williams, Lich et al. 2005). To assess the impact of the microbiota on the increased colitis susceptibility in *Nlrp12*$^{-/-}$ mice, we generated gnotobiotic WT and *Nlrp12*$^{-/-}$ mice and subjected these germ-free (GF) animals to a reduced 1.5% DSS in the drinking water due to the reported increased sensitivity of GF mice to DSS (Kitajima, Morimoto et al. 2001). In contrast to conventionally-raised mice, GF-WT and GF-*Nlrp12*$^{-/-}$ mice showed indistinguishable weight loss, mortality, DAI, colon length and histology scores following DSS treatment (**Fig. 2.3, a-e**). In line with these findings, colons from GF-WT and GF-*Nlrp12*$^{-/-}$ mice showed similar levels of activated NF-KB, ERK and STAT3 (**Fig. 2.3, f-h**). These results implicate a role for the microbiota in severe colitis found in *Nlrp12*$^{-/-}$ mice.

The presence of NLRP12 curtails the activation of inflammatory cell signaling pathways induced by bacteria-derived ligands (Lich, Williams et al. 2007, Zaki, Vogel et al. 2011, Allen, Wilson et al. 2012, Zaki, Man et al. 2014), which suggests *Nlrp12*$^{-/-}$ mice may present increased basal colonic inflammation in the presence of commensal bacteria at the steady state. In line with this hypothesis, colons from naïve specific-pathogen free (SPF) *Nlrp12*$^{-/-}$ mice displayed elevated NF-KB p65 and p52 activation compared to wild type colons (**Fig. 2.4a**), which indicates that Nlrp12 limits low-grade

basal colonic inflammation in the steady state. To determine the role of NLRP12 in regulating basal colon inflammation during intestinal colonization by the microbiota, we conventionalized GF-WT and GF-*Nlrp12*$^{-/-}$ mice by housing these animals in a SPF vivarium for 4 weeks (**Fig. 2.4b**). GF-*Nlrp12*$^{-/-}$ mice colonized for 4 weeks (exGF-*Nlrp12*$^{-/-}$) displayed increased colon NF-KB activation compared to conventionalized WT mice (exGF-WT) and control animals maintained in sterile isolators (i.e., GF-WT and GF-*Nlrp12*$^{-/-}$ mice) at steady state (**Fig. 2.4c**). These results demonstrate that NF-KB immune signaling pathways activated at the basal state requires two factors: *Nlrp12*-deficiency and microbiota from mice housed in conventional conditions. We also found that the C-type lectin antimicrobial peptide REG3γ and cathelin-related antimicrobial peptide (CRAMP) were increased in the exGF-*Nlrp12*$^{-/-}$ mice compared to exGF-WT mice and control GF animals (**Fig. 2.4, d-e**). This result agrees with the literature where increased inflammation promotes antimicrobial peptides expression, which may skew intestinal microbial populations, resulting in a dysbiotic intestinal microbiome (Gallo and Hooper 2012). Together, these findings indicate that intestinal microbiota is required for the enhanced basal colonic inflammation and exacerbated experimental colitis in *Nlrp12*$^{-/-}$ mice.

NLRP12-deficiency generates a unique microbiome resembling dysbiotic microbiome in IBD patients

To determine if NLRP12 alters the microbiome, high throughput 16S rRNA gene sequencing analysis was performed on fecal bacterial DNA isolated from WT and *Nlrp12*$^{-/-}$ mice that were originally generated from the same heterozygous *Nlrp12*$^{+/-}$ parents and raised in our facilities for more than nine generations (**Fig. 2.5a**). Housing and diet are key factors that can influence the intestinal microbiota (Carmody, Gerber et al. 2015); thus, we repeated the microbiome analysis three years later with mice housed in a second vivarium with different formula chow, and findings were similar. Rarefaction analysis was used to compare bacterial diversity within individuals of a group (Kuczynski, Stombaugh et al. 2012). Compared to WT mice, *Nlrp12*$^{-/-}$ mice harbored a microbiota with significantly reduced diversity (**Fig. 2.5b**). Additionally, the community composition of the microbiota from *Nlrp12*$^{-/-}$ mice was strikingly different from that observed in WT animals (**Fig. 2.5c**). Comparing within and between group dissimilarity (**Fig. 2.5d, calculated from Fig. 2.5c**) indicated that the microbiome difference between the WT vs. *Nlrp12*$^{-/-}$ mice was significantly larger than the differences between animals of each genotype. These results suggest that *Nlrp12*-deficiency results in the assembly of a significantly different intestinal microbiome. These results demonstrate that *Nlrp12*$^{-/-}$ mice retained this altered microbiome in different housing conditions over many generations.

Because the analyzed WT and *Nlrp12*$^{-/-}$ mice had been bred separately for multiple generations, it is possible that familial transmission instead of *NLRP12*-deficiency was responsible for the altered microbiome in *Nlrp12*$^{-/-}$ mice (Ubeda, Lipuma et al. 2012). Therefore, we analyzed feces from WT and *Nlrp12*$^{-/-}$ littermates birthed from the same *Nlrp12* heterozygous parents (*Nlrp12*$^{+/-}$) and housed separately by genotype after weaning (**Fig. 2.5e**). Compared to WT littermates, *Nlrp12*$^{-/-}$ mice from this heterozygous mating harbored a microbiota with significantly reduced diversity compared to WT littermates (**Fig. 2.5f**). But the separation of microbiome between WT and *Nlrp12*$^{-/-}$ littermates was not as great as the microbiome difference between WT and *Nlrp12*$^{-/-}$ mice had been raised separately for generations (**Fig. 2.5g**).

To establish rigor of the microbiota results, we used high throughput 16S rRNA gene sequencing to characterize the microbiome of the WT and *Nlrp12*$^{-/-}$ mice in three mouse cohorts (vivarium 1, vivarium 2 and littermate studies). Among all three sets of microbiome studies, we observed a consistent decrease in *Bacteroidales*, *Clostridiales* and *Lachnospiraceae* and an increase in *Erysipelotrichaceae* in the *Nlrp12*$^{-/-}$ mice compared to WT animals (**Fig. 2.5h**). This microbiome alteration in the *Nlrp12*$^{-/-}$ mice is noteworthy, as IBD patients have been reported to display a similar microbiome profile (Gevers, Kugathasan et al. 2014) (**Fig. 2.5i**). Thus, we focused on these consistently altered bacterial groups for further study.

Transferring normal microbiota reverses gut microbial dysbiosis and attenuates colitis severity in *Nlrp12*$^{-/-}$ mice

To determine if the altered microbiome observed in *Nlrp12*$^{-/-}$ mice is responsible for the exacerbated colon inflammation in *Nlrp12*$^{-/-}$ mice, we conducted microbiota transfer studies by cohousing mice, which led to the exchange of the microbiota through coprophagia (Elinav, Strowig et al. 2011, Henao-Mejia, Elinav et al. 2012, Ridaura, Faith et al. 2013). To test the hypothesis that the passive exchange of the microbiota between WT and *Nlrp12*$^{-/-}$ mice influences colitis severity in either group, age-and-sex matched WT and *Nlrp12*$^{-/-}$ mice were either single-housed (SiHo) or cohoused (CoHo) for six weeks prior to 3% DSS treatment (**Fig. 2.6a**). Control single-housed WT and *Nlrp12*$^{-/-}$ mice showed significant differences in disease severity (**Fig. 2.6, b-f**) as expected. After receiving DSS, *Nlrp12*$^{-/-}$ mice that were cohoused with WT mice (CoHo *Nlrp12*$^{-/-}$) displayed reduced disease compared to their SiHo *Nlrp12*$^{-/-}$ littermates, which was manifested as significantly lessened weight loss, mortality, DAI, histopathology and NF-KB, ERK and STAT3 activation, with increased colon lengths (**Fig. 2.6, b-i**). Cohoused *Nlrp12*$^{-/-}$ and WT cage-mates displayed similar reduced colitis and were indistinguishable in all other measurements (**Fig. 2.6, b-i**).

To investigate detailed microbiome changes after cohousing WT mice with *Nlrp12*$^{-/-}$ mice, we performed 16S rRNA gene microbiome sequencing analysis on feces from WT and *Nlrp12*$^{-/-}$ mice before and after cohousing (**Fig. 2.6j**). Consistent with **Fig. 2.5**,

we observed significantly different community composition between the WT and *Nlrp12*$^{-/-}$ mice before cohousing. After six weeks of cohousing, the microbiota composition of the cohoused *Nlrp12*$^{-/-}$ mice was analyzed and found to be more similar to that of the WT mice and distinct from the single-housed *Nlrp12*$^{-/-}$ littermate microbiota composition (**Fig. 2.6j**). In particular, cohoused WT and *Nlrp12*$^{-/-}$ cage-mates had the lowest microbiome dissimilarity values while control single-housed WT vs. single-housed *Nlrp12*$^{-/-}$ mice had the greatest dissimilarity (**Fig. 2.6k**). Most importantly, the microbiome dissimilarity between cohoused and single-housed *Nlrp12*$^{-/-}$ mice was as equally high as control single-housed WT vs. *Nlrp12*$^{-/-}$ mice (**Fig. 2.6k**). These results indicate that *Nlrp12*$^{-/-}$ mice cohoused with WT mice developed a microbiota that was closer in community structure to that of WT animals. To assess if the transferred microbiota resulted in changes in specific bacteria, we performed a two-way ANOVA test on all sequenced fecal bacteria identified by 16S rRNA gene sequencing after cohousing WT and *Nlrp12*$^{-/-}$ mice. Bacterial strains from the *Clostridiales* order and *Lachnospiraceae* family were significantly higher, and *Erysipelotrichaceae* was lower in the cohoused *Nlrp12*$^{-/-}$ mice compared to the single-housed *Nlrp12*$^{-/-}$ mice (**Fig. 2.6l**). This reinforced the findings in **Fig. 2.5** of specific microbiota changes in *Nlrp12*$^{-/-}$ mice compared to controls. Additionally, because co-housed *Nlrp12*$^{-/-}$ mice exhibit less disease severity compared to single-housed *Nlrp12*$^{-/-}$ mice, these data demonstrate

that transferred microbiota from WT mice ameliorated disease susceptibility in *Nlrp12*$^{-/-}$ mice in a co-house setting.

As a control, we found cohousing WT with inflammasome-deficient *Asc*$^{-/-}$ mice failed to ameliorate colitis in DSS-treated *Asc*$^{-/-}$ mice, but instead increased death, DAI and histopathology in WT mice (**Fig. 2.7, a-e**), which is in agreement with other previous reports that deletion of inflammasome components generate transmissible colitogenic microbiota (Elinav, Strowig et al. 2011, Henao-Mejia, Elinav et al. 2012, Couturier-Maillard, Secher et al. 2013). This is in contrast to improved survival and lessened colitis in CoHo *Nlrp12*$^{-/-}$ mice and makes *Nlrp12*-deficiency the first case where elevated colitis susceptibility resulting from an NLR deficiency can be reversed by transferring normal microbiota.

The experiments utilizing *Nlrp12*$^{+/+}$ and *Nlrp12*$^{-/-}$ littermate mice and GF animals suggest NF-KB dysregulation occurs prior to alterations in the microbiota, as *Nlrp12*$^{-/-}$ mice developed a different microbiome from that of *Nlrp12*$^{+/+}$ littermates after weaning (**Fig. 2.5, e-g**), and GF *Nlrp12*$^{-/-}$ mice display increased basal colon inflammation when commensal bacteria colonized (**Fig. 2.4**). However, compared to single-housed *Nlrp12*$^{-/-}$ mice, cohoused *Nlrp12*$^{-/-}$ mice displayed attenuated NF-KB activation during DSS-induced colitis, suggesting the altered microbiota in *Nlrp12*$^{-/-}$ mice also contributes to heightened NF-KB activation (**Fig. 2.6g**). To investigate the causality between NF-KB hyperactivation and altered microbiota in *Nlrp12*$^{-/-}$ mice, we performed reciprocal fecal

transplantation experiments in which GF WT mice were reconstituted with the microbiota of SPF *Nlrp12*$^{-/-}$ mice, and GF *Nlrp12*$^{-/-}$ mice were reconstituted with the microbiota of SPF WT mice prior to DSS treatment (**Fig. 2.8a**). As expected, transfer of the fecal microbiota (FM) from an SPF WT donor into GF WT mice (designated as FM_{WT} > $_{GF}$WT) resulted in significantly reduced DSS-induced colitis, survival and disease index, but greater colon length compared to the transfer of FM from an SPF *Nlrp12*$^{-/-}$ donor into GF *Nlrp12*$^{-/-}$ mice ($FM_{Nlrp12-/-}$ > $_{GF}$*Nlrp12*$^{-/-}$) (**Fig. 2.8, a-d).** However, FM_{WT} > $_{GF}$*Nlrp12*$^{-/-}$ and $FM_{Nlrp12-/-}$ > $_{GF}$WT mice exhibited similar weight loss, survival, disease index and colon length, which were less severe compared to control $FM_{Nlrp12-/-}$ > $_{GF}$*Nlrp12*$^{-/-}$ mice **(Fig. 2.8, a-d)**. This indicates that both the *Nlrp12*$^{-/-}$-shaped microbiome and host genetic deficiency in *Nlrp12* are required to produce the fulminant colitis observed in *Nlrp12*$^{-/-}$ mice. Next, we examined the contribution of FM vs. host genetics on immune signaling pathways. As expected, colon samples from control FM_{WT} > $_{GF}$WT mice exhibited minimal NF-KB and STAT3 activation, while $FM_{Nlrp12-/-}$ > $_{GF}$*Nlrp12*$^{-/-}$ samples showed elevated p52, pp65 and pSTAT3 (**Fig. 2.8e**). Remarkably, colons from $FM_{Nlrp12-/-}$ > $_{GF}$WT and FM_{WT} > $_{GF}$*Nlrp12*$^{-/-}$ mice showed intermediate, but distinct activation of the following inflammatory pathways. $FM_{Nlrp12-/-}$ > $_{GF}$WT colons had elevated pp65 that were similar to $FM_{Nlrp12-/-}$ > $_{GF}$*Nlrp12*$^{-/-}$ colons, but reduced p52 nuclear translocation and STAT3 activation. By contrast, FM_{WT} > $_{GF}$*Nlrp12*$^{-/-}$ colons showed elevated p52 and pp65 but displayed a modest level of STAT3

activation. This supports the conclusion that both the microbiome shaped by *Nlrp12*$^{-/-}$ animals and *Nlrp12* gene deficiency are required to cause the full activation of p52, p65 and STAT3.

Collectively, the fecal reciprocal transplantation studies indicate that the cumulative insult of increased inflammation due to NLRP12 deficiency and the presence of a dysbiotic microbiota result in fulminant colitis in *Nlrp12*$^{-/-}$ mice.

Administration of Lachnospiraceae suppresses colitis and reduces Erysipelotrichaceae in *Nlrp12*$^{-/-}$ mice

The results thus far show that the *Clostridiales* order and *Lachnospiraceae* family were significantly higher, and *Erysipelotrichaceae* was lower in *Nlrp12*$^{-/-}$ mice compared to WT mice. *Lachnospiraceae* strains were recently found to be decreased in Crohn's patients (Gevers, Kugathasan et al. 2014), and *Lachnospiraceae* limits experimental *C. difficile*-induced colitis (Reeves, Koenigsknecht et al. 2012). To determine if administration of bacterial groups that are lacking in *Nlrp12*$^{-/-}$ mice can restrict the development of colitis, we inoculated WT and *Nlrp12*$^{-/-}$ mice with 23 strains of *Lachnospiraceae* via oral gavage for 21 days followed by one week of rest before DSS treatment (**Fig. 2.9a**). During the 3-week bacterial administration period, we observed no significant weight loss in mice given *Lachnospiraceae* compared to WT mice fed brain-heart infusion (BHI) vehicle control, which was used to grow *Lachnospiraceae*, indicating these strains were not overtly pathogenic. Strikingly, DSS-treated *Nlrp12*$^{-/-}$

mice given *Lachnospiraceae* strains displayed reduced signs of colitis including significantly reduced weight loss, DAI, colon histopathology and increased colon lengths compared to *Nlrp12*$^{-/-}$ mice given BHI vehicle control (**Fig. 2.9, a-d)**. This reduction in disease among *Lachnospiraceae* inoculated *Nlrp12*$^{-/-}$ mice was accompanied by a reduction of proinflammatory cytokines to levels found in WT controls (**Fig. 2.9e**) and significantly decreased activation of canonical and non-canonical NF-KB, ERK and STAT3 (**Fig. 2.9, f-h**).

To examine whether administration of *Lachnospiraceae* modulates severity of inflammation by altering the composition of the microbiota of *Nlrp12*$^{-/-}$ mice, we sequenced the microbiome of the mice receiving *Lachnospiraceae* or control BHI. For both WT and *Nlrp12*$^{-/-}$ mice, the diversity of the microbiota from *Lachnospiraceae*-receiving mice was significantly increased compared to that of the BHI-treated littermates, although the impact of the *Lachnospiraceae* transfer was greater in *Nlrp12*$^{-/-}$ mice **(Fig. 2.9i)**. Next, UniFrac distance analysis was used to quantify the dissimilarity between bacterial communities among the groups. The distance between the BHI-treated *Nlrp12*$^{-/-}$ mice vs. *Lachnospiraceae*-treated *Nlrp12*$^{-/-}$ mice was as large as the distance between the control BHI-treated WT vs. BHI-treated *Nlrp12*$^{-/-}$ mice (**Fig. 2.9j**). This result indicates that the microbiome in *Lachnospiraceae*-treated *Nlrp12*$^{-/-}$ mice was significantly distinct from that of littermate control *Nlrp12*$^{-/-}$ mice given BHI. Additionally, the microbiome dissimilarity distance between the BHI-treated WT and

Lachnospiraceae-treated *Nlrp12*$^{-/-}$ mice was significantly decreased compared to the distance between the BHI-treated *Nlrp12*$^{-/-}$ mice and *Lachnospiraceae*-treated *Nlrp12*$^{-/-}$ mice, suggesting that *Nlrp12*$^{-/-}$ mice administered *Lachnospiraceae* develop a microbiome more reminiscent of WT animals (**Fig. 2.9k**). Administration of *Lachnospiraceae* also promoted the expansion of *Clostridiales* in *Nlrp12*$^{-/-}$ mice (**Fig. 2.5l**), which was reduced in the intestine of *Nlrp12*$^{-/-}$ mice as shown earlier. Among all identified strains, only *Erysipelotrichaceae* was significantly reduced after the *Lachnospiraceae* administration. Given the fact that the abundance of *Erysipelotrichaceae* was increased in the *Nlrp12*$^{-/-}$ mice, which positively correlated with disease severity, administration of *Lachnospiraceae* may limit colitis in part by suppressing intestinal expansion of *Erysipelotrichaceae.*

NLRP12 expression in the hematopoietic compartment prevents commensal dysbiosis

We and others have previously reported the increased intestinal inflammation in *Nlrp12*$^{-/-}$ mice is driven by both hematopoietic and non-hematopoietic components (Zaki, Vogel et al. 2011, Allen, Wilson et al. 2012), but the cellular compartment expressing NLRP12 that shapes the intestinal commensals is unknown. To address this, we generated radiation bone marrow chimeric mice by lethally irradiating WT and *Nlrp12*$^{-/-}$ mice and performed adoptive bone marrow transplantation (BMT) using bone marrow derived from WT and *Nlrp12*$^{-/-}$ donors to generate WT mice containing myeloid

cells deficient in *Nlrp12* (*Nlrp12*$^{-/-}$>WT) and *Nlrp12*$^{-/-}$ mice expressing *Nlrp12* only in myeloid cells (WT>*Nlrp12*$^{-/-}$). We then assessed the microbiome in these animals after a 10-week-reconstituition period (**Fig. 2.10a**). As expected, control WT mice given WT bone marrow retained greater microbiota diversity than *Nlrp12*$^{-/-}$ recipients with *Nlrp12*$^{-/-}$ bone marrow **(Fig. 2.10b)**, Microbiome-sequencing of radiation chimeric mice revealed that WT mice with *Nlrp12*$^{-/-}$ bone marrow (*Nlrp12*$^{-/-}$>WT) displayed reduced bacterial diversity compared to WT>WT mice. Additionally, transplantation of WT bone marrow into *Nlrp12*$^{-/-}$ mice (WT>*Nlrp12*$^{-/-}$) increased bacterial diversity compared to control *Nlrp12*$^{-/-}$>*Nlrp12*$^{-/-}$ mice **(Fig. 2.10b).** These results indicate that NLRP12 expression in the hematopoietic compartment dominantly shapes the diversity of the intestinal bacteria. Analysis of bacterial composition confirmed these findings as the microbiome observed in WT>WT mice were similar to that of WT>*Nlrp12*$^{-/-}$ mice, and the microbiome of *Nlrp12*$^{-/-}$>WT mice were similar to *Nlrp12*$^{-/-}$>*Nlrp12*$^{-/-}$ mice (**Fig. 2.10, c-d**).

Because NLRP12 expression in the hematopoietic compartment shaped the intestinal microbiota, we next characterized the hematopoietic cells in the colon lamina propria (cLP) that could be contributing to increased basal inflammation in *Nlrp12*$^{-/-}$ mice. Although we and others have shown that NLRP12 suppresses inflammatory pathways in bone marrow-derived macrophages (Zaki, Vogel et al. 2011, Zaki, Man et al. 2014) and DCs (Allen, Wilson et al. 2012), there is no evidence to support a role for

NLRP12 in colon-resident macrophages and DCs, which are phenotypically different from their bone marrow-derived counterparts (Denning, Wang et al. 2007). Within the cLP, colon residual macrophages are identified as two subsets that express the fractalkine receptor (CX3CR1), F4/80 and CD11b with or without coexpression of CD11c. DCs within the cLP express CD11c and CD103 and are considered CD11b negative or low (**Fig. 2.10e)**. Other cellular subsets have also been reported to be present in the cLP, however these three populations contribute to the vast majority of the colonic mononuclear phagocytes (Cerovic, Bain et al. 2014). To analyze the impact of NLRP12 on these macrophage and DC populations in the steady state, we isolated cLP cells from naïve wild type and *Nlrp12*$^{-/-}$ mice and gated on CD45^{+}I-A^{b+} cells with differential expression of F4/80, CD11b, CD11c and CD103 by flow cytometry. In accordance with our findings that SPF *Nlrp12*$^{-/-}$ mice have increased colonic basal inflammation, we observed a significantly increased population of CD11c^{+}CD11b^{lo} (**designated R3 in Fig. 2.10e**) that is consistent with intestinal DCs. The cells in the R1 (CD11c^{lo}CD11b^{+}) and R2 (CD11c^{+}CD11b^{+}) populations were modestly elevated in *Nlrp12*$^{-/-}$ mice. These R1-R3 fractions were further stained for F4/80 and CD103 to determine if *NLRP12*-deficiency altered the cellular composition within R1-R3. In both wild type and *Nlrp12*$^{-/-}$ mice, the R1 and R2 populations were found to be primarily macrophages, and R3 were DCs (**Fig. 2.10e**). The composite data of multiple animals showed that CD11b^{lo}CD11c^{+}F4/80^{-}CD103^{+} DCs were significantly increased in the

lamina propria of *Nlrp12*$^{-/-}$ mice. The cLP CD11b^{+}CD11c^{lo}F4/80^{+}CD103^{-} and CD11b^{+}CD11c^{+}F4/80^{+}CD103^{-} populations, which were characterized as macrophages, were also increased in *Nlrp12*$^{-/-}$ mice, but this difference was not significant (**Fig. 2.10f**). These results suggest that *Nlrp12* deficiency increased the number of CD11b^{lo}CD11c^{+}F4/80^{-}CD103^{+} colonic DCs.

To maintain colon homeostasis, macrophages and DCs in the cLP acquire anti-inflammatory phenotypes (Rivollier, He et al. 2012) and become anergic to bacterial stimulation (Denning, Wang et al. 2007). To test if NLRP12 plays a role in maintaining colonic macrophage and DC quiescence, we isolated cLP macrophages and DCs from naïve WT and *Nlrp12*$^{-/-}$ mice and exposed these cells to cecal contents from WT animals to mimic the cell-commensal bacterial interactions *in vivo*. Consistent with the concept that cLP do not readily respond to bacterial stimulation (Denning, Wang et al. 2007), cecal content exposure did not increase inflammatory cytokine gene expression in WT macrophage and DC populations with the exception of a slight level of *Il23p19* expressed by WT DCs (**Fig. 2.10g**). By contrast, cecal content significantly increased *Il6, Tnf, Il12p40* and *Il23p19* expression in *Nlrp12*$^{-/-}$ CD11b^{+}CD11c^{+} macrophages and CD11b^{lo}CD11c^{+} DCs compared to WT controls (**Fig. 2.10g**). Of the measured inflammatory cytokines, only *Tnf* was significantly elevated in *Nlrp12*$^{-/-}$ CD11b^{+}CD11c^{lo} macrophages after exposure to cecal contents. These results suggest that NLRP12

maintains colon homeostasis by suppressing proinflammatory cytokine expression in colonic macrophages and DCs in the presence of cecal material.

Excessive TNF and IL6 production causes microbial dysbiosis in *Nlrp12*$^{-/-}$ mice

The findings in **Fig. 2.8** indicate that the *Nlrp12*$^{-/-}$ genetic deficiency and *Nlrp12*$^{-/-}$-derived microbiome result in elevate immune activation and inflammation. We next directly tested if increased inflammatory responses in turn could drive microbial dysbiosis. Anti-TNF antibody is a common treatment for IBD patients (Peyrin-Biroulet 2010), while anti-IL6R antibody has been discussed as a new therapeutic strategy for colitis (Jones, Scheller et al. 2011, Tanaka, Narazaki et al. 2011). We targeted the inflammatory cytokines TNF and IL6 *in vivo* by injecting mice with anti-TNF and anti-IL6 receptor (IL6R) antibodies (Ab) prior to and during DSS exposure (**Fig. 2.11a**). Blocking TNF and IL6 signaling ameliorated DSS-induced colitis in *Nlrp12*$^{-/-}$ mice indicated by significantly improved weight gain, survival and clinical scores (**Fig. 2.11, b-d**), while the impact was less pronounced in WT controls.

To determine if Ab treatment reversed dysbiosis in *Nlrp12*$^{-/-}$ mice, we performed microbiome analysis before and after Ab treatment. Interestingly, after 4 weeks of anti-TNF and anti-IL6R treatment, antibody-treated *Nlrp12*$^{-/-}$ mice displayed significantly reduced microbiome compositional differences compared to WT mice, with increased intestinal bacterial diversity (**Fig. 2.11, e-g**) and elevated *Bacteroidales* and *Clostridiales*

taxa (**Fig. 2.11h**). This was in contrast to control PBS-treated *Nlrp12*$^{-/-}$ mice, which maintained significantly reduced bacterial diversity, *Bacteroidales* and *Clostridiales* compared to WT mice. These results indicate that blocking excessive levels of inflammatory cytokines recovered the altered microbiome and reduced colitis in *Nlrp12*$^{-/-}$ mice. These combined findings reveal that the absence of NLRP12 promotes a circular feedback loop of exaggerated immune signaling leading to inflammatory cytokine production that in turn drives dysbiosis, resulting in fulminate colitis in *Nlrp12*$^{-/-}$ mice (**Fig. 2.12a**). In addition, reconstitution with *Lachnospiraceae* strains or treatment with anti-IL6R and anti-TNF reverted disease course and dysbiosis.

2.3 DISCUSSION

We and others have previously established a protective role for NLRP12 in intestinal inflammation by suppressing canonical and noncanonical NF-KB (Zaki, Vogel et al. 2011, Allen, Wilson et al. 2012). In this study, we identified an additional critical role for NLRP12 during this process by regulating gut microbial communities. Published IBD-profiling studies using different microarrays and sequencing tools reveal that *NLRP12* expression is negatively correlated with active colitis. In addition, an imbalance in the intestinal microbiota, or dysbiosis, has been linked to IBD pathogenesis (Gevers, Kugathasan et al. 2014). We reveal a link between these two clinical observations by

providing direct evidence that NLRP12 promotes microbial symbiosis, which results in reduced colitis susceptibility.

Unlike conventionally (CV)-raised *Nlrp12*$^{-/-}$ mice, which are more susceptible to colitis compared to similarly raised WT animals, *Nlrp12*$^{-/-}$ mice raised under germ-free conditions were indistinguishable from GF-WT mice during experimental colitis. This indicates interactions between the host and commensal bacteria are required for the severe disease susceptibility in *Nlrp12*$^{-/-}$ mice. Intestinal microbial diversity and human disease have a complex reciprocal cause and effect relationship. A reduction of gut microbiome richness is a biomarker for human metabolic and inflammatory disorders (Le Chatelier, Nielsen et al. 2013), including IBD (Ridaura, Faith et al. 2013). Loss of commensal diversity due to genetic alterations (Kawamoto, Maruya et al. 2014) or an unhealthy diet (Sonnenburg, Smits et al. 2016) correlates with exacerbated colitis. Our results indicate that NLRP12 acts a central component of this relationship by curtailing excessive inflammatory cytokine production to limit intestinal inflammation and maintain commensal diversity and protective microbiota. Neutralization of TNF is a current IBD therapy, and targeting IL6R is being assessed as a similar therapeutic approach. Our findings indicate that in addition to suppressing inflammatory signaling, targeting these cytokines may also alleviate colitis by reversing dysbiosis. Previous studies indicate that TNF and IL6 promote the production of anti-microbial peptides (Choi, McAleer et al.

2013), providing a mechanistic link between inflammatory cytokines and skewing of intestinal microbe populations.

Many protective intestinal bacterial groups are necessary for maintaining gut homeostasis. Similar to the microbiota found in Crohn's patients who have not undergone treatment, we consistently observed a decrease in *Bacteroidales and Clostridiales* (in particular *Lachnospiraceae*) strains in *Nlrp12*$^{-/-}$ mice, which correlated with a greater severity of colitis. Previous reports indicate that *Nod2*- or *Nlrp6*-deficiency results in a colitogenic microbiota that can be transferred to WT animals to exacerbate colitis (Elinav, Strowig et al. 2011, Couturier-Maillard, Secher et al. 2013, Jiang, Wang et al. 2013, Ramanan, Tang et al. 2014). In contrast, this is the first observation where dysbiosis and colitis severity caused by loss of an NLR can be reversed by transferring the microbiota from WT animals, further supporting our conclusion that NLRP12 plays a predominate role in maintaining the presence of protective bacterial groups and limiting colitogenic strains. In line with this, *Nlrp12*$^{-/-}$ mice cohoused with WT mice exhibited elevated intestinal *Clostridiales* and *Lachnospiraceae,* decreased *Erysipelotrichaceae* and reduced DSS-induced colitis. We further explored the therapeutic potential of administering *Lachnospiraceae* isolates to *Nlrp12*$^{-/-}$ mice, which significantly attenuated colitis in these highly susceptible animals. Interestingly, administration of *Lachnospiraceae* had little effect on DSS-induced colitis in wild type animals likely due our finding that these animals already harbor *Lachnospiraceae* strains. This hypothesis

is in line with a recent report demonstrating that effective engraftment and long-term persistence of introduced commensal strains require a niche opportunity that is not already fulfilled by phylogenic or functionally similar groups within the microbiota (Maldonado-Gomez, Martinez et al. 2016). Regardless, accompanied by the human gene profile outcome where mucosal *NLRP12* expression is reduced in active colitis compared to controls or inactive colitis, these results suggest that the same commensal mixtures may be therapeutic when applied to colitis subjects with reduced *NLRP12* expression.

Although studies indicate that *Lachnospiraceae* are decreased in IBD patients (Lepage, Hasler et al. 2011, Gevers, Kugathasan et al. 2014, Haberman, Tickle et al. 2014) and *Clostridium difficile*-associated colitis (Schubert, Rogers et al. 2014), little is known about how these protective strains impact the host immune system. Strikingly, *Lachnospiraceae* are more enriched in the mucosal folds compared to the central lumen (Nava, Friedrichsen et al. 2011). The spatial location of *Lachnospiraceae* favors their interaction with lamina propria residual immune cells, which suggests *Lachnospiraceae* may function as an immune regulator and physical barrier to prevent enteric pathogen adhesion/colonization. *Lachnospiraceae* are also major producers of the short chain fatty acid (SCFA) propionate in the human gut (Reichardt, Duncan et al. 2014). SCFAs act as histone deacetylase (HDAC) inhibitors to promote peripheral regulatory T cell generation (Arpaia, Campbell et al. 2013, Smith, Howitt et al. 2013). Loss of

Lachnospiraceae species in the *Nlrp12*$^{-/-}$ mice may result in reduced SCFA production, which could contribute to the elevated inflammation in the *Nlrp12*$^{-/-}$ mice. Moreover, we showed there is a negative correlation between intestinal *Lachnospiraceae* and *Erysipelotrichaceae. Erysipelotrichaceae* have been recently linked to elevated TNF level and chronic intestinal inflammation in SIV-infected animals and HIV-infected patients received antiretroviral therapy (Dinh, Volpe et al. 2015, Handley, Desai et al. 2016), which suggest these organisms appear to be highly inflammatory. In agreement with these findings, we showed here that *Erysipelotrichaceae*-enriched microbiota from *Nlrp12*$^{-/-}$ mice induced more NF-KB and STAT3 activation. *Lachnospiraceae* may provide a protective function during colon homeostasis and inflammation in part by suppressing over-growth of intestinal *Erysipelotrichaceae.*

As NLRP12 is expressed in both hematopoietic cells and nonhematopoietic cells, we produced bone marrow chimeras to identify the source of cells that impact the microbiome. Our results indicate that a bone marrow-derived source of NLRP12 affects the gut microbiota. Because NLRP12 is primarily expressed by myeloid cells, we focused on gut DC and macrophages and found that NLRP12 limits the number of intestinal DCs and restricts inflammatory response to commensal bacteria stimulation primarily in CD11c^{+}CD11b^{lo} DCs and CD11c^{+}CD11b^{+} macrophages. These results provide a more mechanistic understanding of how NLRP12 regulates colon macrophages and DCs response to the gut microbiota.

In order to address whether the altered microbiota in *Nlrp12*$^{-/-}$ mice is the cause or the effect of deregulated NF-KB, we conducted reciprocal fecal transplantation experiments to test if the altered microbiota is sufficient to induce disease when NLRP12 is present, or whether a healthy microbiota can reduce colitis in *Nlrp12*$^{-/-}$ mice despite their aberrant NF-KB activation. Our results suggest that the altered microbiota from *Nlrp12*$^{-/-}$ mice induces increased NF-KB activation compared to normal WT microbiota. However, when given to WT recipients, the altered *Nlrp12*$^{-/-}$-derived microbiota is insufficient to produce the severe colitis observed in *Nlrp12*$^{-/-}$ mice. This finding provides additional support for an intrinsic protective role for NLRP12 in suppressing colon inflammation. In addition, transplanting normal microbiota can also attenuate colitis in *Nlrp12*$^{-/-}$ mice, suggesting the composition of the microbiota can also limit inflammation, which illustrates the potential for targeting the microbiota when treating inflammatory diseases in patients with intrinsic genetic defects. While both the cohousing and GF reciprocal fecal transplantation studies suggest the interaction between aberrant NF-KB activation and dysbiotic microbiota in *Nlrp12*$^{-/-}$ animals does not proceed in a one-way linear trajectory, but instead in a vicious feed-forward cycle in which increased inflammation driven by NLRP12 mutation selectively produces a proinflammatory microbiota that further escalates inflammation.

2.4 MATERIALS AND METHODS

Mice

All animal procedures were approved by the University of North Carolina Chapel Hill (UNC) Institutional Animal Care and Use Committee (IACUC) according to US National Institutes of Health Guide for the Care and Use of Laboratory Animals. Animal numbers were empirically determined to optimize numbers necessary for statistical significance based on our previous reports utilizing these disease models (minimum of 4–7 animals/group). Animals were excluded if exhibiting signs of disease not associated with the conditions of the colitis (e.g., fight wounds and malocclusion).

Wild type C57BL/6 mice were obtained from Jackson laboratory and house-raised at UNC for at least 9 generations. *Nlrp12*$^{-/-}$ and *Asc*$^{-/-}$ mice are on C57BL/6 background after at least 9 generations backcross. Conventionally raised mice were bred and housed in specific-pathogen-free (SPF) conditions, and germ-free (GF) animals were generated and housed in the National Gnotobiotic Rodent Resource Center of North Carolina at Chapel Hill or in the Center for Gastrointestinal Biology and Disease, Gnotobiotic Core at North Carolina State University. For cohousing experiments, 4-week old mice originating from the same breeders were divided for either single-housed (SiHo) or cohoused (CoHo) with age- and sex-matched mice for 6 weeks. CoHo mice were compared to their SiHo littermates as controls. For conventionalization study, GF animals were transferred into SPF condition and housed for 4 weeks. Conventionalized

(exGF) animals were compared to the mice kept in GF condition as control. For reciprocal fecal transplantation study, GF WT or *Nlrp12*$^{-/-}$ mice were orally gavaged with feces suspension derived from SPF WT or *Nlrp12*$^{-/-}$ mice followed the previously described protocol (Ridaura, Faith et al. 2013). For adoptive bone marrow transplantation study, WT and *Nlrp12*$^{-/-}$ chimeric mice were generated as previously described(Allen, Wilson et al. 2012). No antibiotics were used during the bone marrow reconstitution phase and fecal DNA was collected at the 10th week after the transplantation.

Experimental Colitis

Experimental colitis was initiated by treating mice with 1.5%-3% dextran sulfate sodium (DSS) (36,000-50,000 M.W, MP Biomedicals) in autoclaved drinking water for 5 days. DSS was then replaced by normal autoclaved water for 6-7 days. Body weight was monitored daily, and disease-associated index (DAI) was determined by an investigator blinded to experimental conditions on day 8 post-DSS treatment according to the following parameters: 1) Weight loss (0 points=0% weight loss from baseline, 1 point=1-5% weight loss, 2 points=5-10% weight loss, 3 points=10-20% weight loss, 4 points=more than 20% weight loss); 2) Bleeding (0 points=negative, 2 points=positive hemoccult test, 4 points=gross bleeding), and 3) Stool consistency (0 points=normal, 2 points=semiformed stool, 4 points=liquid that adhere to the anus). The sum of these 3

parameters results in the total DAI ranging from 0 (healthy) to 12 (maximal activity of colitis).

Histopathology

Colons were Swiss-rolled, fixed in 10% neutral-buffered formalin and paraffin embedded and processed for histological analysis. Five-micron-thick colon sections were stained with hematoxylin and eosin (H&E) and semi-quantitatively scored for histopathology by a board-certified veterinary pathologist in a blind manner. Histology score represented the sum of each histological alterations outlined below. This system assessed inflammation, epithelial defect, area of inflammation, area of epithelial defect, crypt atrophy, and dysplasia/neoplasia, by giving each parameter a separate score (0-4) for severity and extent as previously described (Allen, Wilson et al. 2012).

Western Blot

Colons were excised, opened longitudinally and washed with cold PBS. The distal-most-3 cm section of each colon was collected and mechanically homogenized in NE-PER Nuclear and Cytoplasmic Extraction Reagent (Thermo Scientific) containing Complete Protease Inhibitor and PhosphoStop (Roche) per manufacturer's protocol. Cytosolic and nuclear lysates were subjected to SDS-PAGE and western blotting. The following primary antibodies were used for western blot analysis: anti-pIκBα (2859S);

anti-pIKKα (7218S); anti-pp65 (3033S); anti-NIK (4994); anti-pp38 (9216S); anti-p38 (9212S); anti-pERK1/2 (4370S); anti-pSTAT3 (9131S); and anti-STAT3 (4904S) (Cell Signaling Technology); anti-p52 (SC7386); anti-ERK1 (SC93); anti-ERK2 (SC154); anti-CRAMP (SC166055) and anti-Actin-HRP (SC1615) (Santa Cruz Biotechnology); anti-REG3γ (ab198216) (Abcam); and anti-Histone H3 (07-690) (Millipore). Goat anti-rabbit-HRP (111-035-144) and goat anti-mouse-HRP (115-035-146) (Jackson Laboratories) were used as secondary antibodies. Protein densitometry were quantified by Image J software.

Colon Explant Cultures

Colons were excised, washed several times in cold PBS containing 2x penicillin/streptomycin (Sigma Aldrich) and cultured for 15 hours in RPMI media (Gibco) containing 2x penicillin/streptomycin at 37°C. Supernatants were collected, centrifuged to clear debris and assessed for cytokines by Luminex Bio-Plex System per manufacturer's instructions.

Fecal DNA Extraction

Fecal samples were collected from live mice, snap-frozen and stored at -80°C. DNA was isolated by incubating fecal material at 65°C for 30 min in Lysing Matrix E tubes (MP Biomedicals) containing 200 mM NaCl, 100 mM Tris, 20 mM EDTA (pH 8.0),

SDS and proteinase K (Qiagen). Phenol:Choloroform:Isoamyl alcohol (Invitrogen) was added, and the samples were homogenized at 4°C for 3 min using a bead beater homogenizer. The samples were centrifuged at 8000 rpms for 3 min at 4°C, and the supernatant was incubated with Phenol:Chloroform (Invitrogen) for 10 min at room temperature. The samples were centrifuged at 13,000 rpms for 5 min at 4°C, and the aqueous phase was incubated with isopropanol and 3M sodium acetate, pH 5.2, at -20°C for 15 hrs to precipitate DNA. The precipitated DNA was collected by centrifugation at 13000 rpm at 4°C for 20 min, washed twice with 100% cold ethanol and resuspended in TE buffer. The DNA was further purified using a DNeasy Blood and Tissue Kit (Qiagen) according to the manufactures protocol.

16S rRNA Gene Sequencing and Data Analysis

Fecal DNA samples were amplified by PCR using barcoded primer pairs targeting the V1-V2 region of the 16S gene. PCR amplicons were sequenced at the V1-V2 region using Roche 454 for the vivarium #1 study, and the same V1-V2 region was sequenced using a Mi-Seq Illumina sequencer for all other described experiments. The resulting bacterial sequence fragments were clustered into Operational Taxonomic Units (OTUs) and aligned to microbial genes with 97% sequence similarity from Greengenes Database using UCLUST method in QIIME. Bacterial taxa summarization and rarefaction analyses of microbial diversity or compositional differences (dissimilarity

value indicated by Unweighted UniFrac Distance) were calculated in QIIME (1.8.0) as previously described(Kuczynski, Stombaugh et al. 2012) using QIIME scripts (including pick_open_reference_otus.py, summarize_taxa.py, alpha_rarefaction.py, jackknifed_beta_diversity.py and make_distance_boxplots.py). PCoA plots indicating compositional difference were generated by QIIME script, make_2d_plots.py. Each point represents one mouse, and the ellipses represent the interquartile range (IQR) during the rarefaction analyses(Schmidt, Koberl et al. 2014) (see http://www.wernerlab.org/teaching/qiime/overview for scripts details). All 16S rRNA microbiome sequences have been deposited at the open-source microbiome deposition site: QIITA (https://qiita.ucsd.edu) with Study IDs 10427, 10429 and 10428.

Mouse colonic lamina propria macrophage and dendritic cells isolation and stimulation

Mouse colons were opened longitudinally and washed with cold PBS to remove the fecal contents. Pooled colons from 2 mice were further cut into 1.5 cm pieces and washed twice with 30 ml of HBSS containing 10% FBS and 2mM EDTA on an orbital shaker at 250 rpms for 30 min at 37°C. After washing, the colons were finely minced and digested with 20 ml of HBSS containing 10% FBS, 1.5 mg/ml Type VIII Collagenase (C2139; Sigma-Aldrich) and 40 μg/ml DNase I (4527; Sigma-Aldrich) at 200 rpms for 20 min at 37°C. After the digestion, the digested colonic lamina propria (cLP) cells were filtered through a 100 μm strainer, centrifuged at 1,500 rpm for 5 min at

4 °C and resuspended in 2 ml MACS buffer for flow cytometric analysis or fluorescence-activated cell sorting (FACS) (Geem, Medina-Contreras et al. 2012).

For flow cytometric analysis, cLP cells were incubated with mouse Fcγ II/III receptor blocker (553141; BD Pharmingen) for 15 min on ice and were then stained with the following labeled antibodies for 30 min on ice: Brilliant Violet 421-conjugated anti-CD45 (103133; Biolegend), PE-conjugated anti-IA^b (553552; BD Pharmingen), APC-Cy7-conjugated anti-CD11c (117324; Biolegend), PE-Cy7-conjugated anti-CD11b (101216; Biolegend), APC-conjugated anti-CD103 (17-1031-80; eBioscience), and Alexa Fluor 488-conjugated anti-F4/80 (123120; Biolegend). Samples were washed twice in MACS buffer and were analyzed on a BD LSR II flow cytometry at the UNC Flow Cytometry Core Facility. Dead cells and doublets were excluded from the cLP mononuclear based on appropriate forward and side scatter plots. Antigen-presenting cells (APC) were defined as $CD45^+I\text{-}A^{b+}$. Macrophage and dendritic cell (DC) populations were firstly categorized by the expression of CD11b and CD11c and then further characterized by CD103 and F4/80 expression as previously described(Geem, Medina-Contreras et al. 2012).

For cLP macrophage and DC FACS separation and *ex vivo* stimulation, $CD11b^+$ and $CD11c^+$ microbeads (Miltenyi Biotec) were used to enrich $CD11b^+$ or $CD11c^+$ positive cells. The enriched cells were stained with labeled antibodies aforementioned. Stained cells were sorted to purify the indicated population at the UNC Flow Cytometry

Core Facility. Sorted macrophages and DCs were seeded in a 96-well plates (0.5~1X10^5 cells per well) with 200 µl RPMI medium containing 10% FBS. For cecal content stimulation, cecal contents were generated from WT mice as described elsewhere (Seo, Kamada et al. 2015) and were added to the cell culture medium at a 1:200 dilution for 3 hours. Total RNA was then isolated by TRIzol (Thermo Fisher Scientific) for qRT-PCR analysis.

Design of *Lachnospiraceae* specific primers

Lachnospiraceae strains were identified utilizing an adapted version of the plate wash PCR technique (Stevenson, Eichorst et al. 2004). This allowed for rapid screening by PCR using phylotype specific primers of the 16S rRNA gene to screen selective media plates to identify conditions that enrich for specific bacteria. To generate *Lachnospiraceae* specific primers the near full length 16S rRNA gene sequence from 34 bacterial strains were used to generate CLUSTALW multiple-sequence alignments. The 16S rRNA gene sequences used were the following: 9 of the most represented bacterial sequences from the murine large intestine found in Berry, et al*. (Berry, Schwab et al. 2012)* (*Akkermansia muciniphila*, *Alistipes finegoldii*, *Bacteroides acidifaciens*, *Barnesiella intestinihominis*, C*lostridium propionicum*, *Enterococcus faecalis*, *Eubacterium siraeum*, *Oscillibacter valericigenes*, *Ruminococcus flavefaciens*), 4 *Firmicutes* (*Clostridium difficile*, *Enterococcus faecalis, Lactobacillus murinus*, and

Staphylococcus xylosus), 6 *Lachnospiraceae* (*Clostridium aldenense*, *Clostridium bolteae*, *Clostridium citroniae*, *Clostridium indolis*, *Clostridium propionicum*, *Clostridium xylosus*), 3 *Lachnospiraceae* strains isolated in Reeves et al. (Reeves, Koenigsknecht et al. 2012)(D4, G11, and E7), and 12 of the most represented *Lachnospiraceae*-classified OTUs from Reeves, et al. (Reeves, Koenigsknecht et al. 2012). Areas of homology between *Lachnospiraceae* sequences that were not homologous to other *Firmicutes* and *Bacteroidetes* were used to create 4 *Lachnospiraceae* specific 16S rRNA forward gene primers: Lachno419F (5' –GAC GCC GCG TGA GTG AAG AAG TAT- 3'), Lachno428F (5' –GTA AAG CTC TAT CAG CAG GGA AGA- 3'), Lachno481F (5' –GAC GGT ACC TGA CTA AGA AGC CC- 3'), and Lachno462F (5' –GTC CAC AGG ACT TTG GAC GG- 3'). The primer LachF (5' -CC GCA TAA GCG CAC AGC- 3') from Reeves, et al. (Reeves, Koenigsknecht et al. 2012) was also utilized in this study. These forward primers were used with the 16S rRNA reverse gene primer 1492R (5' -GGT TAC CTT GTT ACG ACT T- 3') for PCR amplification. One *Lachnospiraceae* specific reverse primer was also created: Lachno1261R (5' -TCG CTT CCC TTT GTT TAC GC- 3'), which was used with the 16S rRNA forward gene primer 8F (5' -AGA GTT TGA TCC TGG CTC AG- 3') for PCR amplification. The specificity and coverage of the *Lachnospiraceae* primers was obtained using the Ribosomal Database Project Probe Match tool (https://rdp.cme.msu.edu/probematch/search.jsp accessed on May 19, 2012). Additionally, primers were tested with Gram-negative bacteria *Bacteroides*

fragilis Escherichia coli; Gram-positive bacteria *Lactobacillus murinus*, *Staphylococcus aureus*, *Staphylococcus pneumonia*; *Clostridium difficile* strain VPI 10463 to ensure specificity to *Lachnospiraceae*.

PCR was performed with 1 µl of template DNA (approximately 100 ng), 20 pmol of each primer, 8mM dNTP master mix (Promega-U1511), 1 unit GoTaq DNA polymerase (Promega- M3005), PCR buffer (Promega- M3005) and water in a total of 25 µl per reaction. PCR reaction was performed under the following cycling conditions: 95°C for 2 min, 30 cycles of 95°C for 30 sec annealing at 57°C for 45 sec, and extension at 72°C for 90 sec, 72°C for 10 min.

Bacterial isolation and selective growth conditions

Three of the *Lachnospiraceae* isolates (*Lachnospiraceae* D4, G11, and E7) used in this study were reported previously(Reeves, Koenigsknecht et al. 2012). The remaining 20 strains were isolated from murine cecal content, cecal tissue, and stool. Mouse stool was collected into a sterile tube directly from a restrained mouse and immediately transferred into an anaerobic chamber (Coy Industries, Grass Lake, MI). Ceca from C57BL/6 mice were collected in a sterile manner and immediately transferred into an anaerobic chamber. A sterile scalpel was used to open the cecum and separate cecal content and cecal tissue. Cecal content was added to a sterile tube and diluted into anaerobic 1X phosphate-buffered saline (PBS). Using a sterile syringe 2 ml of PBS was

gently injected into the cecum to remove any additional cecal content. The cecal tissue was then added to 1 ml of anaerobic PBS and placed into a sterile container for tissue homogenization (50 um pore size) using a Medimachine tissue homogenizer (BD Biosciences). The tissue was grinded for 15 seconds and homogenized tissue was used for plating. The cecal content, cecal tissue homogenization, and stool was serial diluted in anaerobic PBS and plated in duplicate onto brain heart infusion agar (BD Biosciences) with 0.01% cysteine (BHI).

A variety of media conditions were used to enrich for *Lachnospiraceae* isolates. Bacterial growth from the first agar plate was collected and genomic bacterial DNA was isolated using an Easy-DNA (Invitrogen) kit. Using the *Lachnospiraceae* specific primers and PCR conditions described above we identified several media conditions that enriched for *Lachnospiraceae* strains. Once a media condition was identified that enriched for Lachnospiraceae strains, single colonies from the duplicate plate were used to inoculate 1 ml of BHI + 5% fetal bovine serum (FBS) into a sterile 96-well plate. These cultures were grown anaerobically for 3 days at 37°C then 1 µl of the liquid culture was used as a template for the PCR reaction described above. The *Lachnospiraceae* specific primers previously mentioned were used to identify potential *Lachnospiraceae* isolates. If any of the primers used yielded a successful PCR reaction, 50 µl of the corresponding culture was plated for single colonies anaerobically on BHI + 5% FBS for one to three days at 37°C. A single colony was used to inoculate a 5 ml BHI

+ 5% FBS culture that grew anaerobically for one to three days at 37°C. This culture was used to create 20% final concentration glycerol stocks of all the isolates that were stored at -80°C.

The following media conditions were used to isolate *Lachnospiraceae* strains in this study: BHI + 5% FBS; BHI + 1 µg/mL aztreonam + 10 µg/mL colistin + 2 µg/mL gentamicin; and BHI + 0.5 µg/mL ampicillin + 2 µg/mL erythromycin + 0.25 µg/mL vancomycin. Single colonies from the duplicate plate were used to inoculate 1 ml of BHI + 5% FBS.

Taxonomic classification of bacterial isolates.

Genomic DNA was isolated using an Easy-DNA (Invitrogen) kit. PCR reaction conditions were described above and PCR product cleanup was performed using ExoSAP-IT (Affymetrix) per the manufactures protocol. Near full-length 16S rRNA amplicons were sequenced at the University of Michigan DNA Sequencing Core using primers 8F (5’ -AGA GTT TGA TCC TGG CTC AG- 3’), 515F (5’ -GTG CCA GCM GCC GCG GTA- 3’), E939R (5’ -CTT GTG CGG GCC CCC GTC AAT TC- 3’), and 1492R (5’ -GGT TAC CTT GTT ACG ACT T- 3’). CLUSTALW multiple-sequence alignments were generated for each isolate and a near-full length 16S rRNA gene consensus sequence was obtained. The consensus sequence was taxonomically classified using the RDP

classifier (https://rdp.cme.msu.edu/classifier/classifier.jsp accessed between 6-29-2012 and 3-7-2013)(Wang, Garrity et al. 2007).

Mouse Colonization with *Lachnospiraceae* Bacteria

Mice were orally gavaged with a mixture containing the 23 *Lachnospiraceae* stains (~1X10^8 bacteria) described above in brain-heart infusion broth (BHI) twice a week for 3 weeks. BHI broth was used as vehicle control. The mice were given DSS 1 week after the final gavage.

***In vivo* anti-IL6R and anti-TNF Treatment**

Mice were given 2mg/kg body weight of anti-IL6R (Tocilizumab, Genentech) and anti-TNF (Infliximab, Janssen Biotech) via intraperitoneal injection twice a week for four weeks prior to DSS exposure and during the 11 day DSS treatment period. Fecal DNA was collected from WT littermates and *Nlrp12*$^{-/-}$ littermates before, and after 4 weeks antibody treatment but prior to DSS initiation.

Metadata Study of Human *NLRP12* profiling and microbiome changes in IBD Patients

Raw data from 8 NCBI GEO human ulcerative colitis studies were renormalized and analyzed by Genespring GX (Agilent Tech). The following studies were used: GSE22619, GSE42911, GSE14580, GSE16879, GSE13367, GSE65114, GSE21231

and GSE57945. In the summary panels, the healthy group includes the samples from healthy participants and normal un-inflamed tissues of the patients, the active group includes the samples from the patients inflamed tissues and the inactive group includes un-inflamed tissue samples of patients in remission due to the treatment (anti-TNF, steroids and others).

For microbiome changes in IBD patients, we downloaded the raw 16S rRNA gene sequencing file published by Dirk Gevers et al. (Gevers, Kugathasan et al. 2014) from the open-source microbiome deposition site: QIITA (https://qiita.ucsd.edu/) under study ID: 1939. This file includes 16S microbiome sequencing results from 28 healthy controls, 63 colonic Crohn's disease patients (cCD), 156 ileal Crohn's disease patients (iCD) and 24 UC patients. Raw sequencing data was reanalyzed as aforementioned. Significantly altered strains were identified by comparing IBD (cCD, iCD and UC) patients against healthy participants.

Statistical Analysis

If not specified in the figure legends, statistical significance between two groups was determined by unpaired, two-tailed Student's *t* test, and significance between more than two groups was determined using one-way analysis of variance (ANOVA), with Fisher's LSD test or two-way ANOVA using Prism software (GraphPad). Statistical significance for survival studies was determined by Log-rank (Mantel Cox) test using

Prism software. One dot or lane represents one mouse. *p<0.05, **p<0.01, ***p<0.001, ****p<0.0001 and n.s. means no significance. Error bar represents mean ± SEM.

2.5 FIGURES

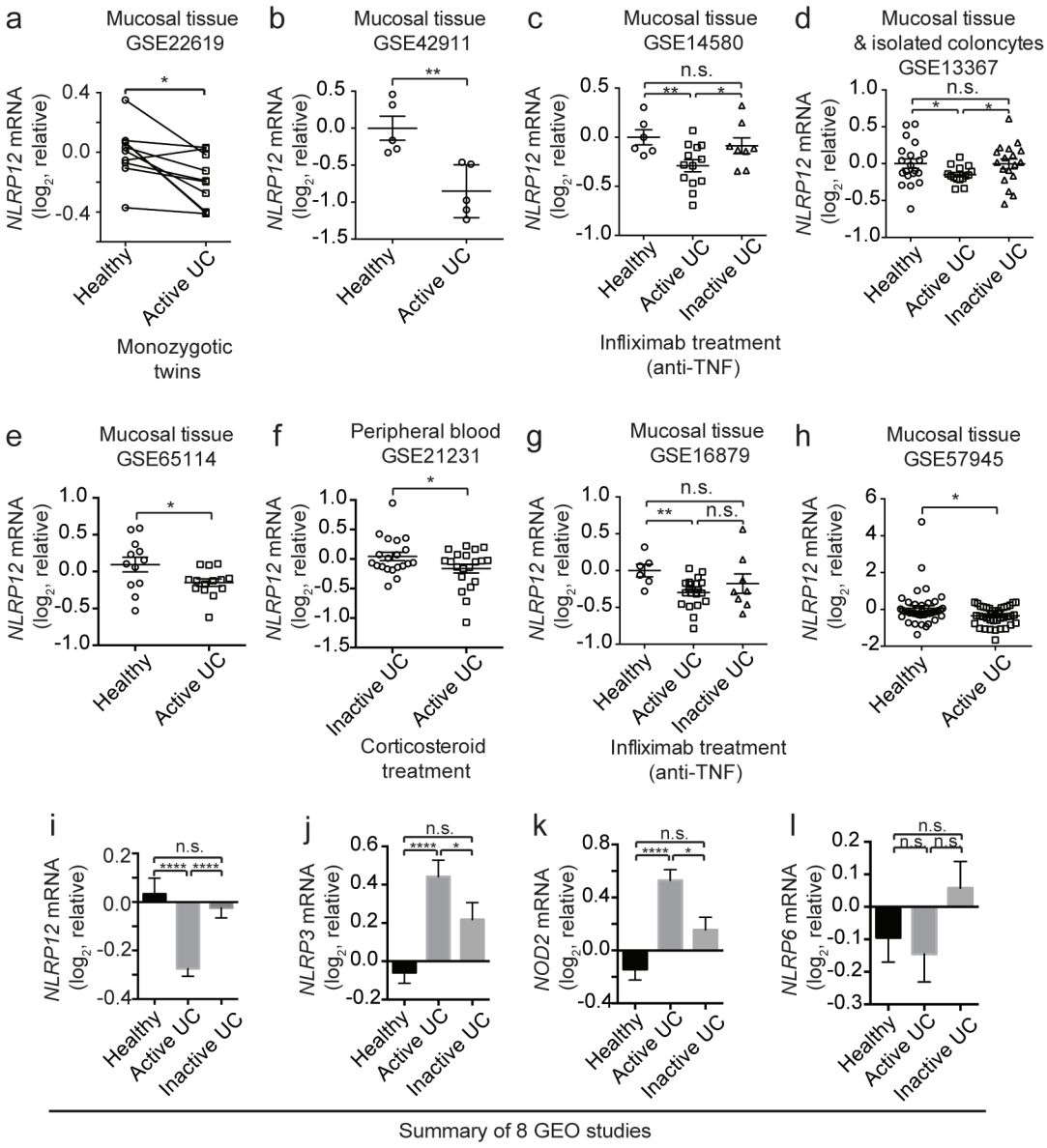

Fig. 2.1. *NLRP12* is down regulated in biopsy samples from active ulcerative colitis (UC) patients. (**a-h**) *NLRP12* gene expression between healthy, active and inactive UC patients from 8 mRNA profiling studies deposited in NCBI GEO database. Disease stages, GEO accession numbers, subject tissues for mRNA purification, and therapeutic treatments including corticosteroid or anti-TNF (infliximab) are listed. For treatment studies (**c, f, g**), inactive UC groups include the samples from patients responsive to the treatment, and active UC groups include the samples from patients not responsive to the treatment or before the treatment. For (**a**) 10 pairs of monozygotic twins, (**b**) n=5/group; (**c**) healthy (n=6), active UC (n=13), inactive UC (n=8); (**d**) healthy

(n=20), active UC (n=15), inactive UC (n=18); (**e**) healthy (n=12), active UC (n=13); (**f**) n=20/group; (**g**) healthy (n=6), active UC (n=20), inactive UC (n=8); (**h**) healthy (n=42), UC (n=40). (**i-l**) Composite gene expression of *NLRP12, NLRP3, NOD2* and *NLRP6* from the 8 GEO databases. Error bars show SEM. *p<0.05, **p<0.01 and n.s. means no significance determined by two-tailed paired (**a**) or unpaired *t* test (**b-l**).

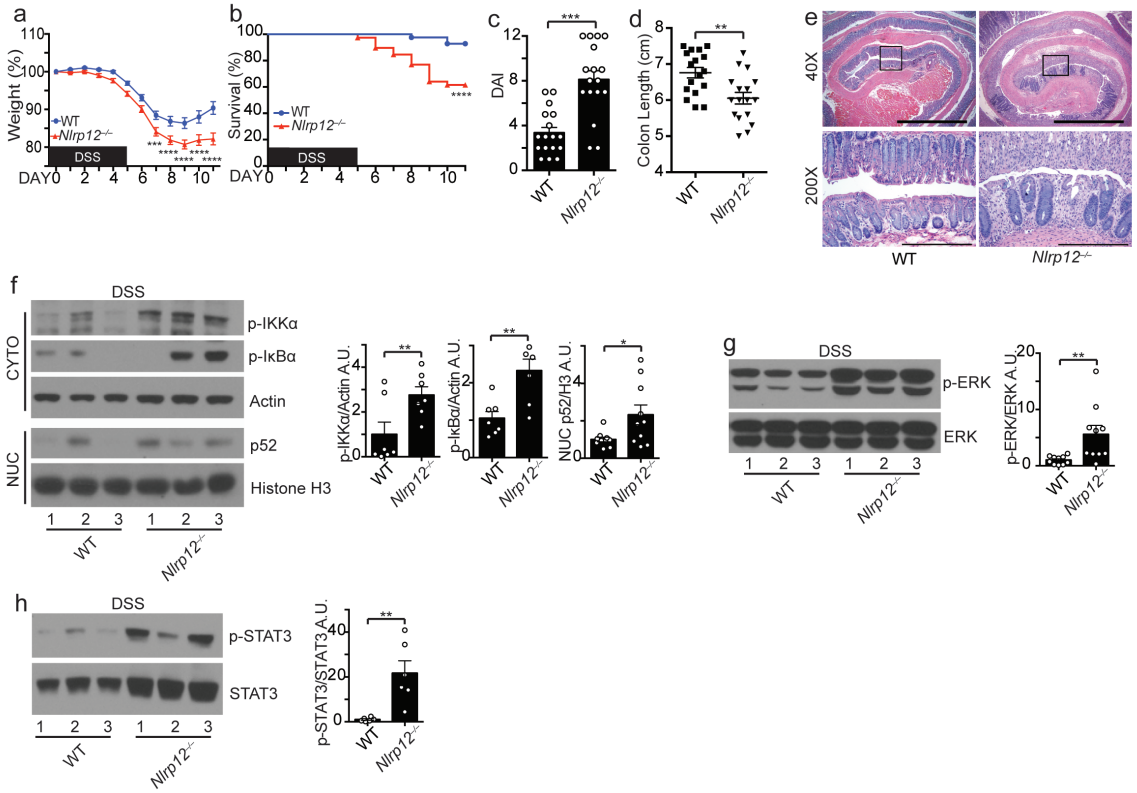

Fig. 2.2. Conventional-raised *Nlrp12*$^{-/-}$ mice are more susceptible to DSS induced colitis. (**a**) Body weight and (**b**) percent survival (WT, n=41; *Nlrp12*$^{-/-}$, n=42), (**c**) DAI and (**d**) colon length (n=17/group) of conventionally-raised mice treated with 3% DSS, compiled from 3 independent experiments. (**e**) Representative images of H&E-stained colons from conventionally-raised mice after DSS-induced colitis. Scale bars represent 1 mm for 40X and 200 μm for 200X. (**f-h**) Representative immunoblots of distal colon proteins and composite densitometry from 2 independent experiments. One dot or one lane represents one mouse. Error bars show SEM. *p<0.05, **p<0.01, ***p<0.001, and n.s. means no significance determined by two-tailed unpaired *t* test.

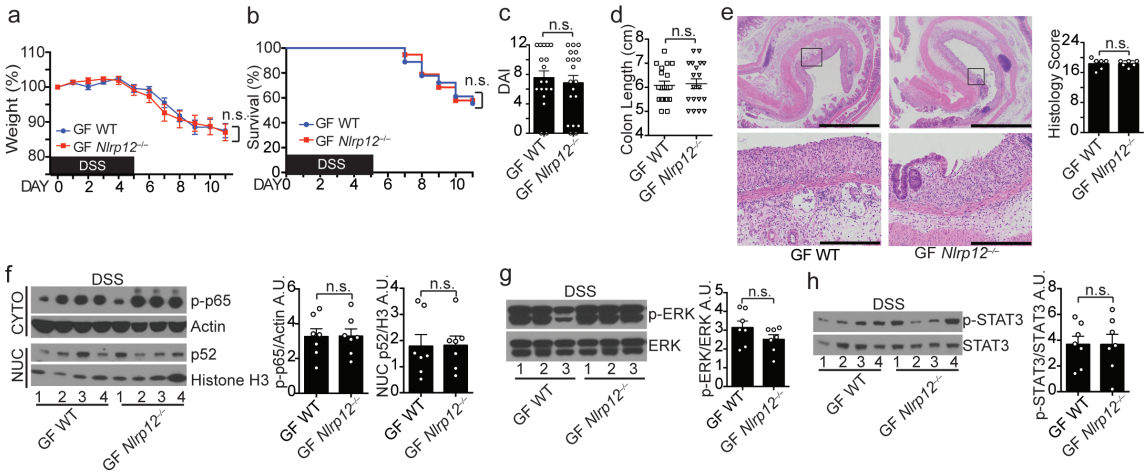

Fig. 2.3. Germ-free WT and *Nlrp12*$^{-/-}$ mice display similar colitis severity. (**a**) Body weight, (**b**) percent survival, (**c**) disease-associated index (DAI) and (**d**) colon length of germ-free (GF) WT (n=18) and *Nlrp12*$^{-/-}$ (n=19) mice given 1.5% DSS. (**e**) Representative images of H&E-stained colons from germ-free mice after DSS-induced colitis. Scale bars represent 1 mm for 40X and 200 μm for 200X. Blinded histopathology scoring of colons (n=6/group). (**f-h**) Western blots of distal colon proteins from DSS-treated GF mice, and densitometry of 2 independent experiments (n=7/group). Error bars show SEM. *p<0.05, **p<0.01, ***p<0.001, and n.s. means no significance determined by two-tailed unpaired *t* test.

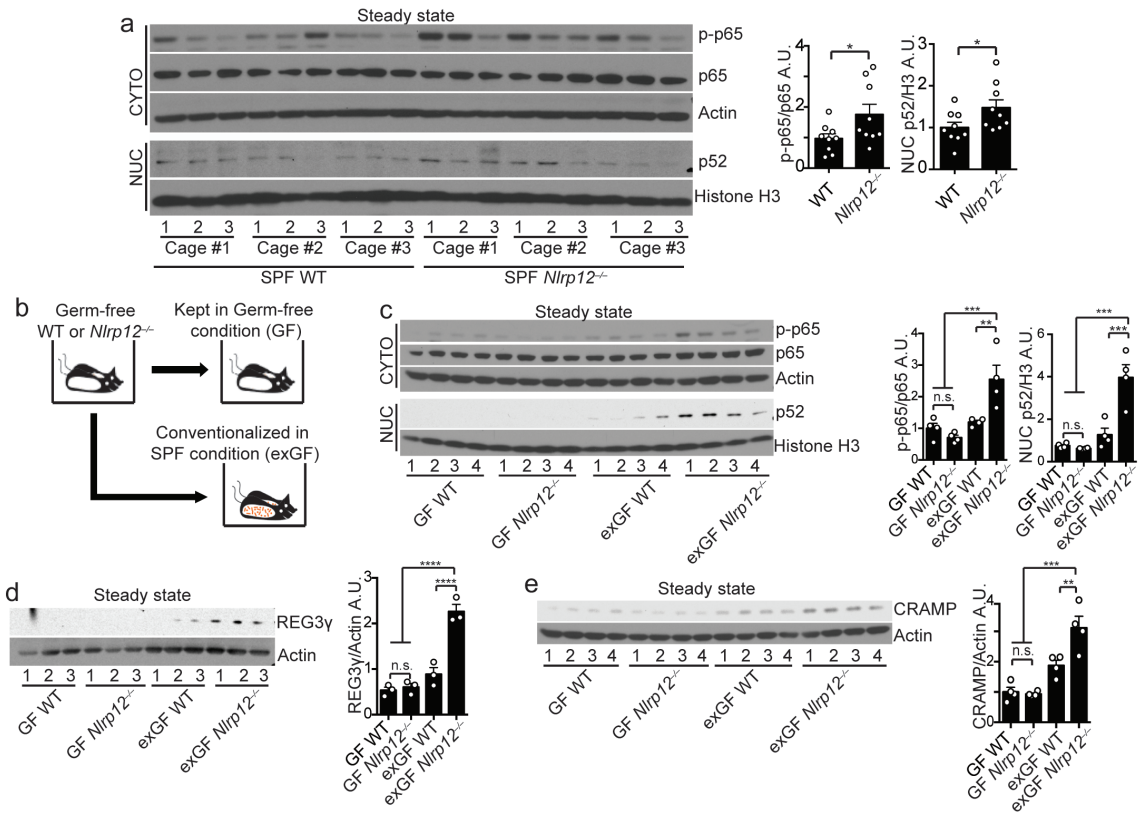

Fig. 2.4. Increased intestinal inflammation in the *Nlrp12*$^{-/-}$ mice contain commensal microbiota. (**a**) Western blots of distal colon proteins from untreated SPF mice, and densitometry (n=9/group). (**b**) Scheme of the comparison between GF and conventionalized (exGF) mice. (**c-e**) Western blots of distal colon proteins from untreated GF and exGF mice, and densitometry (n=3 or 4/group). One dot or one lane represents one mouse. Error bars show SEM. *p<0.05, **p<0.01, ***p<0.001 and ****p<0.0001 and n.s. means no significance by unpaired *t* test.

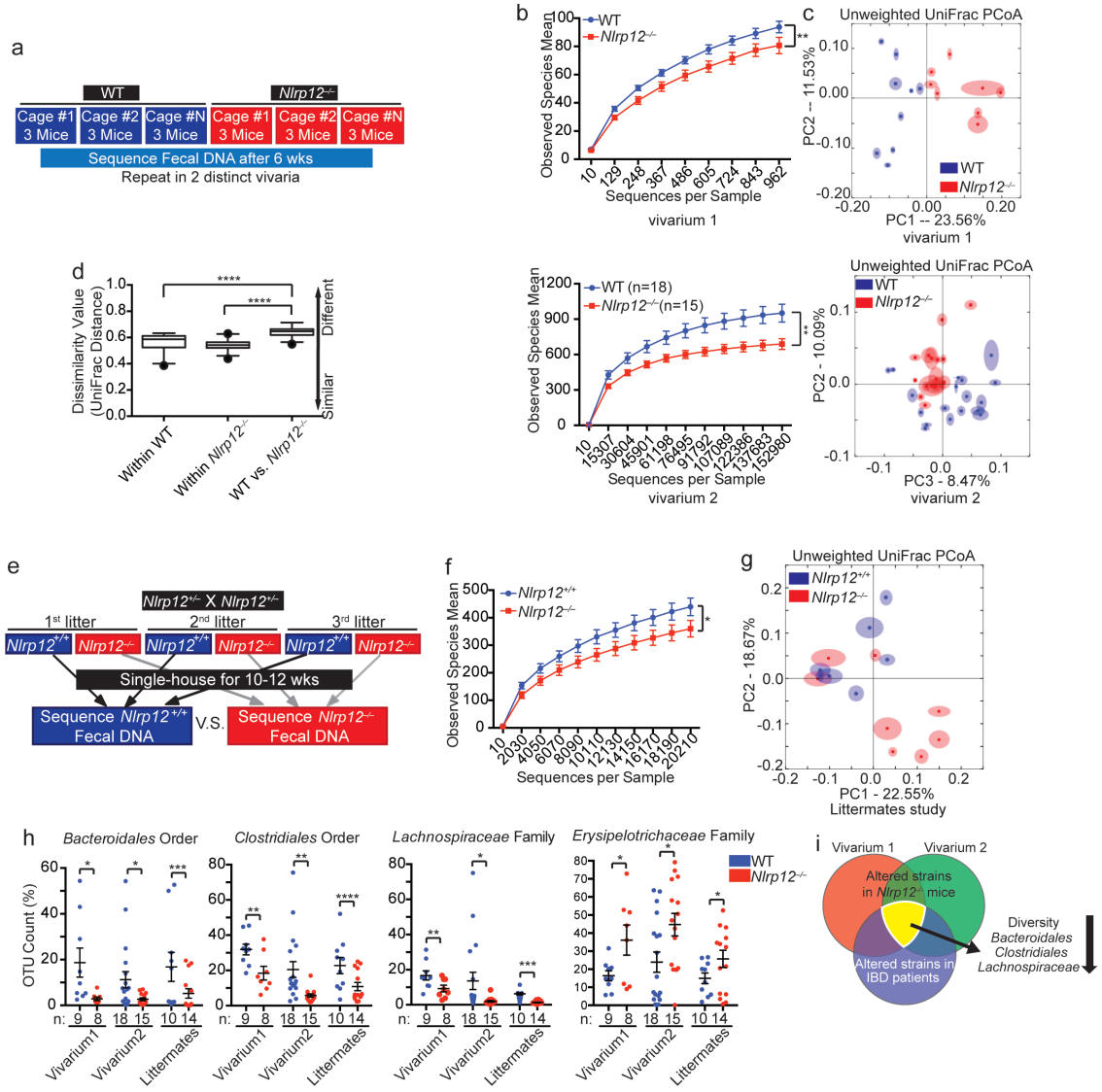

Fig. 2.5. 16s rRNA gene sequencing analysis of WT and *Nlrp12*$^{-/-}$ mice colon microbiome. (**a**) Schematic showing separation of mice into N (N≥3) cages per genotype for fecal 16S rRNA sequencing repeated in two vivaria. (**b**) Bacterial diversity and (**c**) unweighted UniFrac principal coordinate analysis (PCoA) showing microbiota compositional differences between WT and *Nlrp12*$^{-/-}$ mice. Each symbol represents one mouse. For vivarium1, WT (n=9) and *Nlrp12*$^{-/-}$ (n=8); and for vivarium 2, WT (n=18) and *Nlrp12*$^{-/-}$ (n=15). (**d**) Quantification of UniFrac distance from mice study in vivarium 1 (c, upper panel) indicated as dissimilarity value. (**e**) Schematic of experiment comparing *Nlrp12*$^{+/+}$ (n=10) and *Nlrp12*$^{-/-}$ (n=14) littermates. (**f**) Diversity and (**g**) PCoA plots of bacterial composition from *Nlrp12*$^{+/+}$ and *Nlrp12*$^{-/-}$ littermates. (**h**) Consistently altered intestinal bacterial groups in *Nlrp12*$^{-/-}$ vs. WT mice from experiments described in (a) and (e). (**i**) Venn diagram showing overlapped microbiota changes between *Nlrp12*$^{-/-}$ vs.

WT mice and IBD vs. healthy individuals. Error bars denote SEM. *p<0.05, **p<0.01, ***p<0.001 and ****p<0.0001 determined by unpaired *t* test (b, f and h) or ANOSIM test (d).

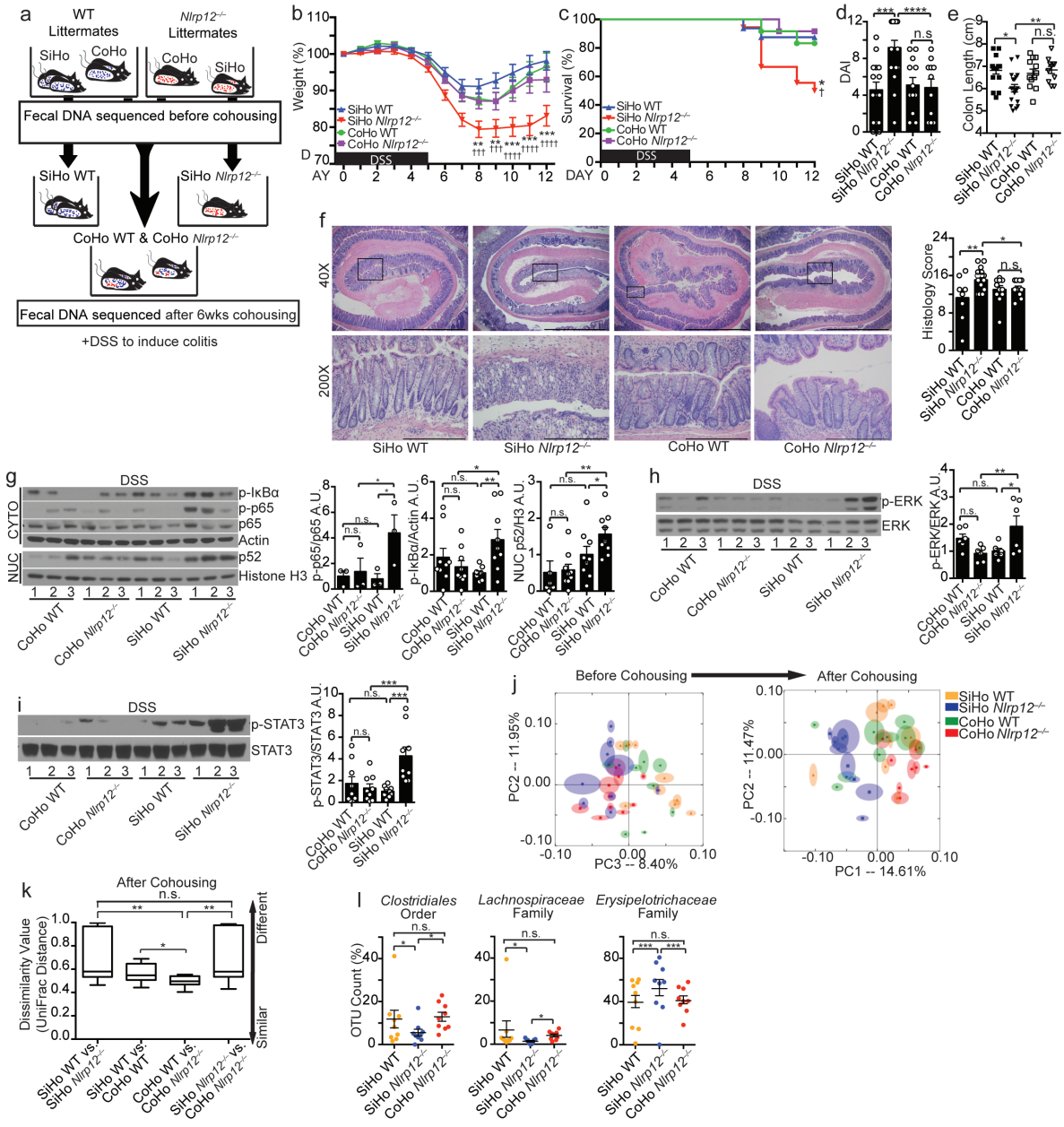

Fig. 2.6. Co-housing with WT animals attenuates exacerbated colitis in *Nlrp12*$^{-/-}$ mice. (**a**) Scheme of comparing DSS-treated cohoused (CoHo) and single-housed (SiHo) littermates of WT or *Nlrp12*$^{-/-}$ mice. (**b**) Body weight and (**c**) percent survival († indicates statistical significance between SiHo WT vs. SiHo *Nlrp12*$^{-/-}$, and * indicates significance between SiHo *Nlrp12*$^{-/-}$ vs. CoHo *Nlrp12*$^{-/-}$), (**d**) DAI and (**e**) colon length of littermate mice treated as in (a). (SiHo WT, n=16; SiHo *Nlrp12*$^{-/-}$, n=18; CoHo WT, n=12; CoHo *Nlrp12*$^{-/-}$, n=12). (**f**) Representative images of H&E-stained colons from DSS-treated cohoused or single-housed WT and *Nlrp12*$^{-/-}$ mice, and histopathology scoring of colons (n=10/group). Scale bars represent 1 mm for 40X and 200 μm for

200X. (**g-i**) Western blots of distal colon proteins from the single- and cohoused mice, and densitometry showing 3 independent experiments. (**j**) PCoA plot showing fecal microbial composition before and after cohousing (n=9/group). (**k**) Quantification of UniFrac distance between mice from (j) after cohousing, indicated as dissimilarity value. (**l**) Significantly altered strains identified by two-way ANOVA test from all sequenced bacteria in SiHo WT, SiHo and CoHo *Nlrp12*$^{-/-}$ mice. One dot or one lane represents one mouse. Error bars show SEM. *p<0.05, **p<0.01, *** p<0.001, **** p<0.0001 and n.s. means no significance determined using unpaired *t* test (b), Log-rank (Mantel Cox) test (c), one-way ANOVA Fisher's LSD test (d-i), ANOISM test (k), and two-way ANOVA (l).

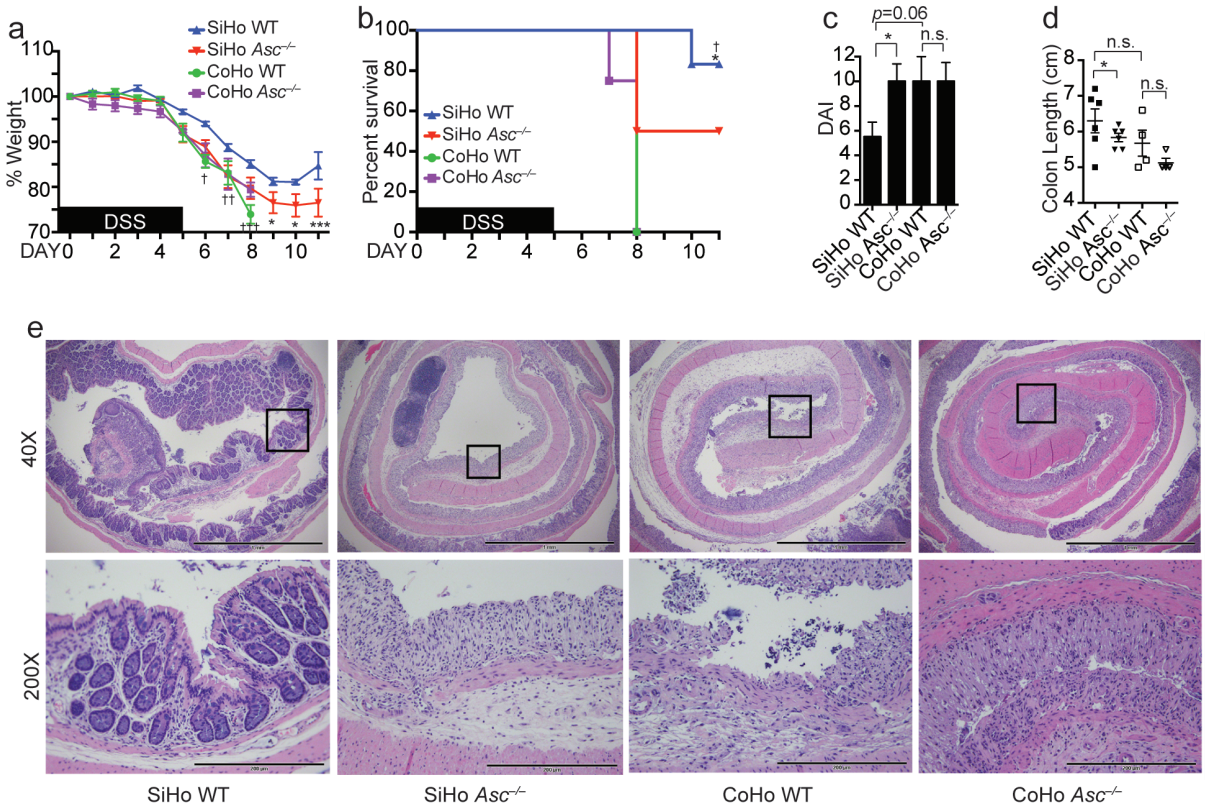

Fig. 2.7. Co-housing with WT animals does not attenuate exacerbated colitis in *Asc*$^{-/-}$ mice. (**a**) Body weight, (**b**) percent survival († indicates statistical significance between SiHo WT vs. SiHo *Asc*$^{-/-}$, and * indicates significance between SiHo WT vs. CoHo WT), (**c**) DAI and (**d**) colon length of DSS-treated cohoused or single-housed WT and *Asc*$^{-/-}$ mice (CoHo WT and CoHo *Asc*$^{-/-}$, n=4; SiHo WT and SiHo *Asc*$^{-/-}$, n=6). (**e**) Representative images of H&E-stained colons of SiHo and Coho WT and *Asc*$^{-/-}$ mice after DSS-induced colitis. Scale bars represent 1 mm for 40X and 200 μm for 200X. Error bars show SEM. *p<0.05, ***p<0.001 and n.s. means no significance, determined by two-tailed unpaired *t* test (a, c, d), and Log-rank (Mantel Cox) test (b).

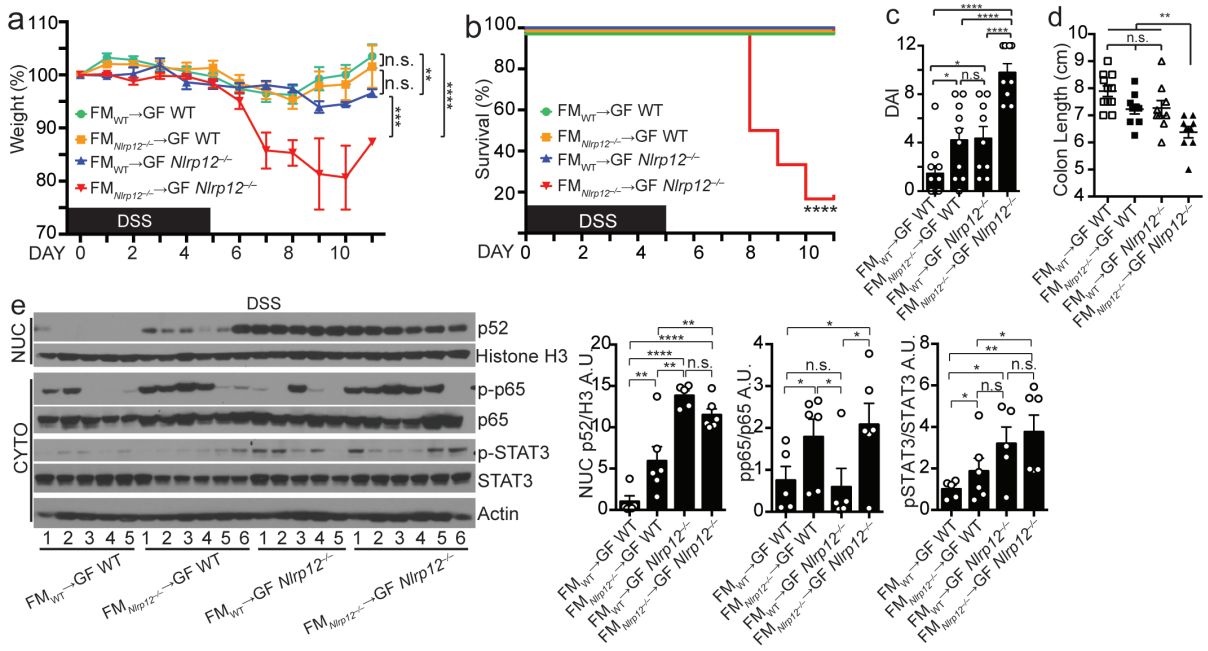

Fig. 2.8. Dysbiotic microbiota and *Nlrp12*-deficiency both contribute to induction of colonic inflammation. (**a**) Body weight and (**b**) percent survival, (**c**) DAI and (**d**) colon length of WT or *Nlrp12*$^{-/-}$ mice received fecal material (FM) derived from WT or *Nlrp12*$^{-/-}$ donors. (**e**) Western blots of the distal colon proteins and densitometry from the mice in (a) treated with DSS to induce colitis. Error bars show SEM. *p<0.05, **p<0.01, *** p<0.001, **** p<0.0001 and n.s. indicates no significance determined using unpaired t test (a, e), Log-rank (Mantel Cox) test (b), and one-way ANOVA Fisher's LSD test (c-d).

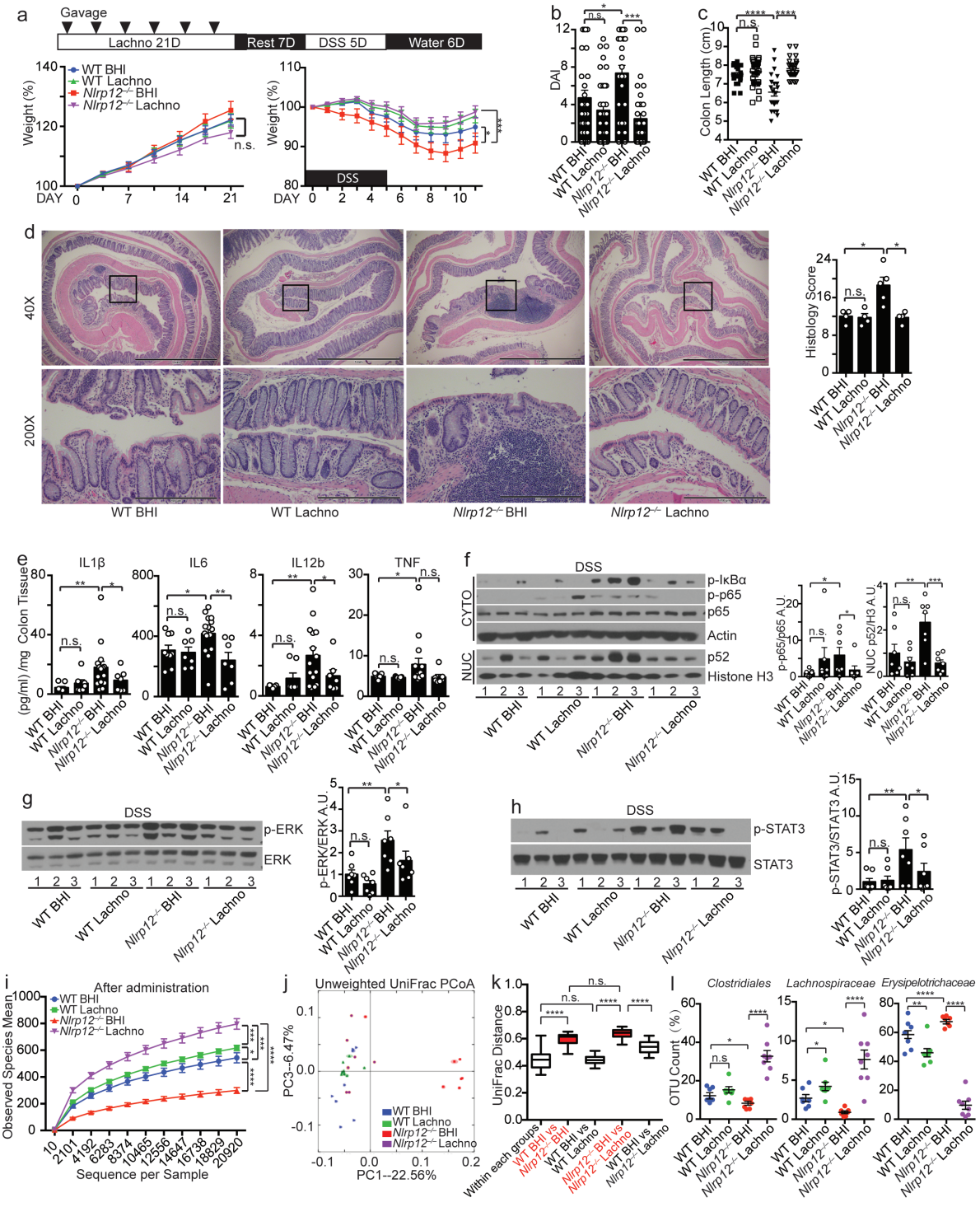

Fig. 2.9. Administration of *Lachnospiraceae* reduces *Erysipelotrichaceae* and suppresses colitis in *Nlrp12*$^{-/-}$ mice. (**a**) Body weights during the 3-week *Lachnospiraceae* treatment (left panel) and the 11-day DSS treatment (right panel) of the WT and *Nlrp12*$^{-/-}$ mice gavaged with *Lachnospiraceae* (Lachno) or brain heart

infusion (BHI) vehicle, and (**b**) DAI, (**c**) colon length after DSS initiation (WT BHI, n=24; WT Lachno, n=33; *Nlrp12*$^{-/-}$ BHI, n=22; *Nlrp12*$^{-/-}$ Lachno, n=22). (**d**) Representative images of H&E-stained colons from DSS-treated mice administered *Lachnospiraceae* or BHI. Scale bars represent 1 mm for 40X and 200 μm for 200X. And histopathology scoring of BHI- or Lachno-treated mice after DSS-induced colitis (n=4 or 5/group). (**e**) Colon explants culture cytokines, and (**f-h**) western blots and densitometry of the distal colons from DSS-treated mice given BHI or Lachno, displaying 3 independent experiments. (**i**) Bacterial diversity, (**j**) PCoA plot showing the microbiome compositional difference quantified by (**k**) UniFrac distance among the mice as treated in (a). (**l**) Significantly altered strains among all identified intestinal bacterial by 16s rRNA gene sequencing due to receiving Lachnospiraceae. One dot or one lane represents one mouse. Error bars show SEM. *p<0.05, **p<0.01, ***p<0.001, ****p<0.0001 and n.s. means no significance determined using unpaired *t* test (a, i), one-way ANOVA Fisher's LSD test (b-h), ANOSIM test (k) and two-way ANOVA (l).

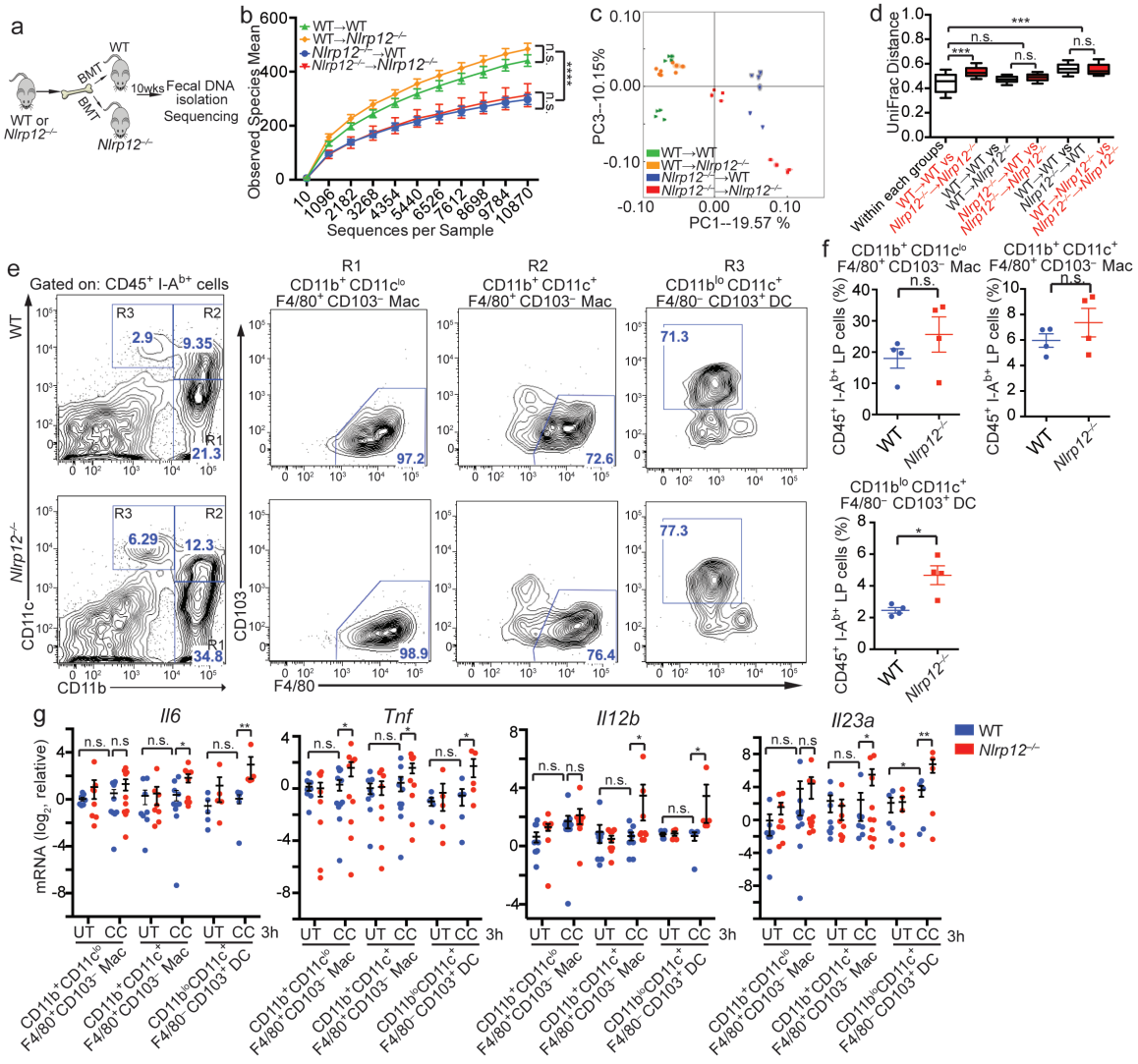

Fig. 2.10. The commensal dysbiosis in *Nlrp12*$^{-/-}$ mice is derived from hematopoietic sources. (**a**) Flowchart illustrating bone-marrow transplantation (BMT) and fecal DNA collection for microbiome analyses. (**b**) Bacterial diversity, (**c**) PCoA plot and (**d**) UniFrac distance plots showing compositional difference of the microbiome from the mice after BMT (n=8/group). One dot represents one mouse. (**e**) Representative concatenated FACS plots, and (**f**) quantifications of colonic lamina propria macrophages and DC subpopulations in SPF mice. Each dot contains pooled cells from 2-3 mice. (**g**) Proinflammatory cytokines expression measurement by RT-qPCR in colon resident macrophages and DC stimulated with cecal contents. Error bars show SEM. *p<0.05, **p<0.01, ***p<0.001, ****p<0.0001 and n.s. means no significance determined using unpaired *t* test (b, g and h) and ANOSIM test (d).

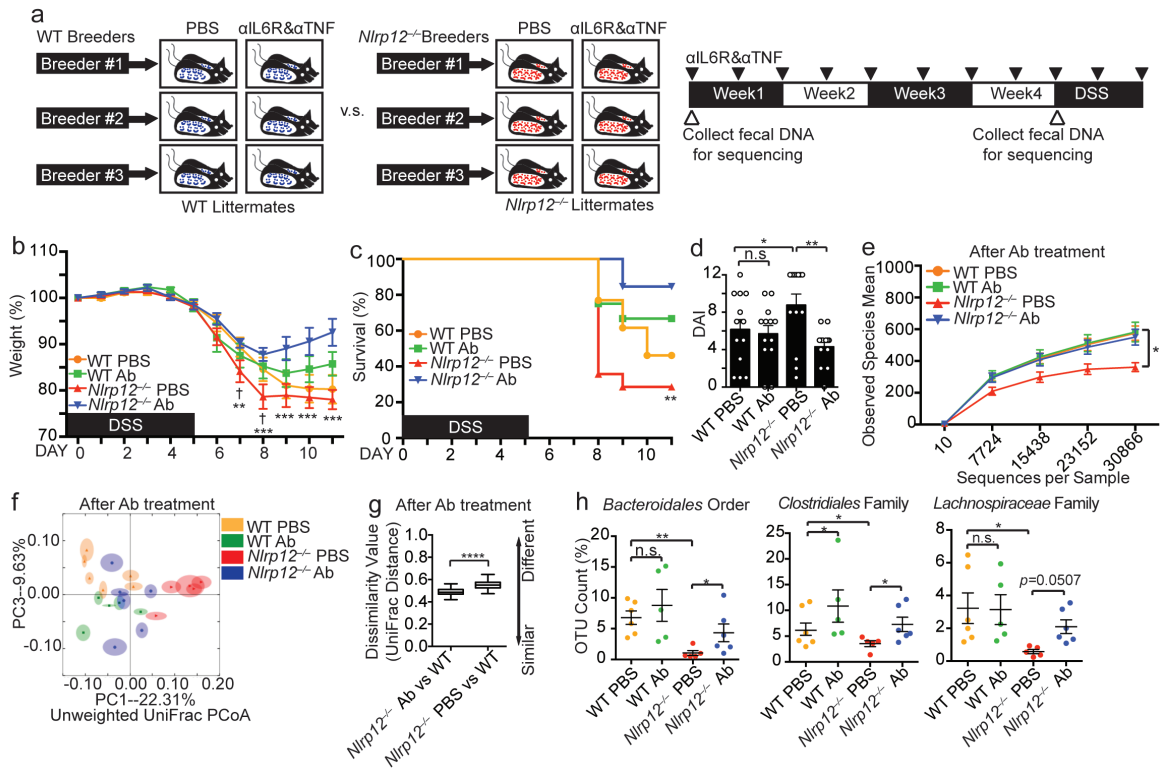

Fig. 2.11. Anti-IL6R and anti-TNF suppresses colitis and increases the missing bacterial groups in *Nlrp12*$^{-/-}$ mice. (**a**) Flow chart showing WT and *Nlrp12*$^{-/-}$ littermates treated with anti-TNF and anti-IL6R antibodies (Ab) or PBS, and experimental strategy for Ab dosing (filled triangles) and fecal collection (open triangles) (n=6 mice/group). (**b**) Body weight, (**c**) percent survival († indicates statistical significance between WT PBS vs. *Nlrp12*$^{-/-}$ PBS; * indicates significance between *Nlrp12*$^{-/-}$ PBS vs. *Nlrp12*$^{-/-}$ Ab), and (**d**) DAI of DSS-treated WT and *Nlrp12*$^{-/-}$ mice injected with anti-IL6R and anti-TNF antibodies (Ab) or PBS (n=12 or 13/group). (**e**) Intestinal microbial diversity, and (**f**) PCoA showing microbiota compositional differences in Ab-treated WT and *Nlrp12*$^{-/-}$ mice (n=6/group). (**g**) Quantification of UniFrac distance from (f). (**h**) Significantly altered groups from sequenced bacteria in Ab- vs. PBS-treated animals. Error bars show SEM. *p<0.05, **p<0.01, ***p<0.001, ****p<0.0001 and n.s. indicates no significance determined by unpaired *t* test (b and e), Log-rank (Mantel Cox) test (c), one-way ANOVA Fisher's LSD test (d), ANOSIM test (g) or two-way ANOVA (h).

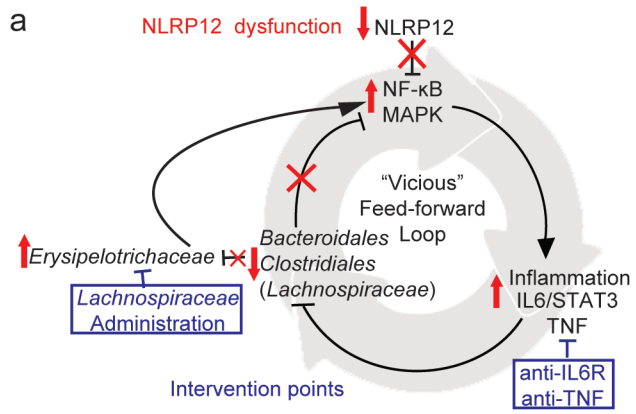

Fig. 2.12. Graphic summary of NLRP12 in maintaining intestinal homeostasis between host innate immunity and intestinal commensal symbiosis. The dysbiosis and inflammation caused by dysfunction of NLRP12 are shown in red. And therapeutic intervention points for the treatment of IBD during NLRP12 dysfunction are shown in blue.

[2]CHAPTER 3: THE INHIBITORY INNATE IMMUNE SENSOR NLRP12 AND SPECIFIC COMMENSAL BACTERIA MAINTAIN A THRESHOLD AGAINST OBESITY

3.1 INTRODUCTION

Obesity is a global health concern afflicting ~30% of the world's population (Flegal, Carroll et al. 2012) and contributes to cardiovascular disease, hypertension, diabetes mellitus and cancer (Hensrud and Klein 2006). While obesity is driven by energy intake and expenditure (e.g., diet and exercise), inflammation is increasingly recognized as an important contributing factor to obesity and obesity-related diseases. Adipose tissues from obese patients and animals given high-fat diet (HFD) display elevated activation of NF-κB and increased TNF, IL-1β and IL-6 (Shoelson, Lee et al. 2003) (Olefsky and Glass 2010). Infiltrating immune cells are predominant sources of cytokines in adipose tissue, with adipose tissue macrophages (ATMs) comprising 40% of total cells in this tissue (Weisberg, McCann et al. 2003). Skewing of ATMs into M1 macrophages is associated with obesity-induced inflammation and pro-inflammatory cytokines (Ouchi, Parker et al. 2011).

In addition to inflammation, obesity is also affected by the gut microbiota. Imbalance of gut microbiota (dysbiosis) is linked to gut inflammation (Sartor and Wu

[2] This chapter is part of a draft entitled "The Inhibitory Innate Immune Sensor NLRP12 and Specific Commensal Bacteria Maintain a Threshold Against Obesity", which in the review process by the *Nature Medicine*.

2017). Innate immune receptors including TLR5 (Vijay-Kumar, Aitken et al. 2010) and the inflammasome adaptor, ASC (apoptotic speck-containing protein with a CARD) (Henao-Mejia, Elinav et al. 2012), have been implicated in obesity-associated dysbiosis (Bouter, van Raalte et al. 2017), although their roles in obesity remain controversial (Chassaing, Ley et al. 2014, Zhang, Hartmann et al. 2016). Inflammasome-activating NOD-like receptor (NLR) proteins, NLRP3 and NLRP6, have been reported to exacerbate obesity-induced inflammation (Stienstra, Joosten et al. 2010, Stienstra, van Diepen et al. 2011, Vandanmagsar, Youm et al. 2011) but others found that co-housing of wildtype (WT) mice with inflammasome-deficient mice caused WT to gain weight (Henao-Mejia, Elinav et al. 2012).

In contrast to pro-inflammatory immune receptors, NLR proteins that dampen inflammation are important for the resolution of inflammation, yet their roles in obesity is completely unknown. NLRP12 is identified as a potent mitigator of inflammation. It is primarily expressed by dendritic cells, granulocytes and macrophages where it inhibits both canonical and non-canonical NF-κB and ERK activation. *Nlrp12*-deficient (*Nlrp12*$^{-/-}$) mice are highly susceptible to experimental models of colitis, colitis-associated colon cancer (CAC) (Zaki, Vogel et al. 2011, Allen, Wilson et al. 2012) and multiple sclerosis (Gharagozloo, Mahvelati et al. 2015, Lukens, Gurung et al. 2015) and they exhibit increased basal colonic inflammation and dysbiosis (Chen, Wilson et al. 2017). This work shows that Nlrp12 is a checkpoint of obesity by maintaining commensals that

produce short-chain fatty acids (SCFA) to restrain HFD-induced inflammation and weight gain.

3.2 RESULTS

Nlrp12$^{-/-}$ mice gained more weight than control animals

We analyzed adipose tissues isolated from healthy and obese individuals and found *NLRP12* expression is negatively correlated with obesity and inflammation index (body mass index, weight, crown-like structure in the fat, serum ferritin), but not with age or sex (**Fig. 3.1**). In addition, *NLRP12* expression is significantly lowered in the obese population (BMI>30) (**Fig. 3.2a**). To determine if NLRP12 regulates obesity, 5-6 week old WT and *Nlrp12*$^{-/-}$ mice were fed HFD (45% kcal from fat) or a control low fat diet (LFD, 10% kcal from fat) for 20 weeks **(Fig. 3.2b)**. *Nlrp12*$^{-/-}$ mice gained significantly more weight **(Fig. 3.2, c-d)** and a greater percentage of body fat than WT mice after 22-weeks of HFD **(Fig. 3.2e)**. Conversely, the percentage of lean mass in HFD-fed *Nlrp12*$^{-/-}$ mice was significantly reduced **(Fig. 3.2f)**. Gonadal white adipose tissues (GWAT) and inguinal white adipose tissues (InWAT) **(Fig. 3.2g, arrows)** were isolated and stained with hematoxylin and eosin to reveal significant increases in adipocyte size in both GWAT and InWAT in *Nlrp12*$^{-/-}$ vs. WT mice on LFD, but this difference was absent in mice on HFD **(Fig. 3.2, h-i)**. *Nlrp12*$^{-/-}$ mice also exhibited a significant increase in adipose tissue weight **(Fig. 3.2, j-k).** The inflammatory cytokines TNF and IL6 have

been positively correlated with obesity and insulin tolerance (Hotamisligil, Arner et al. 1995). *Nlrp12*$^{-/-}$ mice on LFD showed higher serum TNF than WT, indicating enhanced basal inflammation. Both IL6 and TNF were significantly elevated in *Nlrp12*$^{-/-}$ over WT mice on HFD **(Fig. 3.2l),** and this was accompanied by insulin tolerance **(Fig. 3.2m)**. Liver, muscle, and WAT AKT phosphorylation, a readout of intracellular insulin signaling, was reduced in HFD-fed *Nlrp12*$^{-/-}$ mice compared to WT controls **(Fig. 3.2n)**.

Nlrp12$^{-/-}$ mice consumed the same amount of food and water as WT mice **(Fig. 3.3, a-b)** and showed no significant differences in the total respiratory exchange ratio (RER) (ratio of carbon dioxide made during metabolism to oxygen used) (**Fig. 3.3c**) but they had less energy expenditures **(Fig. 3.3d).**

HFD-fed *Nlrp12*$^{-/-}$ mice also showed a significant increase of liver weight but not spleen, heart and kidney weights compared to HFD-fed WT controls and LFD-fed animals **(Fig. 3.4, a-d)**. This coincides with greater HFD-induced steatosis and a trend of higher intrahepatic triglyceride in HFD-fed *Nlrp12*$^{-/-}$ than WT mice **(Fig. 3.4, e-f)**.

Nlrp12$^{-/-}$ animals have increased inflammatory macrophages and exaggerated inflammation in the adipose tissue

In both humans and rodents, macrophages accumulate in adipose tissue during weight gain (Weisberg, McCann et al. 2003, Xu, Barnes et al. 2003), and adipose tissue macrophages (ATMs) are thought to originate from monocytes infiltrating the adipose tissue from the circulation (Weisberg, McCann et al. 2003) or from local proliferation

within adipose tissues (Amano, Cohen et al. 2014). A previous report (Zaki, Vogel et al. 2011) and public databases have shown that NLRP12 is primarily expressed by the myeloid lineage (**Fig. 3.5**). The RNAseq profile of human $CD14^+$ monocytes shows reduced *NLRP12* expression in LPS activated monocytes compared to unstimulated monocytes **(Fig. 3.6a, left)**. The epigenetic activation markers in the *NLRP12* promoter region were also down-regulated in activated monocytes. Conversely, LPS activation increased expression of proinflammatory cytokines *IL1B* **(Fig. 3.6a, middle left)**, *TNF* and *IL6* (**data not shown**), and chemokines *CCL20* **(Fig. 3.6a, middle right)**, *CCL2* and *CCL10* (**data not shown**). As a control, *NLRP13* expression was unaltered by activation (**Fig. 3.6a, right**). When activated monocytes reverted to a quiescent state 24hr after stimulation, proinflammatory cytokine genes (*IL1B, TNF, IL6*) were silenced while *NLRP12* expression was restored (**Fig. 3.6b**). These results suggest that NLRP12 expression is inversely correlated with cytokine and chemokine gene expression, and consistent with its role as an inhibitor of inflammatory response. In agreement with this, LFD fed *Nlrp12*$^{-/-}$ mice had more GWAT $F4/80^+$ macrophages compared to WT mice on LFD, but GWAT from *Nlrp12*$^{-/-}$ mice on HFD had the most abundant $F4/80^+$ cells forming 'crown like structure' (CLS) **(Fig. 3.6c)**, which is an indicator of significant macrophage infiltration in adipose tissue (Cinti, Mitchell et al. 2005, Murano, Barbatelli et al. 2008). This increased macrophage infiltration in the HFD-fed *Nlrp12*$^{-/-}$ mice was also confirmed by flow cytometric analysis **(Fig. 3.6, d-e)**.

ATMs include M1 population that are $CD11b^{+}CD11c^{+}$ and these accumulate in obese mice (Nguyen, Favelyukis et al. 2007). Alternatively activated M2 cells are resident $CD11b^{+}CD11c^{-}$ macrophages which are more abundant in healthy/lean adipose tissue(Martinez and Gordon 2014). As obesity progresses, the expansion of adipose tissue is reported to coincide with activation of ATMs (Olefsky and Glass 2010, Fan, Toubal et al. 2016) and a switch from an M2-like to an M1-like phenotype (Lumeng, Bodzin et al. 2007), consistent with the conclusion that M1 macrophages promote inflammation and obesity. To characterize the ATMs, we isolated GWAT ATMs from WT or *Nlrp12*$^{-/-}$ mice after 20 weeks on HFD and found a higher percentage of $CD11c^{+}$ $CD301^{-}$ M1 macrophage, but lower percentage of $CD11c^{-}CD301^{+}$ M2 cells in the *Nlrp12*$^{-/-}$ ATMs compared to the WT control (**Fig. 3.6, d, f**). These results suggest that the loss of *Nlrp12* may induce ATMs to differentiate into the M1-like phenotype. Analysis of the gene expression in ATMs isolated from WT mice revealed that *Nlrp12* expression was significantly reduced in the proinflammatory M1 cells compared to the M2 cells (**Fig. 3.6g**).

Adipose tissue releases TNF and IL6, which can enhance weight gain (Ohshima, Saeki et al. 1998, Tzanavari, Giannogonas et al. 2010). We found that the GWAT of *Nlrp12*$^{-/-}$ mice had increased expression of *Tnf* and *Il6* at the basal state when compared to WT controls, which was further enhanced with HFD **(Fig. 3.6h)**. MCP-1/CCL2, a chemokine regulating recruitment and infiltration of monocytes into adipose

tissues (Weisberg, McCann et al. 2003, Deshmane, Kremlev et al. 2009) and local macrophage division (Amano, Cohen et al. 2014), was similarly enhanced in *Nlrp12*$^{-/-}$ mice. Additionally, GWAT of HFD-fed *Nlrp12*$^{-/-}$ mice had heightened phosphorylation of p65 and ERK, and production of mature IL1β (**Fig. 3.6i**). These findings suggest that loss of Nlrp12 generated a more inflammatory environment in adipose tissues, which is known to promote obesity. Collectively, these results demonstrate that *Nlrp12* deficiency increases activation and infiltration of monocytes/macrophages into the adipose tissue and contributes to a more M1-enriched status **(Fig. 3.6j)**.

Macrophage-specific deletion of *Nlrp12* resulted in greater obesity, reduced insulin signaling and increased inflammation

Analysis of *Nlrp12* expression revealed reduced *Nlrp12* expression in ATMs isolated from obese mice relative to lean mice (**Fig. 3.7a**). To directly assess if *Nlrp12* in ATM played a role during obesity, we generated myeloid-specific *Nlrp12* knockout mice (*Nlrp12*$^{flox/flox}$ *LysM-Cre*$^{+}$) (**Fig. 3.7b**). *Nlrp12*$^{flox/flox}$ *LysM-Cre*$^{+}$ mice showed greater HFD-induced weight gain (**Fig. 3.7c**). Glucose intolerance measured by OGTT (oral glucose tolerance test) was elevated in *Nlrp12*$^{flox/flox}$ *LysM-Cre*$^{+}$ mice compared to *Nlrp12*$^{flox/flox}$ *LysM-Cre*$^{-}$ control mice but the difference did not reach significance (**Fig. 3.7d**). ITT assay showed that *Nlrp12*$^{flox/flox}$ *LysM-Cre*$^{+}$ mice were in a state of greater insulin tolerance (**Fig. 3.7e**), accompanied by a reduction of insulin signaling (pAKT) in the liver

and WAT (**Fig. 3.7f**). Adipose tissues *Nlrp12*$^{flox/flox}$ *LysM-Cre*$^{+}$ mice have elevated inflammation manifested by increased NF-κB activation and IL1β maturation (**Fig. 3.7g**).

Gut microbiota affects HFD-induced weight gain in *Nlrp12*$^{-/-}$ mice

Others have shown that the intestinal microbiota influences host metabolism and is altered in obesity (Bouter, van Raalte et al. 2017, Plovier, Everard et al. 2017). To address if the resident microbiota contributed to increased HFD-induced-obesity in *Nlrp12*$^{-/-}$ mice, an antibiotic cocktail (Abx) was provided in the drinking water prior to and during feeding with HFD **(Fig. 3.8a)**. There are conflicting reports regarding the impact of antibiotics on the weight gain of WT mice (Cani, Bibiloni et al. 2008, Muccioli, Naslain et al. 2010, Cho, Yamanishi et al. 2012) perhaps due to distinct microbiota at each study site, and the specific antibiotics used. Abx did not significantly affect the weight of WT mice but reduced weight gain among *Nlrp12*$^{-/-}$ mice (**Fig. 3.8b**). Abx-treated *Nlrp12*$^{-/-}$ mice had significantly reduced body fat percentage **(Fig. 3.8c)** compared to untreated *Nlrp12*$^{-/-}$ littermates.

To more stringently investigate the contribution of the microbiota, we examined germ free (GF) WT and *Nlrp12*$^{-/-}$ mice born and reared in sterile isolators. We were unable to administer HFD to GF animals because of difficulty maintaining sterility in irradiated high-fat diets. However specific pathogen-free (SPF) *Nlrp12*$^{-/-}$ mice given standard chow gained significantly more weight at 44 weeks of age compared to

similarly fed WT animals (**Fig. 3.8d**) albeit weight-gain occurred at a later time than mice fed a HFD. SPF-raised *Nlrp12*$^{-/-}$ and WT mice on the standard diet were harvested at 44 weeks of age, and the former displayed significant weight gain and increased GWAT and InWAT (**Fig. 3.8, e-g**). Although 44 week old GF *Nlrp12*$^{-/-}$ mice gained more percentage of weight than GF WT mice (**Fig. 3.8d**), the differences in body weight, GWAT and InWAT were significantly reduced compared to that of animals in the SPF condition (**Fig. 3.8, e-g**).

Colons of Abx-treated *Nlrp12*$^{-/-}$ mice displayed significantly reduced inflammasome activation indicated by the conversion of pro-IL-1β to mature IL-1β compared to untreated mice, while nuclear NF-κB p52, NF-κB phosphorylated p65 (p-p65), and phosphorylated ERK (p-ERK) was also lower but did not reach significance (**Fig. 3.8h**). Abx also reduced IL-6 and TNF in colon explants from HFD-fed *Nlrp12*$^{-/-}$ mice **(Fig. 3.8i).** These results suggest that Abx-mediated changes in the microbiota resulted in attenuated colonic inflammation. This was further confirmed by demonstrating that Abx and GF condition reduced serum IL6 and TNF in *Nlrp12*$^{-/-}$ mice and eliminated cytokine differences that were found in SPF WT and *Nlrp12*$^{-/-}$ mice (**Fig. 3.8, j-k**). These results suggest that the microbiota contribute to basal inflammation and weight gain in *Nlrp12*$^{-/-}$ mice.

Dietary fat can influence the gut microbiota, and mice fed a HFD are reported to have reduced Bacteroidales and increased Firmicutes and Proteobacteria (Eckburg, Bik

et al. 2005, Ley, Backhed et al. 2005, Ley, Turnbaugh et al. 2006). Conversely, the gut microbiota can influence obesity (Backhed, Ding et al. 2004, Ley, Backhed et al. 2005). To determine if *Nlrp12*-deficiency caused microbiome changes during HFD, we profiled bacterial 16S rRNA genes in feces of WT and *Nlrp12*$^{-/-}$ mice fed HFD or LFD for 20 weeks **(Fig. 3.9a).** HFD-fed WT mice showed a loss in bacterial diversity compared to LFD-fed WT mice. However, HFD-fed *Nlrp12*$^{-/-}$ mice showed more significant loss of colonic bacterial diversity compared to similarly fed WT controls (**Fig. 3.9b**). Both *Nlrp12* deficiency and HFD led to a significantly increased microbiome compositional difference between WT and *Nlrp12*$^{-/-}$ mice or LFD and HFD fed mice, shown by a principal component analysis (PCA) and quantified by UniFrac dissimilarity distance (**Fig. 3.9, c-d**).

Loss of intestinal bacterial diversity is reported to correlate with increased inflammation (Le Chatelier, Nielsen et al. 2013) and obesity is frequently accompanied by increased inflammation (Yudkin, Stehouwer et al. 1999, Park, Park et al. 2005, Park, Lee et al. 2010). The reduction of microbial diversity in *Nlrp12*$^{-/-}$ mice on HFD suggests an increased basal intestinal inflammation. Indeed, colon explants from *Nlrp12*$^{-/-}$ mice on HFD showed increased nuclear NF-κB p52, phosphorylated ERK, cleaved caspase-1 p-20 and mature IL-1β when compared to WT mice on HFD **(Fig. 3.9e).** We also observed more anti-microbial peptides Reg3γ (regenerating islet-derived protein III-gamma) and CRAMP (cathelin-related antimicrobial peptides) in the colon of HFD-fed

Nlrp12$^{-/-}$ mice **(Fig. 3.9e)**. These data indicate that HFD increased colonic inflammatory signaling in *Nlrp12*$^{-/-}$ mice and increased antimicrobial peptides which may promote a dysbiotic microbiome.

To ensure that the observed differences in microbiome are not due to housing environment, we performed the same analysis on mice housed in a different vivarium a year later. HFD-fed *Nlrp12*$^{-/-}$ mice showed more significant weight gain (**Fig. 3.10a**), decreased bacterial diversity (**Fig. 3.10b**) and a shift in the colonic microbiome (**Fig. 3.10, c-d**). Thus *Nlrp12*-deficiency caused HFD-induced microbiome perturbation in two vivaria.

To identified if there is any change in gut microbiota at earlier times that might affect the obesity, we collected fecal DNA from the mice on HFD at earlier times (1week, 5 weeks and 15 weeks). There was no significant diversity loss between 1-5 weeks of HFD. After 15 weeks of HFD treatment, we observed significant loss of diversity compared to earlier time points, and there was a more severe loss of diversity in *Nlrp12*$^{-/-}$ mice (**Fig. 3.11, a-b**). There was a trend of decreased Clostridiales and Lachnospiraceae and increased Erysipelotrichaceae along with obesity progression, and this trend was pronounced in *Nlrp12*$^{-/-}$ mice (**Fig. 3.11c**), which correlates with an increased inflammation status in HFD-*Nlrp12*$^{-/-}$ mice (**Fig. 3.11d**). These results indicated the altered bacterial groups might affect obesity outcome ahead of overt obesity. Therefore, transferring probiotics earlier might mitigate weight gain at a later

stage. To test this, we transplanted fecal contents containing high proportion of Lachnospiraceae versus low proportion of Lachnospiraceae but high Erysipelotrichaceae into germ-free recipient mice followed by HFD (**Fig. 3.11e**). After 20 weeks of HFD, fecal contents with higher proportion of Erysipelotrichaceae promoted weight gain, higher fasting glucose level (**Fig. 3.11, f-g**), and elevated inflammation from colon (**Fig. 3.11, h**).

Cohousing with WT mice attenuates HFD-induced obesity in *Nlrp12*$^{-/-}$ mice

The interaction between host and microbiota can be bidirectional. To determine if the altered microbiota in *Nlrp12*$^{-/-}$ mice contributes to excessive weight gain, we cohoused WT and *Nlrp12*$^{-/-}$ mice to achieve microbiota transfer by coprophagia (Henao-Mejia, Elinav et al. 2012, Ridaura, Faith et al. 2013). Weaned age- and gender-matched WT and *Nlrp12*$^{-/-}$ were either single housed (SiHo) or co-housed (CoHo) at 8 weeks of age for another 20 weeks of HFD **(Fig. 3.12a)**. Control SiHo *Nlrp12*$^{-/-}$ mice showed significantly increased body weight **(Fig. 3.12b)** and percentage weight gain **(Fig. 3.12c)** compared to SiHo WT mice. In contrast, *Nlrp12*$^{-/-}$ mice cohoused with WT mice (CoHo *Nlrp12*$^{-/-}$) showed similar body weight as SiHo WT and CoHo WT given HFD, and all were significantly leaner than SiHo *Nlrp12*$^{-/-}$ littermates **(Fig. 3.12, b-c)**. Moreover, CoHo *Nlrp12*$^{-/-}$ mice and CoHo WT cage mates had similar GWAT and InWAT weights **(Fig. 3.12d)** and percentage of body fat **(Fig. 3.12e).**

To investigate changes in the microbiota after cohousing, 16S rRNA gene sequencing analysis was performed on fecal DNA from SiHo or CoHo WT and *Nlrp12*$^{-/-}$ mice fed HFD. Fecal samples from SiHo *Nlrp12*$^{-/-}$ mice showed significantly reduced microbial diversity **(Fig. 3.12f)** compared to SiHo WT and CoHo animals, which agreed with the heat map of bacterial OTUs where more groups of bacteria were found in SiHo WT animals and CoHo WT and *Nlrp12*$^{-/-}$ mice than in SiHo *Nlrp12*$^{-/-}$ mice (**Fig. 3.12g**). This is supported by PCA **(Fig. 3.12h)** and the UniFrac distance metric **(Fig. 3.12i)**. Two-way ANOVA revealed an increased abundance of the Erysipelotrichaceae family but reduced abundance of Bacteroidales and Clostridiales orders and Lachnospiraceae family in the SiHo *Nlrp12*$^{-/-}$ mice compared to SiHo WT mice. A comparison of cohoused *Nlrp12*$^{-/-}$ and WT mice showed no difference in these bacteria (**Fig. 3.12j**). These observations suggest a strong association of Erysipelotrichaceae with HFD-induced-obesity in mice. Indeed, the abundance of Erysipelotrichaceae was negatively correlated with Clostridiales and Lachnospiraceae (**Fig. 3.12k**), raising the possibility that these latter bacterial groups have the potential to reduce Erysipelotrichaceae and obesity.

CoHo *Nlrp12*$^{-/-}$ mice show attenuated nuclear p52, phosphorylated p65, p-ERK and IL1β compared to SiHo *Nlrp12*$^{-/-}$ littermates (**Fig. 3.12l**). These data further support the findings that microbiota is an important contributor of increased obesity and inflammation in *Nlrp12*$^{-/-}$ mice.

Lachnospiraceae maintains microbiota diversity, limits intestinal inflammation and reduces obesity in *Nlrp12*$^{-/-}$ mice on HFD

We next examined if Lachnospiraceae supplementation could reverse a dysbiotic microbiome and prevent weight gain in *Nlrp12*$^{-/-}$ mice. A mixture of 23 Lachnospiraceae isolated from WT mice fed normal chow (Chen, Wilson et al. 2017) was delivered to WT and *Nlrp12*$^{-/-}$ mice by oral gavage three weeks prior to HFD feeding and throughout the duration of HFD feeding. As controls, littermates received the brain heart infusion (BHI) medium in which the bacteria were grown (**Fig. 3.13a)**. Clostridiales and Lachnospiraceae bacterial groups produce short chain fatty acids (SCFAs) via fermentation of dietary polysaccharides (Atarashi, Tanoue et al. 2013, den Besten, van Eunen et al. 2013, Reichardt, Duncan et al. 2014). Increased abundance of Lachnospiraceae is expected to enhance the capability to produce SCFA, and we confirmed that the Lachnospiraceae mixture produced SCFA butyrate and propionate, but not isobutyrate compared to the BHI medium (**Fig. 3.13b**). Consequently, 16S rRNA gene sequencing of the fecal material collected from Lachnospiraceae-fed *Nlrp12*$^{-/-}$ mice on HFD revealed a similar microbiota diversity (**Fig. 3.13c**) to that observed in WT mice on LFD. Lachnospiraceae-treated *Nlrp12*$^{-/-}$ mice on HFD showed a significant increase in the abundance of Clostridiales, but not Bacteroidales (**Fig. 3.13d**). As expected, there was a significant increase of Lachnospiraceae in HFD fed *Nlrp12*$^{-/-}$ mice given Lachnospiraceae compared to BHI-treated *Nlrp12*$^{-/-}$ littermates. Among all sequenced bacterial groups, only Erysipelotrichaceae was significantly decreased after

Lachnospiraceae administration in *Nlrp12*$^{-/-}$ mice on HFD (**Fig. 3.13d**). WT mice on HFD also showed reduced abundance of Erysipelotrichaceae after Lachnospiraceae administration (**Fig. 3.13d**). Most strikingly, compared to littermates given BHI, HFD-fed, Lachnospiraceae-treated *Nlrp12*$^{-/-}$ mice had significantly reduced percentage of weight increase and percentage of body fat **(Fig. 3.13, e-f),** reduced fasting glucose level and improved glucose metabolism (**Fig. 3.13, g-h**), and increased insulin sensitivity marked by increased p-AKT in the liver, muscle and WAT (**Fig. 3.13, i-j**). Although it did not reach significance, Lachnospiraceae reduced HFD-associated intrahepatic triglycerides compared to BHI (**Fig. 3.13, k**).

Dietary hexose and fucose can be used to generate SCFAs, propionate by three independent pathways: succinate, acrylate and propanediol pathways (**Fig. 3.14a, left**). Key enzymes from bacteria that are important in these pathways include *mmdA* encoding methylmalonyl-CoA decarboxylase for the succinate pathway, *lcdA*, encoding lactoyl-CoA dehydratase for the acrylate pathway, and *pduP* encoding propionaldehyde dehydrogenase for the propanediol pathway. Additionally, BCoAT encoding butyryl-CoA transferase is essential for butyrate biosynthesis. Reduced expression of these enzymes correlates with reduced propionate and butyrate (Reichardt, Duncan et al. 2014). The colonic microbiota from *Nlrp12*$^{-/-}$ on HFD showed significantly reduced copy numbers of these genes compared to similarly-treated WT mice, while Lachnospiraceae treatment significantly increased these genes (**Fig. 3.14a, right**), which indicated

successful colonization of Lachnospiraceae. Since our Lachnospiraceae mixture produced SCFA and also mitigated obesity in *Nlrp12*$^{-/-}$ mice, we assessed if SCFA produced by the Lachnospiraceae mixture could limit HFD-induced obesity in the *Nlrp12*$^{-/-}$ mice. Propionate and butyrate were given to WT and *Nlrp12*$^{-/-}$ mice on LFD or HFD via their drinking water *ad libitum*. Both WT and *Nlrp12*$^{-/-}$ mice given propionate and butyrate gained significantly less weight than controls **(Fig. 3.14, b-c)**, which agrees with the previous report (Lin, Frassetto et al. 2012). Since, butyrate and propionate are bitter tasting and might affect eating and drinking activity of mice, we monitored and found that SCFA-supplemented water did not affect food- and drink-intake **(Fig. 3.14, d-e)**. HFD-fed *Nlrp12*$^{-/-}$ mice treated with the BHI had greater activation of NF-κB, MAPK and inflammasome pathways, while Lachnospiraceae dampened these inflammatory pathways to a similar level as WT mice in both small intestine and colon **(Fig. 3.15, a-b**). Thus, we hypothesized that the supplementation of SCFA might reverse excessive weight gain by dampening proinflammatory pathways (Smith, Howitt et al. 2013, Wang, He et al. 2015, Bian, Xiao et al. 2017). To test this, we examined the impact of SCFA on macrophage inflammation by pretreating WT bone-marrow-derived macrophages (BMDMs) with butyrate or propionate, followed by a bacterial ligand, LPS. Dose and kinetic analyses were performed. Both butyrate (**Fig. 3.15, c-d**) and propionate (**Fig. 3.15, e-f**) suppressed proinflammatory-signaling pathways activated by LPS, including pp65 and pSTAT3, and pro-IL1β production. To examine the impact of propionate and

butyrate on inflammasome activation, we employed a typical inflammasome activation protocol using LPS pretreatment followed by nigericin. The addition of propionate or butyrate before LPS priming reduced pro-ILβ levels, which resulted in reduced mature IL1β (**Fig. 3.15g**). We next tested the effect of SCFA on inflammasome activation by adding propionate or butyrate after LPS priming. We tested this with a HFD-relevant inflammasome activator, palmitate, a saturated-fatty acid associated with HFD (Wen, Gris et al. 2011). The addition of butyrate and/or propionate after LPS priming and during palmitate treatment reduced mature IL-1β **(Fig. 3.15h)**. Collectively, these data indicate that SCFA-producing Lachnospiraceae maintains microbiota diversity, reduced inflammation and limited obesity in *Nlrp12*$^{-/-}$ mice.

3.3 DISCUSSION

To address the challenge of the worldwide obesity epidemic, it is important to understand the mechanisms that drive weight gain. Our study provides compelling evidence that NLRP12 is not only an attenuator of innate immunity and inflammation, but also plays an important role in restraining diet-induced obesity. The data support the hypothesis that NLRP12 maintains an intestinal microbiota that lessens the impact of HFD on obesity and inflammation. Deep sequencing analysis of the gut microbiota in HFD-fed *Nlrp12*$^{-/-}$ revealed a deficiency of the Clostridiales order and Lachnospiraceae family. Low abundance of these bacteria has been proposed as markers for increased

intestinal inflammation in pediatric and inflammatory bowel diseases (Gevers, Kugathasan et al. 2014) but its reduction has not been studied in obesity. In addition, these bacteria were described as major producers of anti-inflammatory SCFA (Atarashi, Tanoue et al. 2013, Smith, Howitt et al. 2013, Reichardt, Duncan et al. 2014). As evidence of the importance of Lachnospiraceae and SCFA, reconstitution with either prevented excessive weight gain in HFD-fed *Nlrp12*$^{-/-}$ mice. Lachnospiraceae also suppressed activation of proinflammatory pathways that have been well documented to exacerbate obesity, including increased TNF, IL6, inflammasome activation and M1 polarization.

A new outcome of the Lachnospiraceae treatment is that it reduced Erysipelotrichaceae. Erysipelotrichaceae has been correlated with increased TNF, resulting in chronic intestinal inflammation (Dinh, Volpe et al. 2015) and its abundance was found to be enhanced in IBD patients and animal models of IBD (Chen, Liu et al. 2012, Dey, Soergel et al. 2013), although one study has the opposite finding (Gevers, Kugathasan et al. 2014). By contrast, Erysipelotrichaceae has been consistently associated with obesity (Ley, Backhed et al. 2005, Fleissner, Huebel et al. 2010), which is supported by our finding of a strong correlation between Erysipelotrichaceae abundance and exacerbated weight gain. In Koch's postulate, it is important to show that a microbe causes a disease by directing inoculating it to a host and observing the disease, thus we performed fecal transplantation in the germ-free mice and found the

fecal content enriched with Erysipelotrichaceae promoting more inflammation and obesity. Thus, Erysipelotrichaceae may represent a potential target for treating obesity. Indeed, Lachnospiraceae administration reduced the abundance of Erysipelotrichaceae and the associated weight gain.

This study also reveals that NLRP12 inhibits obesity-associated inflammasome activation. Adipose tissue fibrosis that accompanies obesity generates substantial damage-associated molecular patterns (DAMPs) that activate the inflammasome during adipogenesis(Khan, Muise et al. 2009, Divoux, Tordjman et al. 2010), and elevated IL1β was shown to promote obesity (Vandanmagsar, Youm et al. 2011, Wen, Gris et al. 2011). With one exception (Henao-Mejia, Elinav et al. 2012), other studies showed that deficiencies in various inflammasome components including *Nlrp3, Asc* and *Casp1* caused less weight gain with a HFD (Stienstra, van Diepen et al. 2011, Vandanmagsar, Youm et al. 2011). This agrees with our finding of elevated intestinal IL1β in obese HFD-fed *Nlrp12*$^{-/-}$ mice.

In summary, this study reveals that NLRP12 is an important regulator of obesity and obesity-associated diseases. Characterization of this pathway can help devise therapeutic approaches to control obesity. In support of this, we show that Nlrp12 maintained intestinal SCFA-producing bacteria and mitigated inflammation, obesity and obesity-associated diseases (**Fig. 3.16**).

3.4 MATERIALS AND METHODS

Animals and diets:

All studies were conducted in accordance with IACUC guidelines of UNC Chapel Hill and the NIH guide for the Care and Use of Laboratory Animals. *Nlrp12*$^{-/-}$ mice have been described previously (Arthur, Lich et al. 2010, Allen, Lich et al. 2012, Allen, Wilson et al. 2012). WT and *Nlrp12*$^{-/-}$ mice in this study were generated from common *Nlrp12*$^{+/-}$ parents, which were obtained from at least 9 generations backcross to WT C57BL/6J mice, and were bred in house for several generations. All experiments used littermate controls, or their immediate descendants. GF mice were derived by sterile embryo transfer by the National Gnotobiotic Rodent Resource Center at UNC- Chapel Hill (Chen, Wilson et al. 2017).

Apart from a standard chow, mice were specifically described as receiving a HFD (Research Diets, D12451) (45% energy from fat, 35% from carbohydrates and 20% from protein) or a control LFD (Research Diets, D12450B) (10% energy from fat, 70% from carbohydrates and 20% from protein). Mice were put on special diets at the age of 8 weeks. Special feeding was provided for 20 weeks.

Nlrp12$^{flox/flox}$ mice were generated at UNC Animal Models Core using a targeting construct, which contained loxP sites flanking exon 3 of *Nlrp12*, next to a FRT flanked neomycin resistance cassette inserted in the intron 2. Targeted ES cells were injected into C57BL/6-albino blastocysts. The resulting male chimeras were mated with female

Rosa26-Flpe mice on a C57BL/6-albino background to create heterozygous *Nlrp12*$^{flox/+}$ mice and remove the neomycin cassette. The *Nlrp12*$^{flox/+}$ mice were then bred with C57BL/6 mice for at least another seven generations before being inbred with heterozygous *Nlrp12*$^{flox/+}$ mice to get the *Nlrp12*$^{flox/flox}$ mice. To generate myeloid-specific *Nlrp12* KO (*Nlrp12*$^{flox/flox}$, LysM-Cre+) mice, *Nlrp12*$^{flox/flox}$ mice were crossed with LysM-Cre mice for the F1 generation. And *Nlrp12*$^{flox/flox}$ LysM-Cre^{+} and *Nlrp12*$^{flox/flox}$ LysM-Cre^{-} (control) littermates from the F2 generation were used for future breeders or experiments.

Human subjects

Subcutaneous adipose tissues were obtained from 80 donors (Ballak, van Diepen et al. 2014). Some measurements were not carried out in all subjects. All subjects were given informed consent. The studies were approved by the ethical committee of the Radboud University Medical Centre, Nijmegen.

Antibiotic treatment, cohousing studies, Lachnospiraceae and SCFA administration:

For antibiotic treatment (Abx), mice received a mixture of antibiotics (0.17g/L of gentamicin, 1g/L bacitracin, 2g/L of streptomycin and 0.125mg/L of ciprofloxacin) (Chen, Shaw et al. 2008) in drinking water *ad libitum* one week before the special diet feeding. Antibiotics were replaced twice a week for 20 weeks along with the special diet feeding.

For the cohousing study, 3-4 week old WT mice born from the same breeders were divided for either single housing (SiHo) or cohousing (CoHo) with age- and sex-matched *Nlrp12*$^{-/-}$ mice for 4-5 weeks before starting the LFD/HFD. Cohoused mice were compared to their single-housed littermates as controls.

For Lachnospiraceae treatment, mice were orally gavaged with a mixture containing 23 sequenced Lachnospiraceae stains (~10^8 bacteria) (Chen, Wilson et al. 2017) in the culture medium consisting of brain-heart infusion broth (BHI) supplemented with 5% FBS, 0.01% L-cysteine and 1% corn starch twice a week for 3 weeks before the special diet feeding. Plain BHI medium was used as vehicle control. Mice continually received the mixture twice a week for 20 weeks along with the LFD/HFD.

For SCFA treatment of mice, a cocktail of 200mM propionate (Sigma) and butyrate (Sigma) were given to mice in the drinking water accompanied with the HFD feeding.

For fecal contents transplant experiments, we transplanted the feces collected from lean WT mice with high relative abundance of Clostridiales and Lachnospiraceae but low Erysipelotrichaceae, compared to the feces from obese *Nlrp12*$^{-/-}$ mice with low abundance of Clostridiales and Lachnospiraceae but high amount of Erysipelotrichaceae, identified by 16S sequencing. Fresh collected feces were diluted in the saline at the ratio of 40mg feces/ml saline, and homogenized by a sterile blender. The insoluble particles were removed by passing the mixture through a laboratory stainless sieve (pore size: 0.25mm). Total bacterial protein concentration was

determined by BCA assay to normalize the amount of bacterial cell. The feces mixtures were mixed with 10% autoclaved glycerol, aliquoted and frozen at −80 °C until used. We oral-gavaged the 6-7 weeks old germ-free mice with 200 µl feces mixture for 3 times in 2 weeks before HFD feeding. During the 20 weeks of HFD, the recipients' cages were replaced by the used cages of the fecal donors once a week.

Oral glucose tolerance test (OGTT) and insulin tolerance test (ITT):

We performed OGTT and ITT on mice fed LFD/HFD for 20 weeks. The mice were fasted for 10-12 (overnight) hours before the experiment. Fasting glucose level were measured, followed by ITT and OGTT. For ITT, fasted mice were intraperitoneally injected with insulin (Lantus) (0.7 U/kg body weight, SANOFI, USA). For OGTT, fasted mice were oral-gavaged with 20% (w/v) glucose solution (2 g/kg body weight, Sigma). Glucose levels were measured using a glucometer (Freestyle, Abbott, USA) at the indicated time point.

Body composition, indirect calorimetry, food and water intake, and activity measurement:

Mouse body composition (fat and lean mass) was measured using a mice whole-body composition analyzer (Bruker) at the UNC Nutrition Obesity Research Center. Total body mass was measured by standard laboratory scales.

WT and *Nlrp12*$^{-/-}$ animals were placed into individual metabolic cages (TSE Systems International Group, Chesterfield, MO) at UNC Nutrition Obesity Research Center. Respiratory Exchange Ratio (RER), heat production and energy expenditure (EE) were measured. EE was normalized to the mice body mass. Activity was measured as total beam breaks (x+y+z axis) within the cage. Mice had free access to food and water while in the chamber. Food and water intake were measured for the duration of studies. Animals were under indirect calorimetry measurements for 72h.

Histological staining, western blot and ELISA:

For histopathology, organs were collected in 10% formalin. Tissue sections were prepared from paraffin blocks and stained with hematoxylin and eosin (H&E) or F4/80 antibody (Ebiosciences 14-4801-82). F4/80 positive staining or liver steatosis area was quantified by ImageJ and displayed as % to total (stained + non-stained) area.

For western blot analysis, the following primary antibodies were used for western blot analysis: anti-CASPASE1 (4D4) (Genentech); anti-IL1β (cat. AF-401-NA) (R&D systems); anti-pp65 (Ser536) (93H1) (cat. no. 3033); anti-p-ERK1/2 (Thr202/Tyr204) (D13.14.4E) (cat. no. 4370); anti-p65 (D14E12) (cat. no. 8242) (Cell signaling); anti-REG3G (cat. no. ab198216, Abcam); anti-CRAMP (G1) (cat. no. sc-166055), anti-p52 (C-5) (cat. no. sc-7386); anti-ERK1 (C-16) (cat. no. sc-93); anti-ERK2 (C-14) (cat. no. sc-154) and anti-Actin-HRP (C-11) (cat. no. sc-1615) (Santa Cruz Biotechnology); and

anti-Histone H3 (cat. no. 07-690) (Millipore). Goat anti-rabbit-HRP (cat. no. 111-035-144) and goat anti-mouse-HRP (cat. no. 115-035-146) (Jackson Laboratories) were used as secondary antibodies. Protein densitometry was quantified by Image J software. In **Fig. 4n**, the composite densitometry of p-p65/p65, p-ERK/ERK, and nuc p52/H3 for HFD WT and *Nlrp12*$^{-/-}$ mice, includes the data in **Supplementary Fig. 5a**.

IL6 and TNF was measured using ELISA assays according to manufacturer's instructions from BD Bioscience (cat# 555240 for IL6, cat# 560478 for TNF). For colon secreted cytokines, excised colons were flushed with PBS containing penicillin/streptomycin. The distal-most 1cm^2 colon sections were cultured for 15hrs in RPMI media containing penicillin/streptomycin. Supernatants from these cultures were removed, cleared of debris by centrifugation and assessed for cytokines by ELISA. Triglycerides from the liver lysate were measured by a triglyceride detection kit (cat# ab65336, Abcam) and normalized to the total proteins amount quantified by the BCA assay.

RNA isolation and mRNA analysis:

For mRNA detection, total RNA was extracted from GWAT lysate using Qiazol (Qiagen). cDNA was generated from the total RNA by using iScript™ cDNA Synthesis Kit (Cat. 170-8891, Bio-Rad Laboratories, Inc.). Quantitative RT-PCR was performed on a ViiA™ 7 Real-Time PCR System. Taqman probes including mouse *Il6*

(Mm00446190_m1), *Mcp 1* (Mm00441242_m1), *Tnfa* (Mm00443258_m1) *Gapdh* (Mm99999915_g1) and *Actb* (Mm01324804_m1) were used for mRNA detection. Mouse *Nlrp12* was detected using a primer set: F: AATAATGGTCTATGCCTTTTTGAGA, R: CGGACATAGTCTTTGTAGGTTGTCT.

Flow cytometry analysis for adipose tissue macrophages from Gonadal Adipose Tissues：

Stromal vascular cells (SVCs) were prepared from gonadal adipose tissues as previously described (Orr, Kennedy et al. 2013, Cho, Morris et al. 2014). Briefly, the gonadal adipose tissues were resected from mice, and mechanically dissociated into fine pieces by a surgical blade, and then treated by 1mg/ml collagenase II (Sigma) in digestion buffer (HBSS with 0.5% BSA, 10mM EDTA) for 30min in a 37°C shaking incubator (200 rpm). The SVCs suspension was washed with FACS buffer and centrifuged at 4°C (1,200 rpm). Red blood cells were removed with ACK lysing buffer. The remaining cells were washed and counted for FACS staining.

SVCs suspensions from adipose tissue were re-suspended in FACS buffer on ice during the staining process. Cells were firstly stained with anti-CD16/32 (Fc block, eBioscience), followed with antibodies targeting cell surface molecules: CD45.2 (clone# 104, PerCP-Cy5.5, eBioscience), CD11b (clone# M1/70, e450, eBioscience), F4/80 (clone# BM8, PE, Biolegend), CD11c (clone# N418, PE-Cy7, eBioscience) and CD301 (clone# ER-MP23, Alexa Fluor 647, Bio-Rad). All cells were collected using LSRII (BD

Biosciences) flow cytometer or MoFlo (Beckman Coulter) cell sorter. To gate adipocyte tissue macrophages (ATMs), cell aggregates and cellular debris were first excluded, then adipose tissue leukocytes ($CD45.2^{+}$) were selected. ATMs were identified as $F4/80^{high}CD11b^{high}$ to minimize contamination by eosinophils and neutrophils, according to a previous report (Cho, Morris et al. 2014). Finally, $CD45^{+}F4/80^{high}CD11b^{high}$ ATMs were gated for surface expression of $CD11c^{+}CD301^{-}$ (M1 subset) and $CD301^{+}CD11c^{-}$ (M2 subset). All data were analyzed using FlowJo software (Tree Star).

Fecal DNA isolation, propionate-producing enzyme copy number measurement and 16S rRNA gene microbiome sequencing:

Fecal samples were collected from live mice, snap-frozen and stored at -80°C. DNA was isolated by incubating fecal material at 65°C for 30min in Lysing Matrix E tubes (MP Biomedicals) containing 200mM NaCl, 100mM Tris, 20mM EDTA (pH 8.0), SDS and proteinase K (Qiagen). Phenol:Chloroform:Isoamyl alcohol (Invitrogen) was added, and the samples were homogenized at 4°C for 3min using a bead beater homogenizer. The samples were centrifuged at 8000 rpm for 3min at 4°C, and the supernatant was incubated with Phenol:Chloroform (Invitrogen) for 10 min at room temperature. The samples were centrifuged at 13,000rpms for 5min at 4°C, and the aqueous phase was incubated with isopropanol and 3M sodium acetate, pH 5.2, at -20°C for 15hrs to precipitate DNA. The precipitated DNA was collected by centrifugation at 13000rpm at 4°C for 20min, washed twice with 100% cold ethanol and resuspended

in TE buffer. The DNA was further purified using a DNeasy Blood and Tissue Kit (Qiagen) according to the manufacturer's protocol.

Fecal DNA samples were amplified by PCR using barcoded primer pairs targeting the V3-V4 region of the 16S gene. PCR amplicons were sequenced using the Mi-Seq Illumina sequencer. The resulting bacterial sequence fragments were clustered into Operational Taxonomic Units (OTUs) and aligned to Greengenes microbial gene database with 97% sequence similarity in QIIME. Bacterial taxonomy summarization, rarefaction analyses of microbial diversity, compositional differences (dissimilarity value indicated by Unweighted UniFrac Distance) were calculated in QIIME (1.8.0) as previously described using scripts (including pick_open_reference_otus.py, summarize_taxa.py, alpha_rarefaction.py, jackknifed_beta_diversity.py and make_distance_boxplots.py). PCoA plots were generated by QIIME script, make_2d_plots.py. Each point represents one mouse, and the ellipses represent the interquartile range (IQR) during the rarefaction analyses (see http://www.wernerlab.org/teaching/qiime/overview for scripts details). All 16S rRNA microbiome sequences have been deposited in the European Nucleotide Archive (http://www.ebi.ac.uk/ena), see data accessibility section for accession number.

To examine the distribution of three different pathways (succinate, acrylate and propanediol pathway) used by bacteria for propionate formation and Butyryl-CoA transferase for butyrate formation, we measured the genomic copy number of the

specific key enzymes in each pathway by qPCR with reported primer sets (*lcdA*-F: 5′-CTGGTGTGCTGGWSIGCIWSIGTIGCNCC-3′, -R: 5′-CAGATAGGTCCAIAYIGCDATNCCYTCCCA-3′; *pduP*-F: 5′-GTGGATGARACIGGIATGGGNAAYGTNGG-3′, -R: 5′-CAATAGCCYTCICCICCRAAICCIADNGC-3′; and *mmdA*-F: 5′-AATGACTCGGGIGGIGCIMGNATHCARGA-3′, -R: 5′-GATTGTTACYTTIGGIACNGTNGCYTC-3 (Reichardt, Duncan et al. 2014). And *bcoat*-F: 5'-GCIGAICATTTCACITGGAAYWSITGGCAYATG-3', -R: 5'-CCTGCCTTTGCAATRTCIACRAANGC-3'). Copy numbers were normalized to the bacterial total 16S rRNA gene copy number detected by a universal primer set (16S rRNA-F: 5′-AGAGTTTGATYMTGGCTCAG-3′, -R: 5′-ACGGCTACCTTGTTACGACTT-3′). The qPCR was performed using SensiFAST™ SYBR® No-ROX Kit (Bioline) per manufacturing instructions with fecal DNA (200ng for enzyme gene and 10ng for 16S rRNA gene) and 100nM of each primer, at 95°C for 3min, followed by 40 cycles at 95°C for 30s, 56°C for 30s, 72°C for 40s (1min for lcdA, 2min for 16S rRNA gene) and a final extension at 72°C for 5min (10min for 16S rRNA gene)

Short chain fatty acids (SCFA) treatment of BMDM or mice:

WT bone marrow-derived macrophages (BMDM) were pretreated with propionate and butyrate with increased concentrations (0, 0.1, 0.4, 1.6, 6.4 or 25.6mM) for 1hr,

followed by 100ng/ml of LPS stimulation for 30min. Also, the BMDM cells were pretreated with 6.4mM of SCFA for 0, 15, 30, 60 and 120min, followed by 100ng/ml LPS stimulation for 30min. To assay SCFA suppression of mature IL1β production, BMDM cells were pretreated with 6.4mM propionate or butyrate for 1hr, followed by 100ng/ml of LPS stimulation for 30 min and then 1μM nigericin for 30 min. To assay SCFA suppression on IL1β cleavage caused by palmitate, WT BMDM cells were primed with 100ng/ml LPS for 3h, and followed by 0.2mM palmitate-BSA complex for 24hrs with or without propionate and/or butyrate. The palmitate-BSA complex was prepared per previously described (Wen, Gris et al. 2011).

RNA-seq, ChIP-seq and microarray data analysis:

Raw RNA-sequencing and ChIP-sequencing data for untreated and LPS activated human primary CD14+ monocytes were obtained from public dataset: GSE100383(Park, Kang et al. 2017) and GSE85243(Novakovic, Habibi et al. 2016). Microarray data for CD11c+ and CD11c- adipose tissue macrophage isolated from WT mice was obtained from public dataset: GSE53403(Xu, Grijalva et al. 2013). All public datasets were archived in the NCBI GEO database. The raw sequence data was analyzed by Galaxy (usegalaxy.org). Bowtie 2 was used to align the sequence reads to human reference genome (ver. hg19), and MACS 2 was used for peaks identification. Integrated genome browser (IGB) from BioViz was used to generate the peak

distribution plots. For microarray data, raw array data was analyzed by Genespring GX (Agilent), and heatmap was generated by Gene-E (Broad Institute). Human *NLRP12* expression plots were obtained from two datasets: “GeneAtlas U133A, gcrma, Pubmed ID: 15075390” and “Barcode on normal tissue”, archived and analyzed by www.biogps.org(Wu, Jin et al. 2016).

Statistics:

If not specified in the figure legends, statistical significance between two groups was determined by unpaired, two-tailed Student’s *t* test, and significance between more than two groups was determined using one-way ANOVA with Fisher's LSD test using GraphPad. For all data, one dot or lane represents one mouse. Error bar represents mean ± SEM with *p<0.05, **p<0.01, ***p<0.001, ****p<0.0001 and n.s. means no significance.

Data accessibility:

The accession number for the sequencing data are: PRJEB19755 (microbiome of co-housing and Lachno transferring study in vivarium 1 and 2), PRJEB19754 (microbiome of WT *Nlrp12*$^{-/-}$ mice at 1, 5 or 15 weeks of HFD in vivarium 1).

3.5 FIGURES

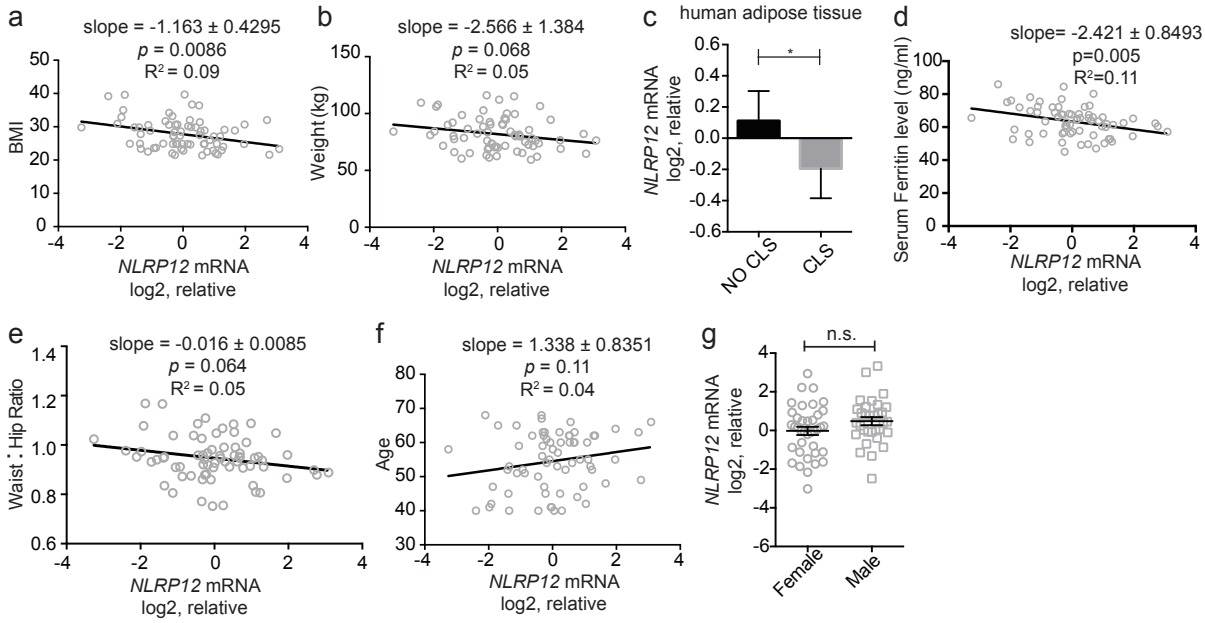

Fig. 3.1. *NLRP12* is reduced in obese patients. Correlation between human *NLRP12* mRNA in adipose tissue and **(a)** BMI, (**b**) Weight, (**c**) appearance of CLS in fat tissue, **(d)** Serum Ferritin level, **(e)** Waist-to-Hip ratio, (**f**) Age (n=70). **(e)** *NLRP12* expression in female (n=38) and male (n=29) individuals. The slope, *p* value, and R^2 are reported for each linear regression (a-f). Each symbol represents one individual patient. Error bars show SEM, n.s. no significance determined by Student's t test (g).

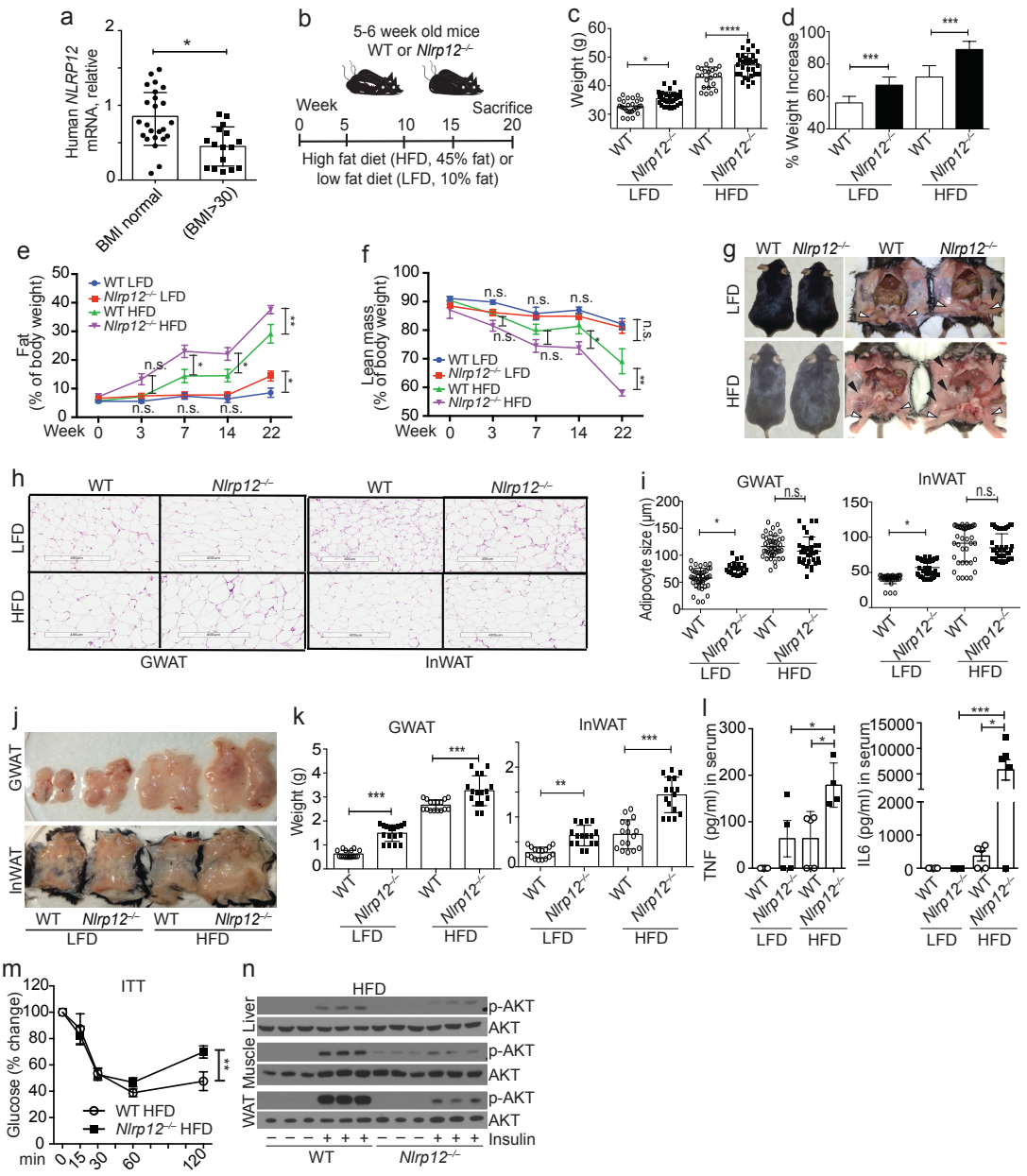

Fig. 3.2. Nlrp12 protects against obesity. (**a**) Expression of human *NLRP12* mRNA in adipose tissue from healthy (n=24) and obese (BMI>30) individuals (n=16). (**b**) Schematic of WT and *Nlrp12*$^{-/-}$ mice fed LFD or HFD. (**c**) Body weight and (**d**) percent weight increase of WT and *Nlrp12*$^{-/-}$ fed LFD/HFD for 20 weeks (WT LFD, n=28; *Nlrp12*$^{-/-}$ LFD, n=30; WT HFD, n=22; *Nlrp12*$^{-/-}$ HFD, n=32). (**e**) Percentage body fat and (**f**) lean mass of WT and *Nlrp12*$^{-/-}$ mice at 0 to 22 weeks of LFD/HFD (WT LFD, n=9; *Nlrp12*$^{-/-}$ LFD, n=8; WT HFD, n=10; *Nlrp12*$^{-/-}$ HFD, n=11). (**g**) Representative image of mice from (b) indicating InWAT (black arrow) and GWAT (white arrow). (**h**) Representative images of H&E staining of WT and *Nlrp12*$^{-/-}$ GWAT and InWAT 20

weeks post-LFD/HFD (Scale bar = 400 μm), with (**i**) composite of adipocyte sizes (n=50/each group). (**j**) Representative images of GWAT and InWAT from mice in (b), with (**k**) composite weight of GWAT and InWAT (n=17/group). (**l**) Serum TNF and IL6 from mice treated as described in (b) (WT LFD, n=3; *Nlrp12*$^{-/-}$ LFD, n=4; WT HFD, n=5; *Nlrp12*$^{-/-}$ HFD, n=5). (**m**) Insulin tolerance test (ITT) in WT and *Nlrp12*$^{-/-}$ mice fed HFD for 20 weeks (WT, n=6; *Nlrp12*$^{-/-}$, n=9). (**n**) Western blot of AKT phosphorylation in the liver, muscle and WAT of HFD-fed WT and *Nlrp12*$^{-/-}$ mice after insulin administration (n=3/group). Each symbol or lane represents one mouse. Error bars represent SEM, with *p<0.05, **p<0.01, *** p<0.001, **** p<0.0001 and n.s. means no significance determined by Student's t test.

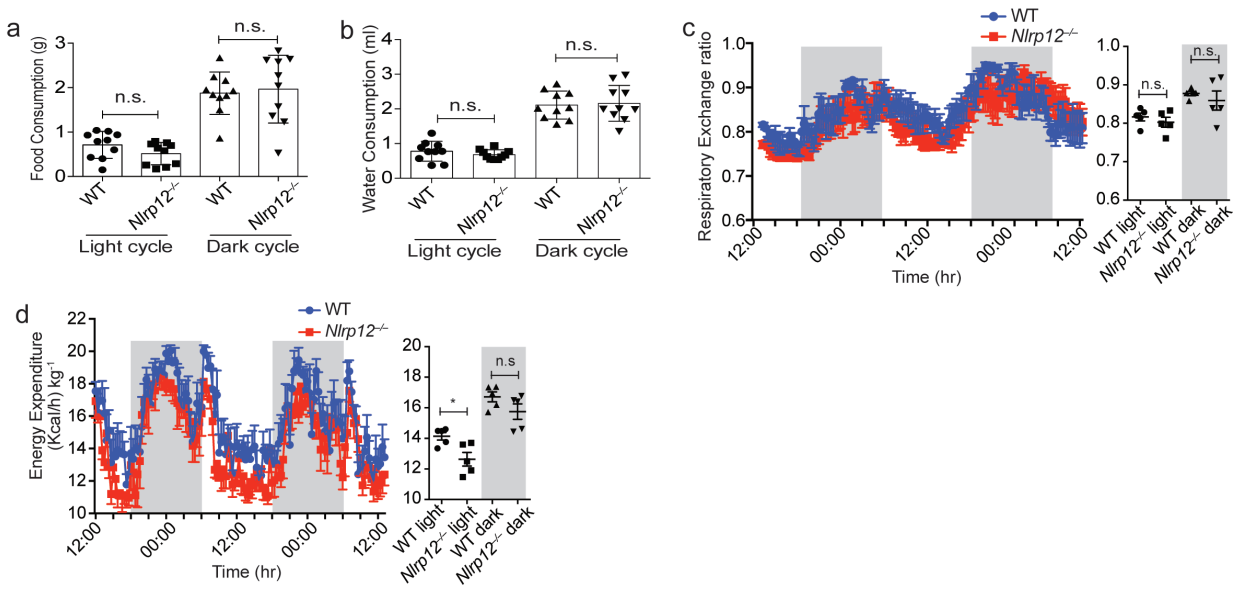

Fig 3.3. *Nlrp12*$^{-/-}$ mice do not exhibit differences in food or water consumption but display reduced energy expenditure. (**a**) Average food and (**b**) water consumption, (**c**) respiratory exchange ratio and (**d**) energy expenditure (normalized to the body mass of each mouse) in WT and *Nlrp12*$^{-/-}$ mice (n=10/group). Error bars show SEM, *p<0.05 and n.s. no significance determined by Student's t test.

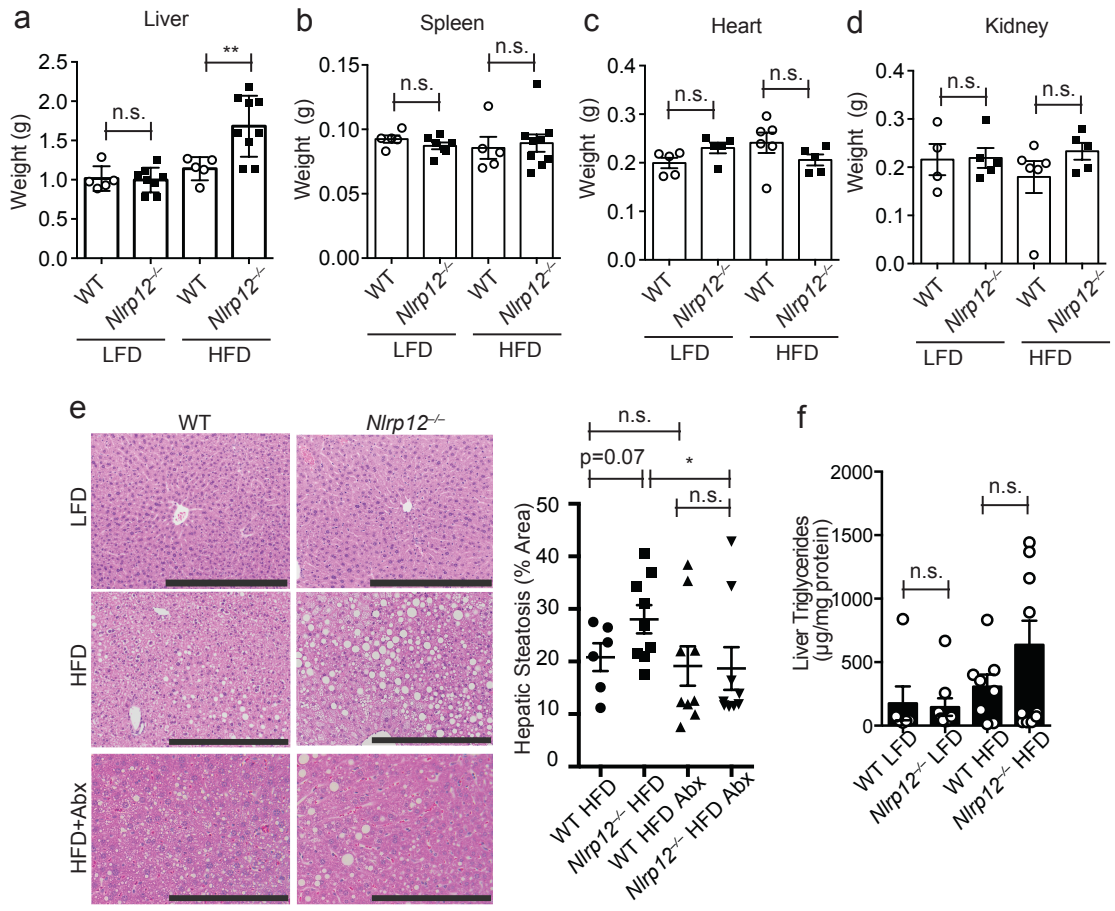

Fig. 3.4. Nlrp12-deficiency increases the risk of HFD diet-induced liver steatosis. (**a**) Weights of liver, (**b**) spleen, (**c**) heart, and (**d**) kidney from WT and *Nlrp12*$^{-/-}$ mice fed LFD or HFD for 20 weeks (n=4-9/group). (**e**) Representative H&E staining of liver with composite semi-quantification of percent steatosis area from mice fed HFD with or without antibiotics (Abx) (WT HFD, n=6, *Nlrp12*$^{-/-}$ HFD, n=9, WT HFD Abx, n=9, *Nlrp12*$^{-/-}$ HFD Abx, n=8). (**f**) Intrahepatic triglyceride content in LFD- vs. HFD-fed mice (WT LFD, n=7, *Nlrp12*$^{-/-}$ LFD, n=8, WT HFD, n=9, *Nlrp12*$^{-/-}$ HFD, n=8). Each dot represents one mouse. Error bars show SEM with *p<0.05, **p<0.01 and n.s. means no significance as determined by one-way ANOVA.

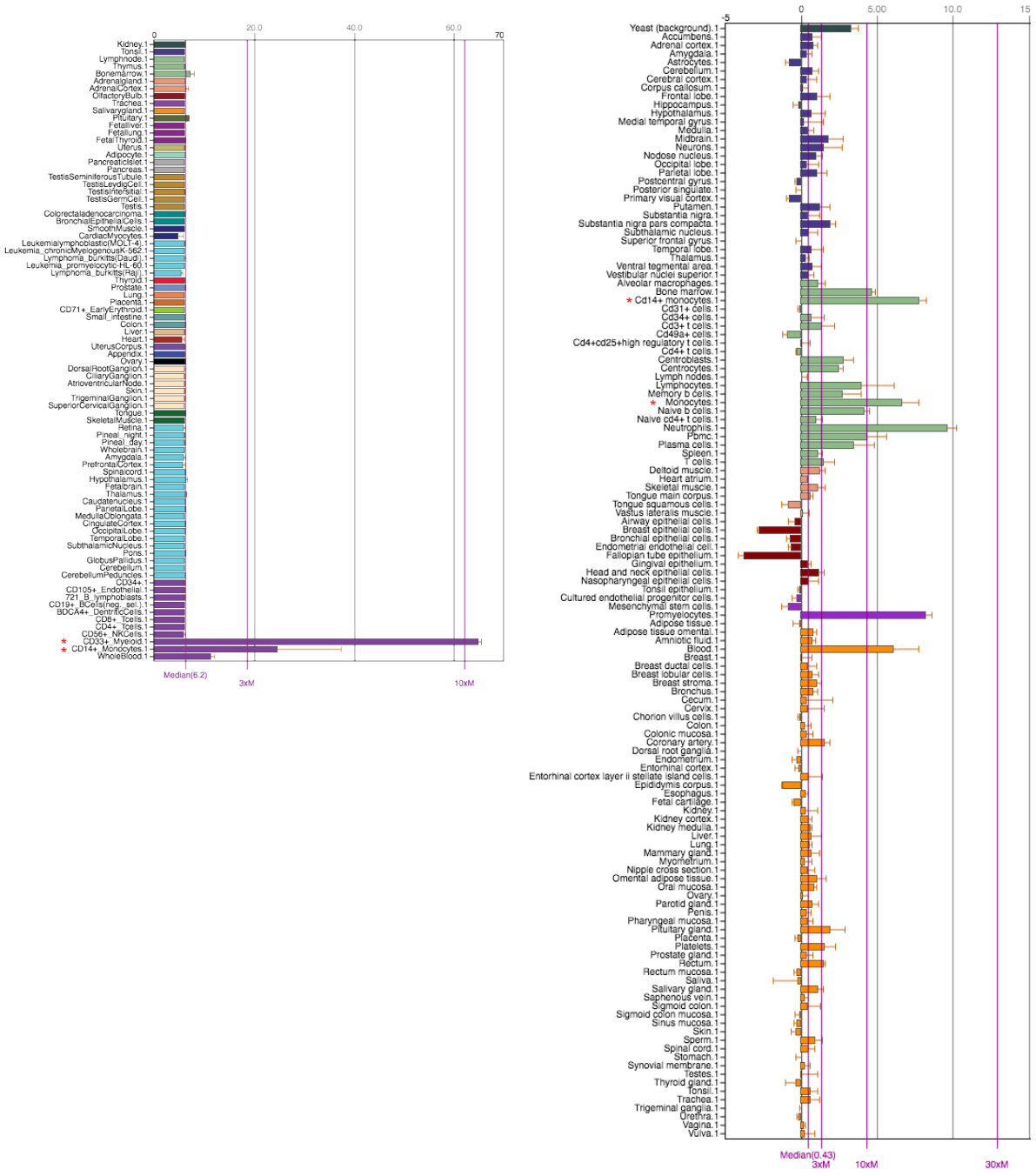

Fig. 3.5. Human *NLRP12* is highly expressed in myeloid monocytes. Human *NLRP12* expression levels in multiple tissues and cells using data extracted and analyzed from the public datasets (**a**) "GeneAtlas U133A, gcrma", Pubmed ID: 15075390, and (**b**) "Barcode on normal tissue", archived at www.biogps.org.

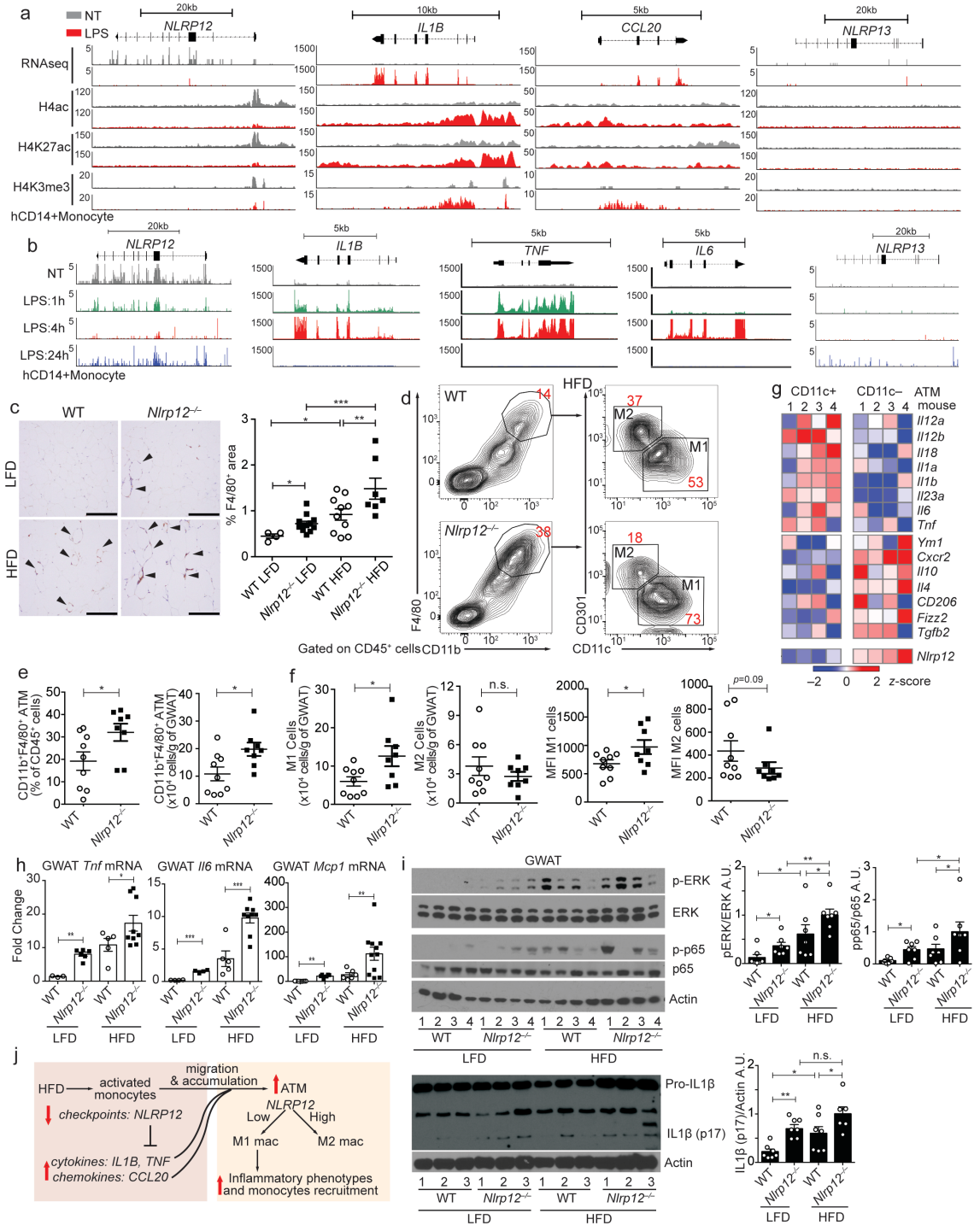

Fig. 3.6. NLRP12 represses macrophage infiltration and inflammation in adipose tissue. (**a**) Peak distributions of RNA-seq at the exons and ChIP-seq at the promoters of *NLRP12*, *IL1B*, *CCL20* and *NLRP13* genes in primary human CD14+ monocytes left non-treated (NT, grey) or given LPS (red). (**b**) RNAseq peak distribution at the exons of

the *NLRP12*, *IL1B*, *TNF, IL6* and *NLRP13* genes in untreated primary human CD14+ monocytes for 1, 4 or 24 hours after LPS stimulation. (**c**) Representative F4/80+ immunohistochemical staining of GWAT from LFD/HFD-fed WT and *Nlrp12*$^{-/-}$ mice (scale bar = 200 μm), with composite percentage of F4/80+ cells (right panel) (WT LFD, n=4; *Nlrp12*$^{-/-}$ LFD, n=8; WT HFD, n=10; *Nlrp12*$^{-/-}$, n=7). (**d**) Representative concatenated FACS plots of cells bearing M1 vs. M2 macrophage markers, with composite quantification of (**e**) GWAT resident macrophage subpopulations and (**f**) mean fluorescence intensity (MFI) of M1 cells (CD11c+ CD301–) and M2 (CD11c– CD301+) from HFD-fed WT and *Nlrp12*$^{-/-}$ mice (WT HFD, n=9; *Nlrp12*$^{-/-}$ HFD, n=8). (**g**) Heatmap of gene expression analysis of CD11c+ and CD11c– adipose tissue macrophages (ATM) isolated from WT mice. (**h**) RT-qPCR analysis of *Tnf*, *Il6* and *Mcp1* mRNA expression, and (**i**) western blots of IL1β and activated p65 and ERK with composite densitometry (n=7/group from 2 studies) from GWAT of LFD- or HFD-fed WT and *Nlrp12*$^{-/-}$ mice. (**j**) Model of NLRP12 inhibition of monocyte/macrophage inflammation and accumulation into adipose tissue. Error bars show SEM, *p<0.05, **p<0.01, *** p<0.001 and n.s. means no significance determined by Student's t test (e,f) and one-way ANOVA (h,i).

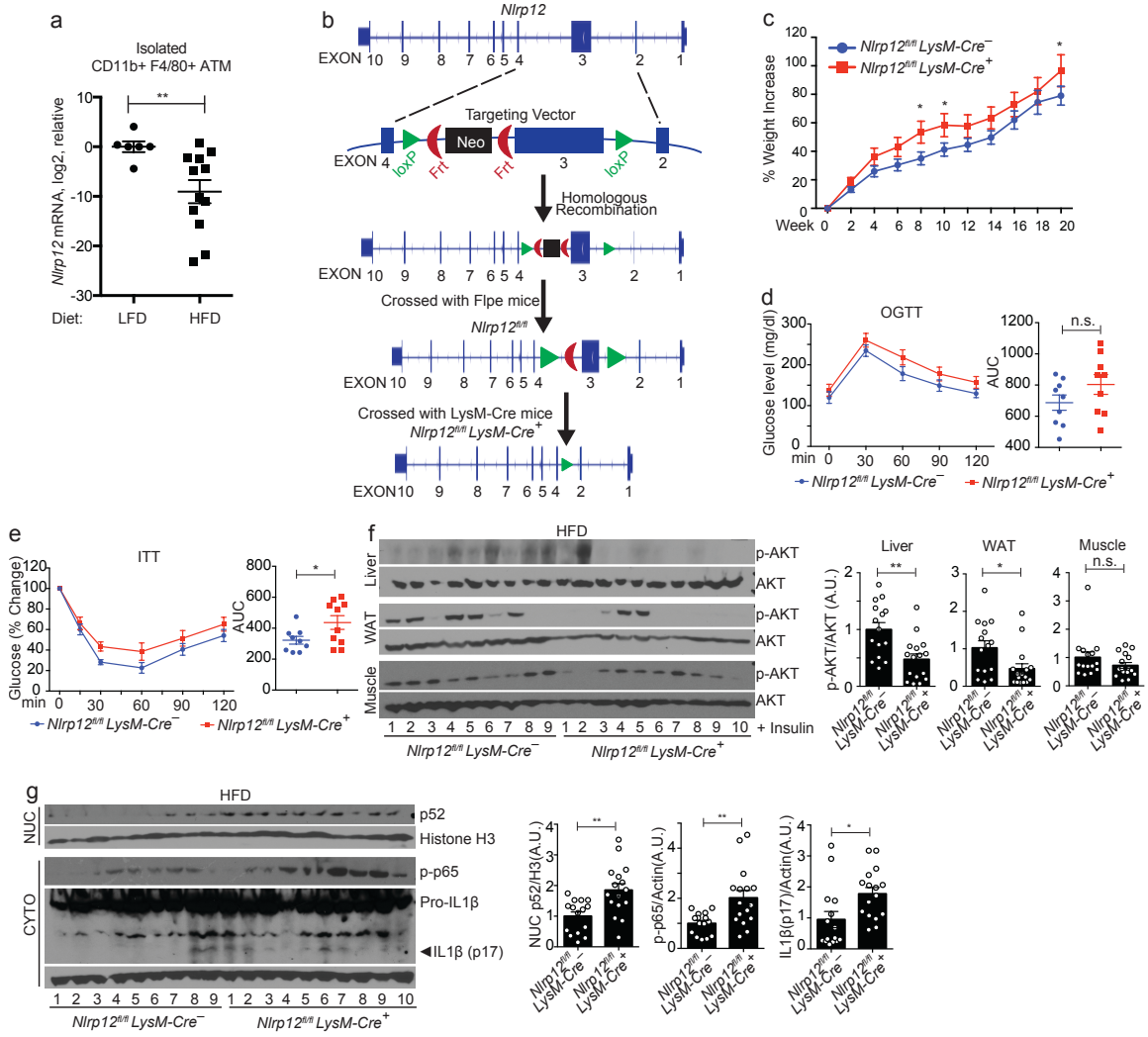

Fig. 3.7. Macrophage NLRP12 prevents obesity and adipose tissue inflammation. (**a**) RT-qPCR analysis of *Nlrp12* expression in ATMs from LFD or HFD fed WT mice. Each dot in the LFD group represents pooled ATM from 2-3 mice, and each dot in the HFD group represents one mouse (LFD WT, n=6; and HFD WT, n=12). (**b**) Schematic of generation strategy for myeloid-specific *Nlrp12*-deficient (*Nlrp12*$^{fl/fl}$ LysM-Cre^{+}) mice. (**c**) Percent weight increase in *Nlrp12*$^{fl/fl}$ LysM-Cre^{+} and *Nlrp12*$^{fl/fl}$ LysM-Cre^{-} (control) mice fed HFD for 20 weeks (*Nlrp12*$^{fl/fl}$ LysM-Cre^{+}, n=17; and *Nlrp12*$^{fl/fl}$ LysM-Cre^{-}, n=18). (**d**) Oral glucose tolerance test (OGTT) and (**e**) ITT of *Nlrp12*$^{fl/fl}$ LysM-Cre^{+} and *Nlrp12*$^{fl/fl}$ LysM-Cre^{-} mice fed HFD for 20 weeks, and western blot analysis with composite quantification of (**f**) AKT phosphorylation in liver, WAT and muscle and (**g**) nuclear p52, p65 phosphorylation and IL1β maturation in adipose tissue (*Nlrp12*$^{fl/fl}$ LysM-Cre^{+}, n=10; *Nlrp12*$^{fl/fl}$ LysM-Cre^{-}, n=9). Error bars show SEM, *p<0.05, **p<0.01 and n.s. means no significance determined by Student's t test.

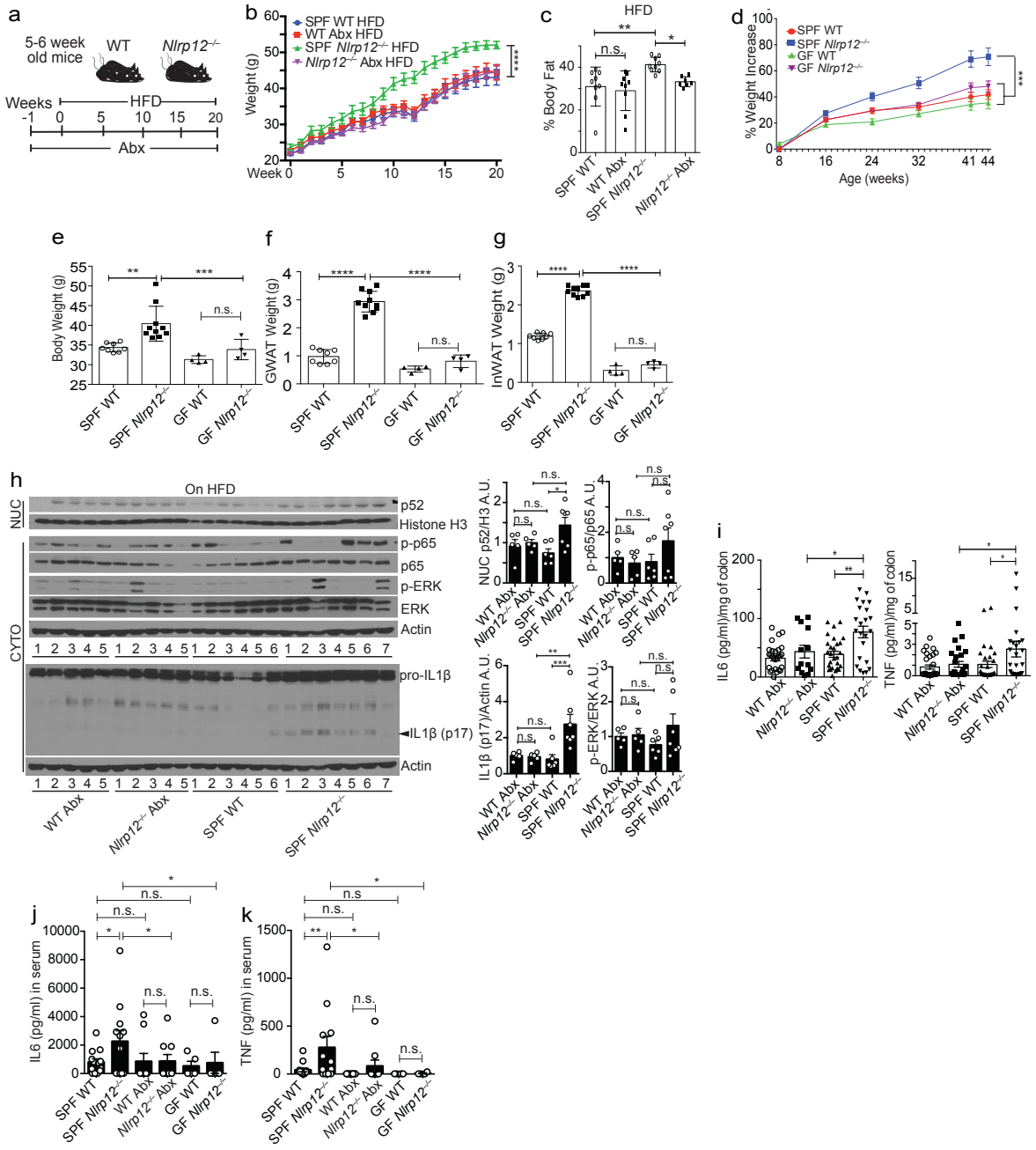

Fig. 3.8. Commensal bacteria contribute to the enhanced obesity in *Nlrp12*$^{-/-}$ mice. (**a**) Schematic of antibiotic (Abx) treatment of WT and *Nlrp12*$^{-/-}$ mice on HFD. (**b**) Body weight and (**c**) percentage body fat of mice shown in (a), (n=9/group). (**d**) Percentage weight increase in specific-pathogen-free (SPF) and germ-free (GF) WT and *Nlrp12*$^{-/-}$ mice on regular chow for 44 weeks; (**e**) Body, (**f**) GWAT and (**g**) InWAT weights of WT and *Nlrp12*$^{-/-}$ mice at week 44 post-HFD (SPF WT, n=8; *Nlrp12*$^{-/-}$ mice, n=10; GF WT and *Nlrp12*$^{-/-}$ mice, n=4/group). (**h**) Western blot analysis and quantification of assayed colonic p52, activated p65, activated ERK and IL1β (n=5-7/group), and (**i**) ELISA of IL6

and TNF from colonic explants of HFD-fed mice with or without antibiotic (Abx) treatment for 20 weeks (n=27/group). (**j**) Serum IL6 and (**k**) TNF from Abx-treated or germ-free mice. (SPF WT, n=13; SPF *Nlrp12*$^{-/-}$, n=12; Abx WT, n=10; Abx *Nlrp12*$^{-/-}$, n=9; GF WT, n=5; GF *Nlrp12*$^{-/-}$, n=5).

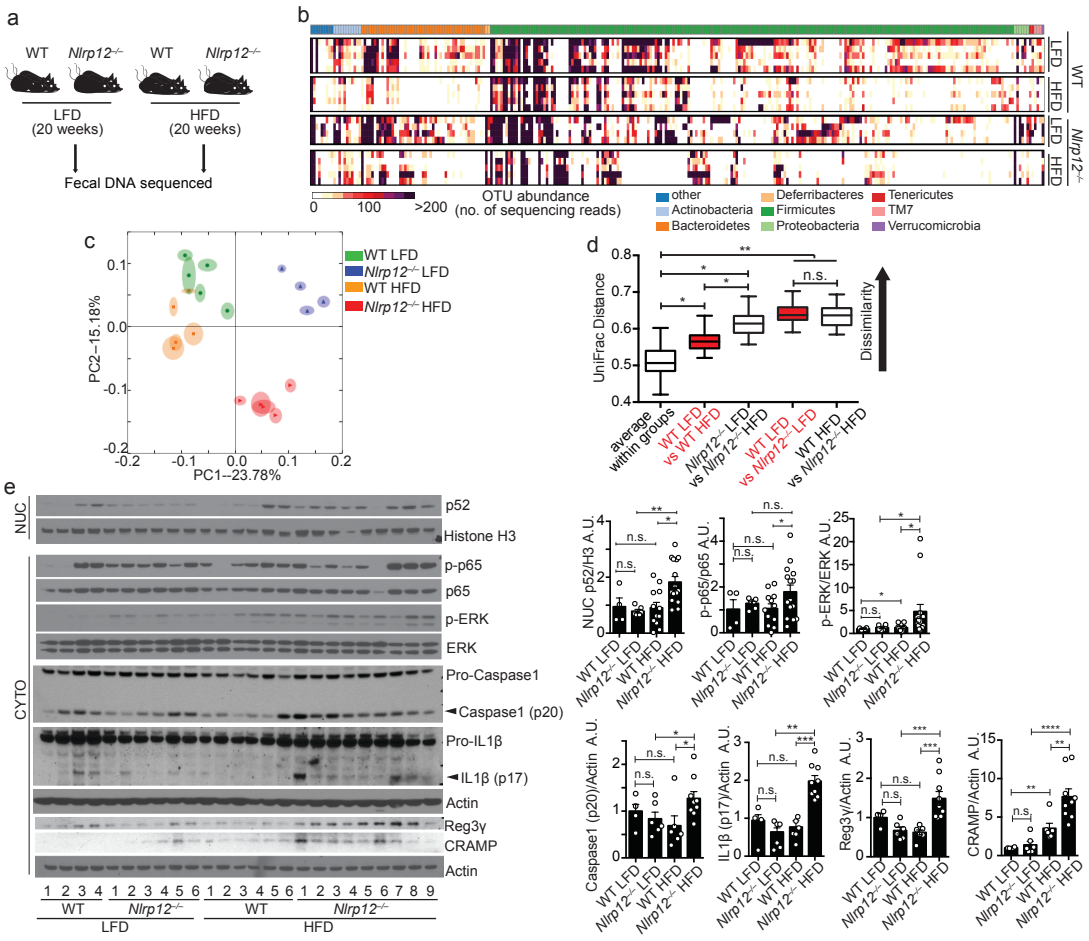

Fig. 3.9. The alteration of commensal bacteria in response to the enhanced obesity in *Nlrp12*$^{-/-}$ mice. (**a**) Schematic of fecal DNA collection from WT and *Nlrp12*$^{-/-}$ mice after 20 weeks of LFD or HFD. (**b**) Heatmap showing microbial diversity with abundance of sequenced bacterial operational taxonomic units (OTU) from fecal samples collected in (a) (n=5/group). (**c**) Principal coordinate analysis (PCoA) showing microbial unweighted UniFrac compositional differences, quantified by (**d**) UniFrac distance between WT and *Nlrp12*$^{-/-}$ mice on HFD vs. LFD. (**e**) Western blot analysis and composite densitometry of small intestine proteins from WT and *Nlrp12*$^{-/-}$ mice on HFD vs. LFD (WT LFD, n=4; *Nlrp12*$^{-/-}$ LFD, n=6; WT HFD, n=12; *Nlrp12*$^{-/-}$ HFD, n=14). Each lane or symbol represents one mouse. Error bars show SEM, *p<0.05, **p<0.01, *** p<0.001, **** p<0.0001 and n.s. means no significance determined by Student's t test (b, d) and one-way ANOVA (c, e).

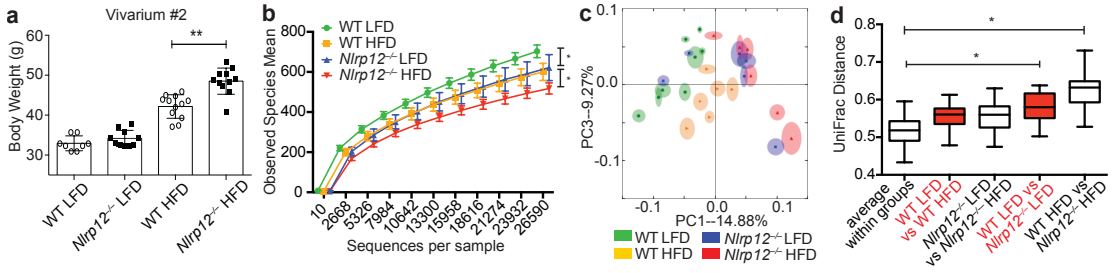

Fig. 3.10. HFD and *Nlrp12*-deficiency causes dysbiotic microbiome in a second vivarium. (**a**) Body weight of WT and *Nlrp12*$^{-/-}$ mice fed HFD or LFD for 20 weeks in a second vivarium (WT LFD, n=8; WT HFD, n=12; *Nlrp12*$^{-/-}$ LFD, n=10; *Nlrp12*$^{-/-}$ HFD, n=11). (**b**) Bacterial diversity of the microbiome from WT and *Nlrp12*$^{-/-}$ mice given LFD or HFD while housed in a second vivarium. (**c**) PCoA and (**d**) UniFrac distance showing microbiome compositional differences between WT and *Nlrp12*$^{-/-}$ mice on HFD or LFD (b-d, WT LFD, n=8; WT HFD, n=6; *Nlrp12*$^{-/-}$ LFD, n=6; *Nlrp12*$^{-/-}$ HFD, n=6). Each symbol represents one mouse. Error bars show SEM, *p<0.05, **p<0.01 and n.s. means no significance as determined by one-way ANOVA (a) and Student's t test (d).

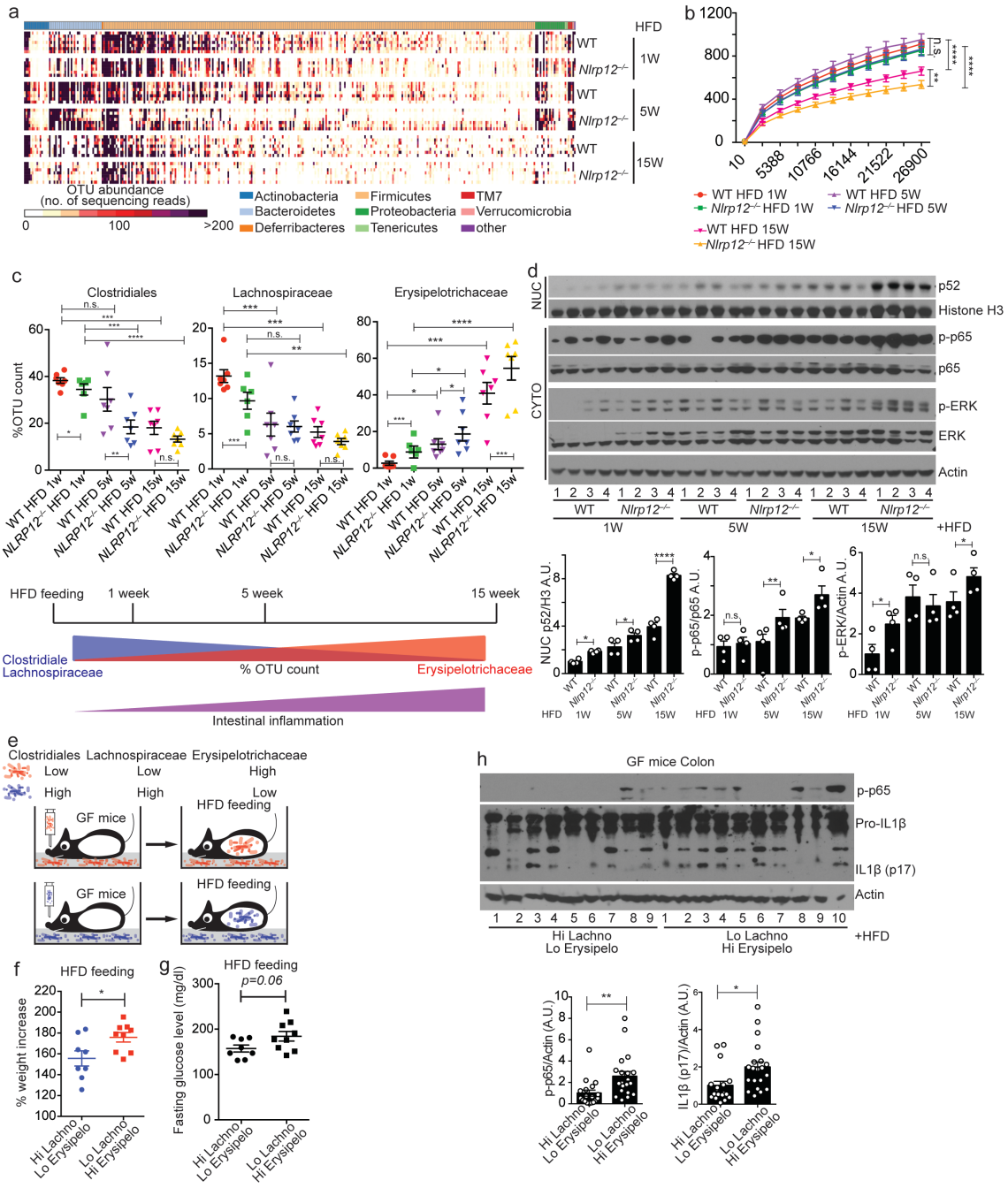

Fig 3.11. HFD induces the development of obesogenic microbial dysbiosis at the early stage of obesity. (**a**) Heatmap of OTU abundance indicating (**b**) bacterial diversity, and (**c**) relative abundance of substantially changed bacterial groups identified by 2-way ANOVA on all sequenced bacteria in fecal samples collected from WT and *Nlrp12*$^{-/-}$ mice at 1 week, 5 weeks and 15 weeks post-HFD feeding (n=6-7/group). (**d**) Western blot analysis and densitometry of colon proteins from WT and *Nlrp12*$^{-/-}$ mice at 1 week, 5 weeks and 15 weeks post-HFD feeding (n=4). **(e)** Experimental schematic of

germ-free WT mice inoculated with fecal contents containing high bacterial diversity and relative abundance of Clostridiales and Lachnospiraceae, but low Erysipelotrichaceae, compared to mice receiving feces containing low bacterial diversity and proportion of Clostridiales and Lachnospiraceae, but high Erysipelotrichaceae. **(f)** Percent weight increase and **(g)** fasting glucose levels of mice in (e) after 20 weeks of HFD feeding; and (**h**) western blot analysis and densitometry of activated p65 and IL1β from the colons of mice in (e), (e-h, n=9-10/group). Each symbol or lane represents one mouse. Error bars show SEM, *p<0.05, **p<0.01, *** p<0.001, **** p<0.0001 and n.s. means no significance as determined by Student's t test.

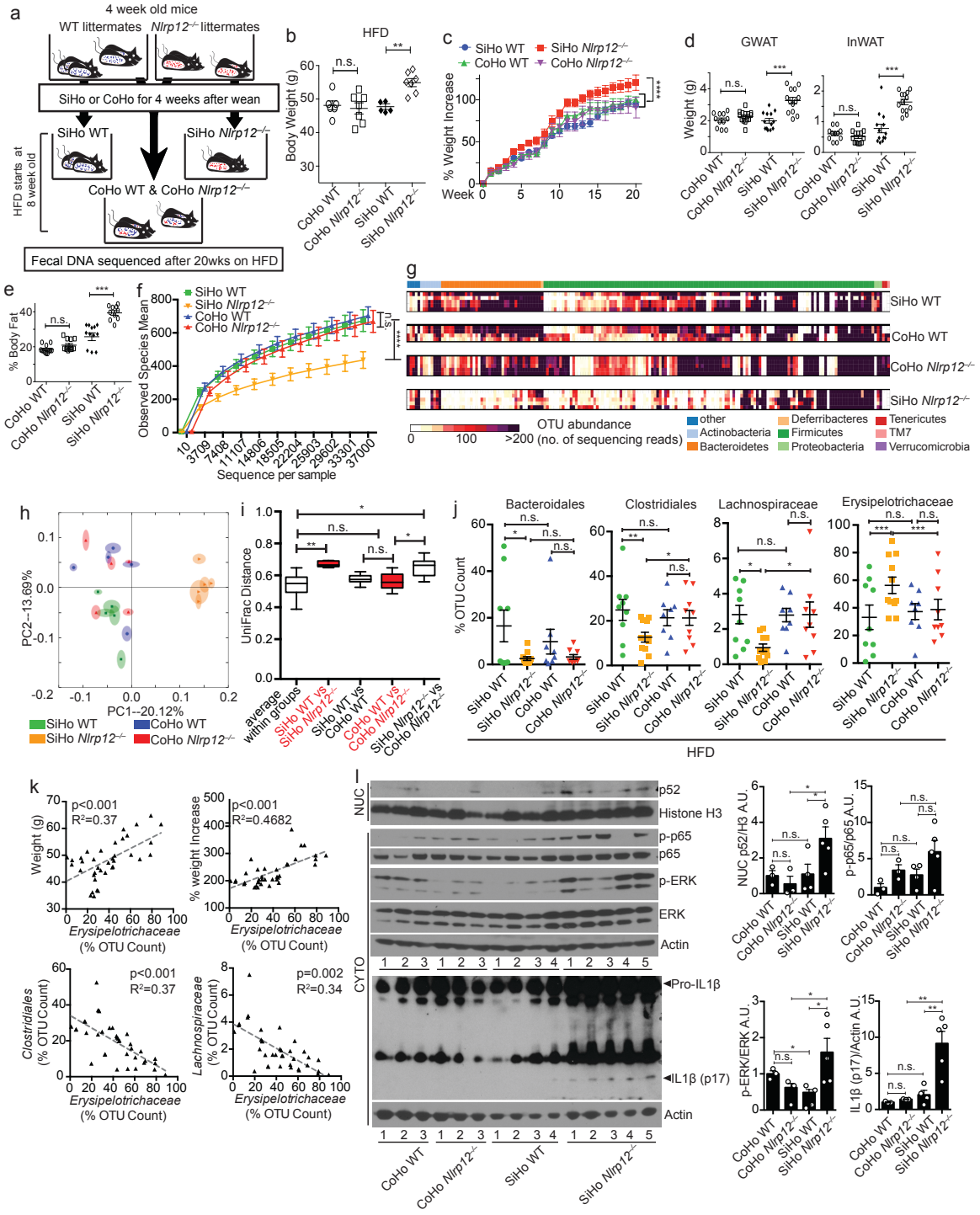

Fig. 3.12. *Nlrp12*$^{-/-}$ mice cohoused with WT mice show attenuated weight gain and inflammation with reduced dysbiosis. (**a**) Illustration of cohoused (CoHo) and single-housed (SiHo) WT and *Nlrp12*$^{-/-}$ mice on HFD for 20 weeks with sequencing of fecal DNA. (**b**) Body weight and (**c**) percent weight increase of animals shown in (a) (CoHo WT, n=6; CoHo *Nlrp12*$^{-/-}$, n=7; SiHo WT, n=5; SiHo *Nlrp12*$^{-/-}$, n=7); **(d)** GWAT and

InWAT weight, and **(e)** percentage body fat of SiHo and CoHo WT and *Nlrp12*$^{-/-}$ mice fed HFD for 20 weeks (CoHo WT, n=11; CoHo *Nlrp12*$^{-/-}$, n=12; SiHo WT, n=12; SiHo *Nlrp12*$^{-/-}$, n=13). (**f**) Bacterial diversity and (**g**) heatmap of OTU abundance of fecal microbiome from WT and *Nlrp12*$^{-/-}$ mice after 20 weeks on HFD; (**h**) PCoA plot with (**i**) UniFrac distances showing microbiome compositional differences. (n=5/group). (**j**) Composite results of substantially changed bacterial groups identified by 2-way ANOVA from all sequenced fecal bacteria isolated from SiHo or CoHo WT and *Nlrp12*$^{-/-}$ mice described in (a). (SiHo WT, n=9; SiHo *Nlrp12*$^{-/-}$, n=11; CoHo WT, n=9; CoHo *Nlrp12*$^{-/-}$, n=9). (**k**) Correlation analysis between Erysipelotrichaceae and weight gain or between Clostridiales and Lachnospiraceae in mice fed HFD (n=34). (**l**) Western blot analysis and densitometry of intestinal proteins from mice described in (a) (CoHo WT, n=3; CoHo *Nlrp12*$^{-/-}$, n=3; SiHo WT, n=4; SiHo *Nlrp12*$^{-/-}$, n=5). Each lane or symbol represents one mouse. Error bars show SEM, *p<0.05, **p<0.01, *** p<0.001, **** p<0.0001 and n.s. means no significance determined by Student's t test (c, f, i) and one-way ANOVA (b, d, l).

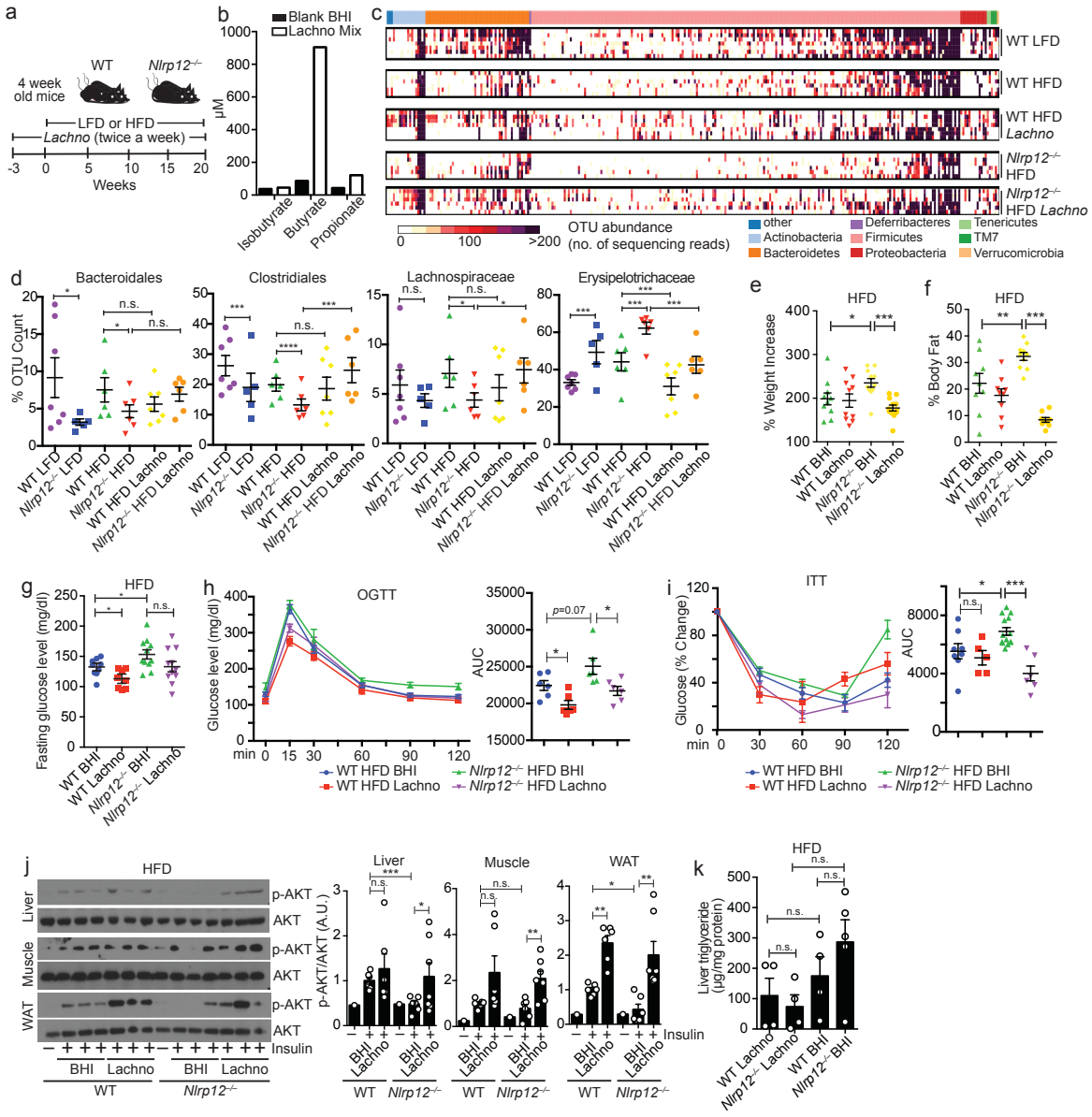

Fig. 3.13. Treatment with SCFA-producing Lachnospiraceae ameliorates weight gain and restores commensal diversity. (**a**) Schematic of Lachnospiraceae (Lachno) vs. control (BHI) treatment of WT and *Nlrp12*$^{-/-}$ mice on LFD or HFD. (**b**) Isobutyrate, butyrate and propionate production by Lachno cultures determined by Mass spectrometry. (**c**) Heatmap of OTU abundance indicating bacterial diversity and (**d**) relative abundance of substantially changed bacterial groups identified by 2-way ANOVA on all sequenced bacteria in fecal samples from mice in (a), (WT LFD, n=7; *Nlrp12*$^{-/-}$ LFD, n=5; WT HFD, n=6; *Nlrp12*$^{-/-}$ HFD, n=6; WT HFD Lachno, n=7; *Nlrp12*$^{-/-}$ HFD Lachno, n=6). (**e**) Percent weight increase and (**f**) percent body fat of WT and *Nlrp12*$^{-/-}$ mice in (a), (n=10/groups). (**g**) Fasting glucose levels (WT HFD, n=9; *Nlrp12*$^{-/-}$

HFD, n=11; WT HFD Lachno, n=9; *Nlrp12*$^{-/-}$ HFD Lachno, n=11), (**h**) OGTT (n=6/group) and (**i**) ITT (WT HFD, n=8; *Nlrp12*$^{-/-}$ HFD, n=13; WT HFD Lachno, n=5; *Nlrp12*$^{-/-}$ HFD Lachno, n=6) of HFD-fed mice with Lachno or BHI, with (**j**) representative western blots and composite densitometry of phosphorylation of AKT in liver, muscle and WAT following treatment of 0.7 U/kg of insulin (n=6-7/group). (**k**) Intrahepatic triglyceride (TG) content in HFD-fed mice given Lachno or BHI (n=4/group). Each lane or symbol represents one mouse. Error bars show SEM, *p<0.05, **p<0.01, *** p<0.001, **** p<0.0001 and n.s. means no significance determined by one-way ANOVA.

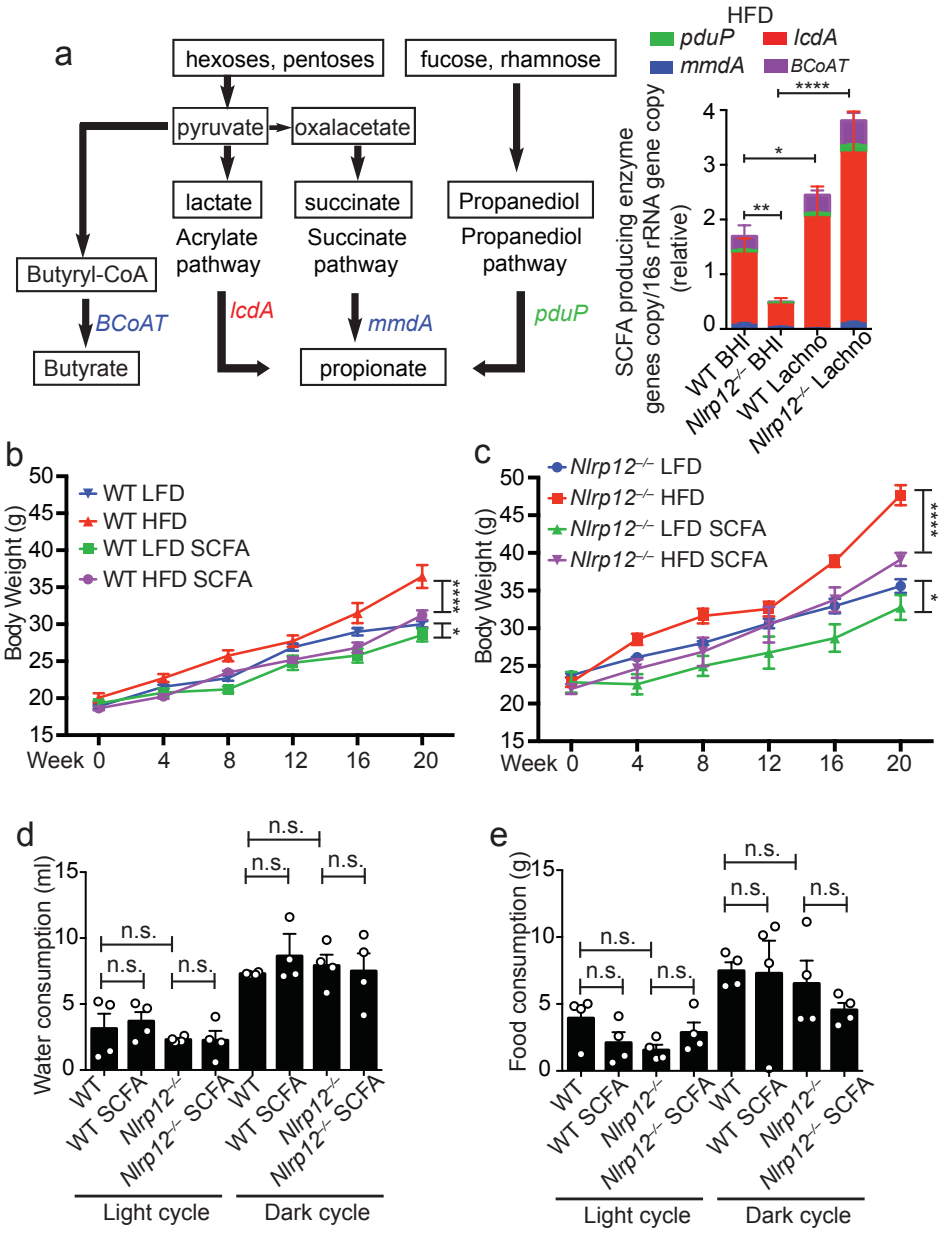

Fig. 3.14. Lachnospiraceae prevents diet-induced obesity via SFCA production. (**a**) Schematic of SCFA propionate and butyrate synthesis pathways utilized by bacteria (**Left**). Relative genomic DNA copy number of the key enzymes of propionate and butyrate synthesis normalized to total bacterial 16S rRNA gene copy number (**Right**) in the fecal microbial DNA from mice treated with Lachnospiraceae (Lachno) or BHI (*mmdA*: methylmalonyl-CoA decarboxylase, *lcdA*: lactoyl-CoA dehydratase, *pduP*: propionaldehyde dehydrogenase, and BCoAT: butyryl-CoA transferase), (WT Lachno, n=9; *Nlrp12*$^{-/-}$ Lachno, n=9; WT BHI, n=19; *Nlrp12*$^{-/-}$ BHI, n=17). (**b**) Body weight of WT and (**c**) *Nlrp12*$^{-/-}$ mice on LFD vs. HFD treated with or without propionate and butyrate (SCFAs) (n=5/group). (**d**) Water and (**e**) food consumption of WT and *Nlrp12*$^{-/-}$ mice

given HFD with or without SCFAs, (n=5/group). Error bars show SEM, *p<0.05, **p<0.01 **** p<0.0001 and n.s. means no significance determined by Student's t test (b, c) and one-way ANOVA (a, d, e).

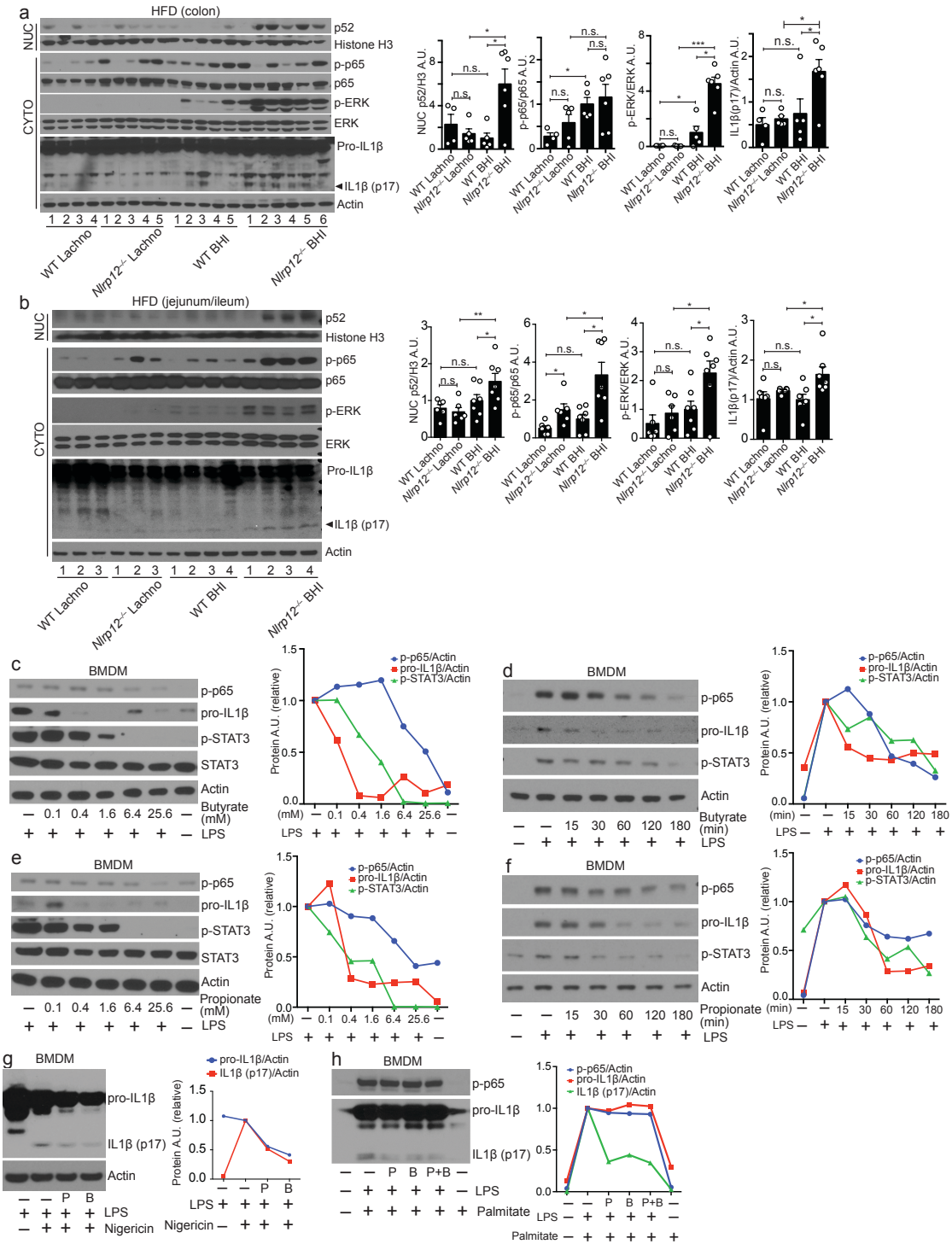

Fig. 3.15 Lachnospiraceae-derived short chain fatty acids attenuate inflammation induced by HFD and LPS. Representative western blots and composite densitometry of (**a**) colon (WT Lachno, n=4; *Nlrp12*$^{-/-}$ Lachno, n=5; WT BHI, n=5; *Nlrp12*$^{-/-}$ BHI, n=6) and (**b**) small intestinal (WT Lachno, n=6; *Nlrp12*$^{-/-}$ Lachno, n=6; WT BHI, n=7; *Nlrp12*$^{-/-}$

BHI, n=7) proteins from HFD-fed mice inoculated with Lachno or BHI. (**c-f**) Dose-response and kinetic analysis of WT bone marrow-derived macrophages (BMDMs) pretreated with propionate (P) or butyrate (B) followed by LPS (100 ng/ml) stimulation. Levels of pro-IL1β and phosphorylated p65 and STAT3 were measured by western blot analysis with densitometry. (**g**) Western blot analysis of pro-IL1β, IL1β (p17) and p-p65 in WT BMDMs untreated or treated with 6.4 mM of P or B for 1hr followed by 100 ng/ml of LPS and 1 μM of Nigericin stimulation. (**h**) Western blot analysis of pro-IL1β, IL1β (p17) and p-p65 in WT BMDMs primed with LPS for 3 hr, followed by a 24 hr stimulation with 0.2 mM of palmitate with or without P or/and B. Error bars show SEM, *p<0.05, **p<0.01, *** p<0.001, **** p<0.0001 and n.s. means no significance as determined using one way ANOVA.

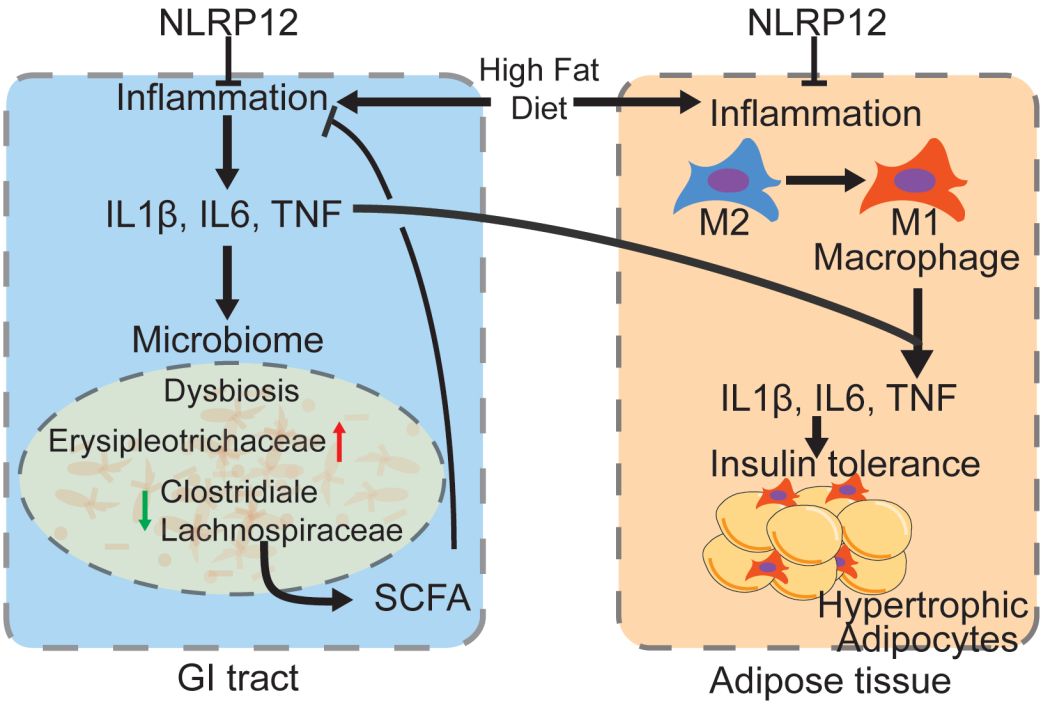

Fig. 3.16. Graphical abstract. NLRP12 suppresses diet-induced inflammation, commensal dysbiosis, M1 macrophage polarization, insulin tolerance and obesity via interactions with the intestinal microbiota that promote microbial SCFA production.

[3]CHAPTER 4: CONCLUSIONS AND PERSPECTIVES

4.1 SUMMARY OF FINDINGS

This thesis provides evidence that suggests NLRP12 expression in the mucosal tissue is negatively correlated with colitis severity in UC patients by analyzing multiple gene profiling studies comparing active UC and inactive UC. Furthermore, commensal bacteria were shown to be pivotal for the increased colitis severity in *Nlrp12*$^{-/-}$ mice. We attributed this commensal bacteria-induced basal inflammation to the NLRP12-deficient hematopoietic cell compartment (such as CD11c^{+} macrophages and DCs). In addition, we found this augmented basal inflammation and drove a dysbiotic microbiome manifested by a loss of diversity and protective stains (Clostridiales and Lachnospiraceae), but increased abundance of colitogenic strains (Erysipelotrichaceae) in *Nlrp12*$^{-/-}$ mice. In this fashion, both the genetic defects of NLRP12 and the consequent dysbiotic microbiome worked together to achieve a full pathology. Finally, we found cohousing with WT mice or treating mice with Lachnospiraceae can attenuate colitis severity.

[3] The Further Questions section contains the research plans proposed by Dr. Jenny PY Ting and listed in her research grants.

In addition to colitis, we extended our knowledge of NLRP12 to obesity. We found that *NLRP12* expression in human adipose tissue was relatively lower in the high BMI population, and *Nlrp12*$^{-/-}$ mice were more prone to high-fat-diet (HFD) induced obesity and insulin tolerance. Loss of *Nlrp12* caused excessive systemic inflammation fueled by the HFD, which further generated a skewed gut microbiome composition. This skewed gut microbiome promoted obesity in *Nlrp12*$^{-/-}$ mice, and restoration of the decreased beneficial strains by cohousing with WT mice or Lachnospiraceae inoculation attenuated obesity progression and improved insulin sensitivity. Finally, we characterized our isolated Lachnospiraceae cultures and showed that it produced anti-inflammatory short-chain-fatty-acids (SCFA) and promoted IL10 secretion. Accordingly, we found that feeding mice with Lachnospiraceae suppressed the intestinal inflammation caused by HFD and *Nlrp12*-deficiency, and restricted obesity with improved insulin sensitivity.

4.2 FURTHER QUESTIONS

Examine if NLRP12 functions as a nuclear transcriptional suppressor.

Coupled with interferon regulatory factor 4 (IRF4), NLRP3 is able to bind nuclear DNA at the promoter and enhancer regions of the IL4 gene to turn on its transcription in activated Th2 cells (Bruchard, Rebe et al. 2015). Similarly, by performing confocal microscopy analysis and nuclear protein extraction, others in our lab have preliminary

evidence to suggest that NLRP12 is found in both the nucleus and cytoplasm. Additionally, bioinformatics analysis shows that NLRP12 may contain a nuclear localization sequence (NLS). Furthermore, we have found that NLRP12-deficiency caused altered gene regulation (e.g., *Ppar*-γ) by microarray analysis. NLRP12 expression in human monocytes is down-regulated at 2-4 hour after LPS or TNF stimulation, but is restored at 6-24h post stimulation, which negatively correlates with the expression of proinflammatory cytokines (e.g., IL1B, IL6 and TNF). Thus, it is reasonable to hypothesize that NLRP12 might function as a nuclear protein that suppresses pro-inflammatory gene transcription. Utilizing next-generation RNA sequencing methods to investigate the transcriptomic change caused by *Nlrp12-deficiency* after various stimulation, it is possible to identify genes and pathways that are affected by NLRP12 at the transcriptional level. Combining RNA-seq with ChIP-seq analysis will help us identify gene and binding regions within the genome which are regulated by NLRP12. However, commercial antibodies for most NLRs are not effective, which prevents us from stringently investigating the function of endogenous NLRs. With the advent of Crispr/Cas9 technology, we can engineer multiple tags into NLR genes and then perform Co-IP and ChIP-seq analysis to understand the endogenous function of NLR proteins. Thus far, we are aiming to engineer an endogenously tagged NLRP12 with a triple FLAG tag in the THP1 cell line where I found the expression of NLRP12 was downregulated after LPS and TNF stimulation but was later restored at 24 hours

post stimulation. Using this strategy, we hope to identify the binding region of endogenous NLRP12 to nucleic acids and dissect if it regulates gene transcription.

Determine the contribution of NLRP12 in different immune cell populations to the development of colitis and obesity.

Although we have previously demonstrated that both hematopoietic and non-hematopoietic cell components contribute to the onset of colon inflammation and colorectal carcinoma, NLRP12 has been found to be expressed mainly in human monocytes and neutrophils (data source: www.biogps.com). In addition, we have found that *Nlrp12* expression in mucosal tissues is inversely correlated with colitis severity by examining multiple databases, which compared tissues from active UC and inactive UC patients. However, since the mucosal tissue is comprised of multiple types of cells, it is still unclear which cells are affected by the loss of Nlrp12 function leading to inflammatory disease development. This raises the need to determine the expression of NLRP12 in different immune cells from active IBD and healthy biopsy. Additionally, early immune cell microarray studies (e.g., https://www.immgen.org/) use Affymetrix MoGene 1.0 ST microarray, which does not contain the probes for NLRP12, therefore it is important to fill this gap by revisiting these cells for NLRP12 expression with new platforms that can survey the entire transcriptome. Our lab has successfully generated cell-specific *Nlrp12* knockout mice. These mice should allow us to verify how *Nlrp12* within subpopulations contributes to disease development and microbiome dysbiosis.

So far, we have generated mice with *Nlrp12*-specific deletion in macrophages (LysM-Cre) and dendritic cells (CD11c-Cre). Our preliminary data show that increased NF-kB activity caused by *Nlrp12*-deficiency also induces more anti-inflammatory IL10 secretion by the colon lamina propria CD11b+ CD11c-macrophages, but not the CD11c+ macrophages and DCs. In another spontaneous colitis model, others in the lab have found that *Nlrp12*$^{-/-}$*Il10*$^{-/-}$ mice develop more severe colitis than wild type mice. Therefore, depletion of Nlrp12 in CD11c+ macrophages and DCs might further exacerbate colitis comparable to that observed in the conventional whole body knock out mice.

Delineate the role of NLRP12 in the dysbiosis-obesity-tumorogenesis axis.

We and others found that *Nlrp12*$^{-/-}$ mice developed exacerbated colitis and inflammatory-driven tumorogenesis in the AOM-DSS model (Allen, Wilson et al. 2012),(Zaki, Vogel et al. 2011). NF-κB activation is a crucial tumor promoter in inflammation-induced colon cancer (Greten et al., 2004; Pikarsky et al., 2004), and NLRP12 can inhibit both canonical and non-canonical NF-κB pathways by reducing IRAK1 and NIK activation via ubiquitination-mediated degradation (Williams, Lich et al. 2005, Lich, Williams et al. 2007). Inflammation and NF-κB activation are also promoters of obesity (Baker, Hayden et al. 2011). Our data showed that Nlrp12 also mitigates HFD-induced obesity development and insulin tolerance. We also found a negative

correlation of *Nlrp12* expression with murine inflammatory cytokine gene expression (e.g., *Mcp1, Il6, Tnf*) in adipose tissue macrophages, which implicates a role for *Nlrp12* in mitigating the risk of obesity and obesity-related inflammation. Our preliminary data also showed that there were increased adenomas in *Nlrp12*-deficient mice treated with HFD/AOM that were followed for more than one year. However, the AOM colorectal tumor model involves a chemical hazard treatment which does not represent spontaneous tumorigenesis observed in the clinic. It is more clinically relevant to study the impact of *Nlrp12* deletion on HFD-induced tumorigenesis using a spontaneous cancer model, such as the HFD-*Apc*$^{+/min}$ obesity-driven colorectal cancer models, where a HFD promotes the abnormal proliferation of the intestinal stem cells carrying the *Apc* gene mutation. (Beyaz, Mana et al. 2016).

Our data indicate that NLRP12 has a profound effect in maintaining commensal bacterial diversity and protective bacterial groups during DSS-induced colitis (Chen, Wilson et al. 2017) and diet induced obesity. However, it is unknown whether the microbiota derived from *Nlrp12*-deficiency affects colorectal cancer development. In this dissertation, we show that *Nlrp12*$^{-/-}$ mice raised under SPF but not germ-free (GF) conditions gained more weight than controls, and cohousing of *Nlrp12*$^{-/-}$ mice with WT controls reduced this weight gain, implicating the role of the microbiome in regulating obesity. *Nlrp12*$^{-/-}$ mice have reduced Clostridiales and Lachnospiraceae and oral gavage of *Nlrp12*$^{-/-}$ mice with these bacterial groups limited obesity. This provides

compelling rationale for using germ-free animal and a cohousing strategy to dissect the role of microbiota in obesity-induced colorectal cancer. First, we are planning to generate germ-free *Apc*$^{+/min}$ mice as the recipient for the obesity-promoting microbiota and normal microbiota. Most recently, I have preliminary data to suggest that inoculation of obesity-promoting fecal contents, with a high proportion of Erysipelotrichaceae, induced more IL-1β in both the colon and small intestine of germ-free mice, which indicates that the Erysipelotrichaceae bacterial group might favor tumorigenesis in germ-free *Apc*$^{+/min}$ mice. Concomitantly, we are generating *Nlrp12*$^{-/-}$ *Apc*$^{+/min}$ mice to test if HFD will induce more tumorigenesis in these mice compared to the control *Apc*$^{+/min}$ mice. Since we have shown that commensal bacteria differentiate the healthy versus inflammatory intestines in WT and *Nlrp12*$^{-/-}$ mice respectively, we also want to use antibiotic treatment and a cohousing strategy to test if this finding is still true for the tumorigenesis of *Nlrp12*$^{-/-}$ *Apc*$^{+/min}$ and control *Apc*$^{+/min}$ mice.

Determine the functional pathways and metabolites of a dysbiotic microbiome that is a result of increased intestinal inflammation and diet-induced obesity.

In this dissertation, we applied bacterial 16S ribosomal RNA (rRNA) genes sequencing and identified the microbiome diversity and taxonomic changes due to Nlrp12-deficiency-associated colitis and obesity. We unveiled the disease-associated microbiome landscape characterized by a loss of diversity, decreased Clostridiales and Lachnospiraceae, and increased Erysipelotrichaceae. However, we do not know how

the bacterial pathways are changed due to these altered microbiome patterns, as the sequence of the bacterial 16S rRNA gene does not capture the microbial gene expression in response to the inflammatory gut environment and HFD feeding. Therefore, high throughput microbial RNA (metatranscriptome) sequencing will rapidly become the method of choice for revealing the gene regulation and the functional pathways in the gut (McNulty, Yatsunenko et al. 2011). We want to apply this new sequencing method to expand our microbiome finding with more insights into mechanism. In the end, we also hope to perform metabolome analysis to identify metabolic products that affect downstream colitis and obesity. The final step is to test the metabolic products in the appropriate mouse model to identify potential beneficial compounds that may alleviate IBD and obesity.

5.3 CONCLUDING REMARKS

This dissertation mainly focuses on the central theme of understanding the roles of the microbiome in colitis and diet induced obesity (DIO) caused by the loss of the *Nlrp12* gene. The first half of the research centered on the identification of the skewed commensal bacterial composition due to the increased basal inflammation caused by a loss of the inhibitory function of NLRP12. We investigated the contribution from commensal dysbiosis to the exacerbated intestinal inflammation in the *Nlrp12*-deficient context by performing a cohousing and reciprocal fecal transplant experiment, and

identified a beneficial bacterial group as a potential colitis treatment. The second half of the research focused on the investigation of the protective role of NLRP12 during diet-induced obesity (DIO) and the therapeutic potential of short chain fatty acid producing Lachnospiraceae for DIO management. These studies revealed that colitis and obesity promoted by *Nlrp12*-deficiency are fueled by the dysbiotic commensal bacterial changes caused by increased inflammation. Our findings also point to potential future directions to evaluate the role of NLRP12 in obesity-induced colorectal tumorigenesis and provide evidence to support the idea that targeting the commensal bacteria may lead to improved IBD and obesity treatment.

REFERENCES:

Abe, T., et al. (2017). "Germ-Cell-Specific Inflammasome Component NLRP14 Negatively Regulates Cytosolic Nucleic Acid Sensing to Promote Fertilization." Immunity **46**(4): 621-634.

Aganna, E., et al. (2002). "Association of mutations in the NALP3/CIAS1/PYPAF1 gene with a broad phenotype including recurrent fever, cold sensitivity, sensorineural deafness, and AA amyloidosis." Arthritis Rheum **46**(9): 2445-2452.

Agostini, L., et al. (2004). "NALP3 forms an IL-1beta-processing inflammasome with increased activity in Muckle-Wells autoinflammatory disorder." Immunity **20**(3): 319-325.

Ahmad, M. S., et al. (2000). "Butyrate and glucose metabolism by colonocytes in experimental colitis in mice." Gut **46**(4): 493-499.

Allen, I. C. (2014). "Non-Inflammasome Forming NLRs in Inflammation and Tumorigenesis." Front Immunol **5**: 169.

Allen, I. C., et al. (2012). "Characterization of NLRP12 during the development of allergic airway disease in mice." PLoS One **7**(1): e30612.

Allen, I. C., et al. (2011). "NLRX1 protein attenuates inflammatory responses to infection by interfering with the RIG-I-MAVS and TRAF6-NF-kappaB signaling pathways." Immunity **34**(6): 854-865.

Allen, I. C., et al. (2012). "NLRP12 suppresses colon inflammation and tumorigenesis through the negative regulation of noncanonical NF-kappaB signaling." Immunity **36**(5): 742-754.

Amano, S. U., et al. (2014). "Local proliferation of macrophages contributes to obesity-associated adipose tissue inflammation." Cell Metab **19**(1): 162-171.

Amer, A., et al. (2006). "Regulation of Legionella phagosome maturation and infection through flagellin and host Ipaf." J Biol Chem **281**(46): 35217-35223.

Anand, P. K., et al. (2012). "NLRP6 negatively regulates innate immunity and host defence against bacterial pathogens." Nature **488**(7411): 389-393.

Arpaia, N., et al. (2013). "Metabolites produced by commensal bacteria promote peripheral regulatory T-cell generation." Nature **504**(7480): 451-455.

Arthur, J. C., et al. (2010). "Cutting edge: NLRP12 controls dendritic and myeloid cell migration to affect contact hypersensitivity." J Immunol **185**(8): 4515-4519.

Atarashi, K., et al. (2013). "Treg induction by a rationally selected mixture of Clostridia strains from the human microbiota." Nature **500**(7461): 232-236.

Backhed, F., et al. (2004). "The gut microbiota as an environmental factor that regulates fat storage." Proc Natl Acad Sci U S A **101**(44): 15718-15723.

Baker, R. G., et al. (2011). "NF-kappaB, inflammation, and metabolic disease." Cell Metab **13**(1): 11-22.

Ballak, D. B., et al. (2014). "IL-37 protects against obesity-induced inflammation and insulin resistance." Nat Commun **5**: 4711.

Benko, S., et al. (2010). "NLRC5 limits the activation of inflammatory pathways." J Immunol **185**(3): 1681-1691.

Berry, D., et al. (2012). "Phylotype-level 16S rRNA analysis reveals new bacterial indicators of health state in acute murine colitis." ISME J **6**(11): 2091-2106.

Bertin, J., et al. (1999). "Human CARD4 protein is a novel CED-4/Apaf-1 cell death family member that activates NF-kappaB." J Biol Chem **274**(19): 12955-12958.

Beyaz, S., et al. (2016). "High-fat diet enhances stemness and tumorigenicity of intestinal progenitors." Nature **531**(7592): 53-58.

Bian, F., et al. (2017). "Inhibition of NLRP3 Inflammasome Pathway by Butyrate Improves Corneal Wound Healing in Corneal Alkali Burn." Int J Mol Sci **18**(3).

Borghini, S., et al. (2011). "Clinical presentation and pathogenesis of cold-induced autoinflammatory disease in a family with recurrence of an NLRP12 mutation." Arthritis Rheum **63**(3): 830-839.

Bouter, K. E., et al. (2017). "Role of the Gut Microbiome in the Pathogenesis of Obesity and Obesity-Related Metabolic Dysfunction." Gastroenterology.

Bruchard, M., et al. (2015). "The receptor NLRP3 is a transcriptional regulator of TH2

differentiation." Nat Immunol **16**(8): 859-870.

Bruey, J. M., et al. (2004). "PAN1/NALP2/PYPAF2, an inducible inflammatory mediator that regulates NF-kappaB and caspase-1 activation in macrophages." J Biol Chem **279**(50): 51897-51907.

Cai, X., et al. (2014). "Prion-like polymerization underlies signal transduction in antiviral immune defense and inflammasome activation." Cell **156**(6): 1207-1222.

Cani, P. D., et al. (2008). "Changes in gut microbiota control metabolic endotoxemia-induced inflammation in high-fat diet-induced obesity and diabetes in mice." Diabetes **57**(6): 1470-1481.

Carmody, R. N., et al. (2015). "Diet dominates host genotype in shaping the murine gut microbiota." Cell Host Microbe **17**(1): 72-84.

Cerovic, V., et al. (2014). "Intestinal macrophages and dendritic cells: what's the difference?" Trends Immunol **35**(6): 270-277.

Charoenthongtrakul, S., et al. (2012). "The NLRP4-DTX4 axis: a key suppressor of TBK1 and innate antiviral signaling." Cell Mol Immunol **9**(6): 431-433.

Chassaing, B., et al. (2014). "Intestinal epithelial cell toll-like receptor 5 regulates the intestinal microbiota to prevent low-grade inflammation and metabolic syndrome in mice." Gastroenterology **147**(6): 1363-1377 e1317.

Chen, G. Y., et al. (2011). "A functional role for Nlrp6 in intestinal inflammation and tumorigenesis." J Immunol **186**(12): 7187-7194.

Chen, G. Y., et al. (2008). "The innate immune receptor Nod1 protects the intestine from inflammation-induced tumorigenesis." Cancer Res **68**(24): 10060-10067.

Chen, L., et al. (2017). "NLRP12 attenuates colon inflammation by maintaining colonic microbial diversity and promoting protective commensal bacterial growth." Nat Immunol.

Chen, L., et al. (2017). "NLRP12 attenuates colon inflammation by maintaining colonic microbial diversity and promoting protective commensal bacterial growth." Nat Immunol **18**(5): 541-551.

Chen, W., et al. (2012). "Human intestinal lumen and mucosa-associated microbiota in patients with colorectal cancer." PLoS One **7**(6): e39743.

Cho, I., et al. (2012). "Antibiotics in early life alter the murine colonic microbiome and adiposity." Nature **488**(7413): 621-626.

Cho, K. W., et al. (2014). "Flow cytometry analyses of adipose tissue macrophages." Methods Enzymol **537**: 297-314.

Choi, S. M., et al. (2013). "Innate Stat3-mediated induction of the antimicrobial protein Reg3gamma is required for host defense against MRSA pneumonia." J Exp Med **210**(3): 551-561.

Cinti, S., et al. (2005). "Adipocyte death defines macrophage localization and function in adipose tissue of obese mice and humans." J Lipid Res **46**(11): 2347-2355.

Corridoni, D., et al. (2014). "The Dual Role of Nod-Like Receptors in Mucosal Innate Immunity and Chronic Intestinal Inflammation." Front Immunol **5**.

Couturier-Maillard, A., et al. (2013). "NOD2-mediated dysbiosis predisposes mice to transmissible colitis and colorectal cancer." J Clin Invest **123**(2): 700-711.

Cui, J., et al. (2012). "NLRP4 negatively regulates type I interferon signaling by targeting the kinase TBK1 for degradation via the ubiquitin ligase DTX4." Nat Immunol **13**(4): 387-395.

Cui, J., et al. (2010). "NLRC5 negatively regulates the NF-kappaB and type I interferon signaling pathways." Cell **141**(3): 483-496.

Davis, B. K., et al. (2011). "Cutting edge: NLRC5-dependent activation of the inflammasome." J Immunol **186**(3): 1333-1337.

Davis, B. K., et al. (2011). "The inflammasome NLRs in immunity, inflammation, and associated diseases." Annu Rev Immunol **29**: 707-735.

den Besten, G., et al. (2013). "The role of short-chain fatty acids in the interplay between diet, gut microbiota, and host energy metabolism." J Lipid Res **54**(9): 2325-2340.

Denning, T. L., et al. (2007). "Lamina propria macrophages and dendritic cells differentially induce regulatory and interleukin 17-producing T cell responses." Nat Immunol **8**(10): 1086-

1094.

Deshmane, S. L., et al. (2009). "Monocyte chemoattractant protein-1 (MCP-1): an overview." J Interferon Cytokine Res **29**(6): 313-326.

Dey, N., et al. (2013). "Association of gut microbiota with post-operative clinical course in Crohn's disease." BMC Gastroenterol **13**: 131.

Dicksved, J., et al. (2008). "Molecular analysis of the gut microbiota of identical twins with Crohn's disease." ISME J **2**(7): 716-727.

Dinh, D. M., et al. (2015). "Intestinal microbiota, microbial translocation, and systemic inflammation in chronic HIV infection." J Infect Dis **211**(1): 19-27.

Divoux, A., et al. (2010). "Fibrosis in human adipose tissue: composition, distribution, and link with lipid metabolism and fat mass loss." Diabetes **59**(11): 2817-2825.

Duncan, S. H., et al. (2002). "Acetate utilization and butyryl coenzyme A (CoA):acetate-CoA transferase in butyrate-producing bacteria from the human large intestine." Appl Environ Microbiol **68**(10): 5186-5190.

Eckburg, P. B., et al. (2005). "Diversity of the human intestinal microbial flora." Science **308**(5728): 1635-1638.

Elinav, E., et al. (2011). "NLRP6 inflammasome regulates colonic microbial ecology and risk for colitis." Cell **145**(5): 745-757.

Fan, R., et al. (2016). "Loss of the co-repressor GPS2 sensitizes macrophage activation upon metabolic stress induced by obesity and type 2 diabetes." Nat Med **22**(7): 780-791.

Feldmann, J., et al. (2002). "Chronic infantile neurological cutaneous and articular syndrome is caused by mutations in CIAS1, a gene highly expressed in polymorphonuclear cells and chondrocytes." Am J Hum Genet **71**(1): 198-203.

Feng, H., et al. (2017). "NLRX1 promotes immediate IRF1-directed antiviral responses by limiting dsRNA-activated translational inhibition mediated by PKR." Nat Immunol **18**(12): 1299-1309.

Fiorentino, L., et al. (2002). "A novel PAAD-containing protein that modulates NF-kappa B

induction by cytokines tumor necrosis factor-alpha and interleukin-1beta." J Biol Chem **277**(38): 35333-35340.

Flegal, K. M., et al. (2012). "Prevalence of obesity and trends in the distribution of body mass index among US adults, 1999-2010." JAMA **307**(5): 491-497.

Fleissner, C. K., et al. (2010). "Absence of intestinal microbiota does not protect mice from diet-induced obesity." Br J Nutr **104**(6): 919-929.

Fontalba, A., et al. (2007). "NLRP2, an inhibitor of the NF-kappaB pathway, is transcriptionally activated by NF-kappaB and exhibits a nonfunctional allelic variant." J Immunol **179**(12): 8519-8524.

Franchi, L., et al. (2006). "Cytosolic flagellin requires Ipaf for activation of caspase-1 and interleukin 1beta in salmonella-infected macrophages." Nat Immunol **7**(6): 576-582.

Fransen, F., et al. (2015). "BALB/c and C57BL/6 Mice Differ in Polyreactive IgA Abundance, which Impacts the Generation of Antigen-Specific IgA and Microbiota Diversity." Immunity **43**(3): 527-540.

Furlan, R., et al. (1999). "Caspase-1 regulates the inflammatory process leading to autoimmune demyelination." J Immunol **163**(5): 2403-2409.

Gallo, R. L. and L. V. Hooper (2012). "Epithelial antimicrobial defence of the skin and intestine." Nat Rev Immunol **12**(7): 503-516.

Geem, D., et al. (2012). "Isolation and characterization of dendritic cells and macrophages from the mouse intestine." J Vis Exp(63): e4040.

Gevers, D., et al. (2014). "The treatment-naive microbiome in new-onset Crohn's disease." Cell Host Microbe **15**(3): 382-392.

Gevers, D., et al. (2014). "The treatment-naive microbiome in new-onset Crohn's disease." Cell Host Microbe **15**(3): 382-392.

Gharagozloo, M., et al. (2017). "NLR-Dependent Regulation of Inflammation in Multiple Sclerosis- Dependent Regulation of Inflammation in Multiple Sclerosis." Front Immunol **8**: 2012.

Gharagozloo, M., et al. (2015). "The nod-like receptor, Nlrp12, plays an anti-inflammatory role in experimental autoimmune encephalomyelitis." J Neuroinflammation **12**: 198.

Greenberg, A. S. and M. S. Obin (2006). "Obesity and the role of adipose tissue in inflammation and metabolism." Am J Clin Nutr **83**(2): 461S-465S.

Greenblum, S., et al. (2012). "Metagenomic systems biology of the human gut microbiome reveals topological shifts associated with obesity and inflammatory bowel disease." Proc Natl Acad Sci U S A **109**(2): 594-599.

Grenier, J. M., et al. (2002). "Functional screening of five PYPAF family members identifies PYPAF5 as a novel regulator of NF-kappaB and caspase-1." FEBS Lett **530**(1-3): 73-78.

Gris, D., et al. (2010). "NLRP3 plays a critical role in the development of experimental autoimmune encephalomyelitis by mediating Th1 and Th17 responses." J Immunol **185**(2): 974-981.

Guo, H., et al. (2015). "Inflammasomes: mechanism of action, role in disease, and therapeutics." Nat Med **21**(7): 677-687.

Guo, H., et al. (2016). "NLRX1 Sequesters STING to Negatively Regulate the Interferon Response, Thereby Facilitating the Replication of HIV-1 and DNA Viruses." Cell Host Microbe **19**(4): 515-528.

Haberman, Y., et al. (2014). "Pediatric Crohn disease patients exhibit specific ileal transcriptome and microbiome signature." J Clin Invest **124**(8): 3617-3633.

Halff, E. F., et al. (2012). "Formation and structure of a NAIP5-NLRC4 inflammasome induced by direct interactions with conserved N- and C-terminal regions of flagellin." J Biol Chem **287**(46): 38460-38472.

Halme, L., et al. (2006). "Family and twin studies in inflammatory bowel disease." World J Gastroenterol **12**(23): 3668-3672.

Handley, S. A., et al. (2016). "SIV Infection-Mediated Changes in Gastrointestinal Bacterial Microbiome and Virome Are Associated with Immunodeficiency and Prevented by Vaccination." Cell Host Microbe **19**(3): 323-335.

Harton, J. A., et al. (2002). "Cutting edge: CATERPILLER: a large family of mammalian genes

containing CARD, pyrin, nucleotide-binding, and leucine-rich repeat domains." J Immunol **169**(8): 4088-4093.

Henao-Mejia, J., et al. (2012). "Inflammasome-mediated dysbiosis regulates progression of NAFLD and obesity." Nature **482**(7384): 179-185.

Hensrud, D. D. and S. Klein (2006). "Extreme obesity: a new medical crisis in the United States." Mayo Clin Proc **81**(10 Suppl): S5-10.

Hoffman, H. M., et al. (2001). "Mutation of a new gene encoding a putative pyrin-like protein causes familial cold autoinflammatory syndrome and Muckle-Wells syndrome." Nat Genet **29**(3): 301-305.

Hotamisligil, G. S., et al. (1995). "Increased adipose tissue expression of tumor necrosis factor-alpha in human obesity and insulin resistance." J Clin Invest **95**(5): 2409-2415.

Hu, B., et al. (2016). "The DNA-sensing AIM2 inflammasome controls radiation-induced cell death and tissue injury." Science **354**(6313): 765-768.

Hu, Y. (2015). "A feedforward loop of NLRC5 (de)ubiquitination keeps IKK-NF-kappaB in check." J Cell Biol **211**(5): 941-943.

Hugot, J. P., et al. (2001). "Association of NOD2 leucine-rich repeat variants with susceptibility to Crohn's disease." Nature **411**(6837): 599-603.

Inohara, N., et al. (1999). "Nod1, an Apaf-1-like activator of caspase-9 and nuclear factor-kappaB." J Biol Chem **274**(21): 14560-14567.

Inohara, N. and G. Nunez (2003). "NODs: intracellular proteins involved in inflammation and apoptosis." Nat Rev Immunol **3**(5): 371-382.

Inoue, M., et al. (2012). "NLRP3 inflammasome induces chemotactic immune cell migration to the CNS in experimental autoimmune encephalomyelitis." Proc Natl Acad Sci U S A **109**(26): 10480-10485.

Janda, J. M. and S. L. Abbott (2007). "16S rRNA gene sequencing for bacterial identification in the diagnostic laboratory: pluses, perils, and pitfalls." J Clin Microbiol **45**(9): 2761-2764.

Jeon, M., et al. (2016). "Elevated IL-1beta expression induces invasiveness of triple negative

breast cancer cells and is suppressed by zerumbone." Chem Biol Interact **258**: 126-133.

Jeru, I., et al. (2008). "Mutations in NALP12 cause hereditary periodic fever syndromes." Proc Natl Acad Sci U S A **105**(5): 1614-1619.

Jeru, I., et al. (2011). "Role of interleukin-1beta in NLRP12-associated autoinflammatory disorders and resistance to anti-interleukin-1 therapy." Arthritis Rheum **63**(7): 2142-2148.

Jha, S., et al. (2010). "The inflammasome sensor, NLRP3, regulates CNS inflammation and demyelination via caspase-1 and interleukin-18." J Neurosci **30**(47): 15811-15820.

Jiang, W., et al. (2013). "Recognition of gut microbiota by NOD2 is essential for the homeostasis of intestinal intraepithelial lymphocytes." J Exp Med **210**(11): 2465-2476.

Johansson, M. E., et al. (2011). "The two mucus layers of colon are organized by the MUC2 mucin, whereas the outer layer is a legislator of host-microbial interactions." Proc Natl Acad Sci U S A **108 Suppl 1**: 4659-4665.

Jones, S. A., et al. (2011). "Therapeutic strategies for the clinical blockade of IL-6/gp130 signaling." J Clin Invest **121**(9): 3375-3383.

Jounai, N., et al. (2011). "NLRP4 negatively regulates autophagic processes through an association with beclin1." J Immunol **186**(3): 1646-1655.

Kaakoush, N. O. (2015). "Insights into the Role of Erysipelotrichaceae in the Human Host." Front Cell Infect Microbiol **5**: 84.

Kang, S., et al. (2010). "Dysbiosis of fecal microbiota in Crohn's disease patients as revealed by a custom phylogenetic microarray." Inflamm Bowel Dis **16**(12): 2034-2042.

Kanneganti, T. D. (2017). "Inflammatory Bowel Disease and the NLRP3 Inflammasome." N Engl J Med **377**(7): 694-696.

Kanneganti, T. D., et al. (2006). "Bacterial RNA and small antiviral compounds activate caspase-1 through cryopyrin/Nalp3." Nature **440**(7081): 233-236.

Karki, R., et al. (2016). "NLRC3 is an inhibitory sensor of PI3K-mTOR pathways in cancer." Nature.

Karrasch, T. and C. Jobin (2008). "NF-kappaB and the intestine: friend or foe?" Inflamm Bowel Dis **14**(1): 114-124.

Kau, A. L., et al. (2011). "Human nutrition, the gut microbiome and the immune system." Nature **474**(7351): 327-336.

Kawamoto, S., et al. (2014). "Foxp3(+) T cells regulate immunoglobulin a selection and facilitate diversification of bacterial species responsible for immune homeostasis." Immunity **41**(1): 152-165.

Kennedy, K., et al. (2014). "Evaluating bias of illumina-based bacterial 16S rRNA gene profiles." Appl Environ Microbiol **80**(18): 5717-5722.

Khan, T., et al. (2009). "Metabolic dysregulation and adipose tissue fibrosis: role of collagen VI." Mol Cell Biol **29**(6): 1575-1591.

Khosravi, R., et al. (2013). "Tumor necrosis factor- alpha and interleukin-6: potential interorgan inflammatory mediators contributing to destructive periodontal disease in obesity or metabolic syndrome." Mediators Inflamm **2013**: 728987.

Kirchgessner, T. G., et al. (1997). "Tumor necrosis factor-alpha contributes to obesity-related hyperleptinemia by regulating leptin release from adipocytes." J Clin Invest **100**(11): 2777-2782.

Kis-Toth, K., et al. (2011). "Cytosolic DNA-activated human dendritic cells are potent activators of the adaptive immune response." J Immunol **187**(3): 1222-1234.

Kitajima, S., et al. (2001). "Dextran sodium sulfate-induced colitis in germ-free IQI/Jic mice." Exp Anim **50**(5): 387-395.

Koblansky, A. A., et al. (2016). "The Innate Immune Receptor NLRX1 Functions as a Tumor Suppressor by Reducing Colon Tumorigenesis and Key Tumor-Promoting Signals." Cell Rep **14**(11): 2562-2575.

Kofoed, E. M. and R. E. Vance (2011). "Innate immune recognition of bacterial ligands by NAIPs determines inflammasome specificity." Nature **477**(7366): 592-595.

Kostic, A. D., et al. (2014). "The microbiome in inflammatory bowel disease: current status and the future ahead." Gastroenterology **146**(6): 1489-1499.

Kuczynski, J., et al. (2012). "Using QIIME to analyze 16S rRNA gene sequences from microbial communities." Curr Protoc Microbiol **Chapter 1**: Unit 1E 5.

Larsen, N., et al. (2010). "Gut microbiota in human adults with type 2 diabetes differs from non-diabetic adults." PLoS One **5**(2): e9085.

Le Chatelier, E., et al. (2013). "Richness of human gut microbiome correlates with metabolic markers." Nature **500**(7464): 541-546.

Leemans, J. C., et al. (2011). "Sensing damage by the NLRP3 inflammasome." Immunol Rev **243**(1): 152-162.

Lei, Y., et al. (2013). "The NLR protein, NLRX1, and its partner, TUFM, reduce type I interferon, and enhance autophagy." Autophagy **9**(3): 432-433.

Lei, Y., et al. (2012). "The mitochondrial proteins NLRX1 and TUFM form a complex that regulates type I interferon and autophagy." Immunity **36**(6): 933-946.

Lepage, P., et al. (2011). "Twin study indicates loss of interaction between microbiota and mucosa of patients with ulcerative colitis." Gastroenterology **141**(1): 227-236.

Lewis, A. M., et al. (2006). "Interleukin-1 and cancer progression: the emerging role of interleukin-1 receptor antagonist as a novel therapeutic agent in cancer treatment." J Transl Med **4**: 48.

Ley, R. E., et al. (2005). "Obesity alters gut microbial ecology." Proc Natl Acad Sci U S A **102**(31): 11070-11075.

Ley, R. E., et al. (2006). "Microbial ecology: human gut microbes associated with obesity." Nature **444**(7122): 1022-1023.

Lich, J. D., et al. (2006). "Cryopyrin: in from the cold." Immunity **24**(3): 241-243.

Lich, J. D., et al. (2007). "Monarch-1 suppresses non-canonical NF-kappaB activation and p52-dependent chemokine expression in monocytes." J Immunol **178**(3): 1256-1260.

Lightfield, K. L., et al. (2008). "Critical function for Naip5 in inflammasome activation by a conserved carboxy-terminal domain of flagellin." Nat Immunol **9**(10): 1171-1178.

Lin, H. V., et al. (2012). "Butyrate and propionate protect against diet-induced obesity and regulate gut hormones via free fatty acid receptor 3-independent mechanisms." PLoS One **7**(4): e35240.

Lin, M., et al. (2016). "USP38 Inhibits Type I Interferon Signaling by Editing TBK1 Ubiquitination through NLRP4 Signalosome." Mol Cell **64**(2): 267-281.

Liu, R., et al. (2015). "Expression profile of innate immune receptors, NLRs and AIM2, in human colorectal cancer: correlation with cancer stages and inflammasome components." Oncotarget **6**(32): 33456-33469.

Loftus, E. V., Jr. (2004). "Clinical epidemiology of inflammatory bowel disease: Incidence, prevalence, and environmental influences." Gastroenterology **126**(6): 1504-1517.

Lord, C. A., et al. (2009). "Blimp-1/PRDM1 mediates transcriptional suppression of the NLR gene NLRP12/Monarch-1." J Immunol **182**(5): 2948-2958.

Lu, A., et al. (2014). "Unified polymerization mechanism for the assembly of ASC-dependent inflammasomes." Cell **156**(6): 1193-1206.

Lukens, J. R., et al. (2015). "The NLRP12 Sensor Negatively Regulates Autoinflammatory Disease by Modulating Interleukin-4 Production in T Cells." Immunity **42**(4): 654-664.

Lumeng, C. N., et al. (2007). "Obesity induces a phenotypic switch in adipose tissue macrophage polarization." J Clin Invest **117**(1): 175-184.

Lumeng, C. N. and A. R. Saltiel (2011). "Inflammatory links between obesity and metabolic disease." J Clin Invest **121**(6): 2111-2117.

Ma, S. R. and X. W. Xie (2017). "NLRC5 deficiency promotes myocardial damage induced by high fat diet in mice through activating TLR4/NF-kappaB." Biomed Pharmacother **91**: 755-766.

Ma, Z., et al. (2017). "NLRX1 negatively modulates type I IFN to facilitate KSHV reactivation from latency." PLoS Pathog **13**(5): e1006350.

Maldonado-Gomez, M. X., et al. (2016). "Stable Engraftment of Bifidobacterium longum AH1206 in the Human Gut Depends on Individualized Features of the Resident Microbiome."

Cell Host Microbe **20**(4): 515-526.

Manichanh, C., et al. (2006). "Reduced diversity of faecal microbiota in Crohn's disease revealed by a metagenomic approach." Gut **55**(2): 205-211.

Manji, G. A., et al. (2002). "PYPAF1, a PYRIN-containing Apaf1-like protein that assembles with ASC and regulates activation of NF-kappa B." J Biol Chem **277**(13): 11570-11575.

Mariathasan, S., et al. (2004). "Differential activation of the inflammasome by caspase-1 adaptors ASC and Ipaf." Nature **430**(6996): 213-218.

Mariathasan, S., et al. (2006). "Cryopyrin activates the inflammasome in response to toxins and ATP." Nature **440**(7081): 228-232.

Martinez, F. O. and S. Gordon (2014). "The M1 and M2 paradigm of macrophage activation: time for reassessment." F1000Prime Rep **6**: 13.

Matsuki, T., et al. (2006). "Abnormal T cell activation caused by the imbalance of the IL-1/IL-1R antagonist system is responsible for the development of experimental autoimmune encephalomyelitis." Int Immunol **18**(2): 399-407.

Maurice, C. F., et al. (2013). "Xenobiotics shape the physiology and gene expression of the active human gut microbiome." Cell **152**(1-2): 39-50.

McNulty, N. P., et al. (2011). "The impact of a consortium of fermented milk strains on the gut microbiome of gnotobiotic mice and monozygotic twins." Sci Transl Med **3**(106): 106ra106.

Meng, Q., et al. (2015). "Reversible ubiquitination shapes NLRC5 function and modulates NF-kappaB activation switch." J Cell Biol **211**(5): 1025-1040.

Meylan, E., et al. (2006). "Intracellular pattern recognition receptors in the host response." Nature **442**(7098): 39-44.

Miao, E. A., et al. (2006). "Cytoplasmic flagellin activates caspase-1 and secretion of interleukin 1beta via Ipaf." Nat Immunol **7**(6): 569-575.

Monteiro, R. and I. Azevedo (2010). "Chronic inflammation in obesity and the metabolic syndrome." Mediators Inflamm **2010**.

Moore, C. B., et al. (2008). "NLRX1 is a regulator of mitochondrial antiviral immunity." Nature **451**(7178): 573-577.

Muccioli, G. G., et al. (2010). "The endocannabinoid system links gut microbiota to adipogenesis." Mol Syst Biol **6**: 392.

Murano, I., et al. (2008). "Dead adipocytes, detected as crown-like structures, are prevalent in visceral fat depots of genetically obese mice." J Lipid Res **49**(7): 1562-1568.

Nava, G. M., et al. (2011). "Spatial organization of intestinal microbiota in the mouse ascending colon." ISME J **5**(4): 627-638.

Neven, B., et al. (2004). "Molecular basis of the spectral expression of CIAS1 mutations associated with phagocytic cell-mediated autoinflammatory disorders CINCA/NOMID, MWS, and FCU." Blood **103**(7): 2809-2815.

Nguyen, M. T., et al. (2007). "A subpopulation of macrophages infiltrates hypertrophic adipose tissue and is activated by free fatty acids via Toll-like receptors 2 and 4 and JNK-dependent pathways." J Biol Chem **282**(48): 35279-35292.

Novakovic, B., et al. (2016). "beta-Glucan Reverses the Epigenetic State of LPS-Induced Immunological Tolerance." Cell **167**(5): 1354-1368 e1314.

Ogura, Y., et al. (2001). "A frameshift mutation in NOD2 associated with susceptibility to Crohn's disease." Nature **411**(6837): 603-606.

Ohshima, S., et al. (1998). "Interleukin 6 plays a key role in the development of antigen-induced arthritis." Proc Natl Acad Sci U S A **95**(14): 8222-8226.

Olefsky, J. M. and C. K. Glass (2010). "Macrophages, inflammation, and insulin resistance." Annu Rev Physiol **72**: 219-246.

Orr, J. S., et al. (2013). "Isolation of adipose tissue immune cells." J Vis Exp(75): e50707.

Ouchi, N., et al. (2011). "Adipokines in inflammation and metabolic disease." Nat Rev Immunol **11**(2): 85-97.

Park, E. J., et al. (2010). "Dietary and genetic obesity promote liver inflammation and tumorigenesis by enhancing IL-6 and TNF expression." Cell **140**(2): 197-208.

Park, H. S., et al. (2005). "Relationship of obesity and visceral adiposity with serum concentrations of CRP, TNF-alpha and IL-6." Diabetes Res Clin Pract **69**(1): 29-35.

Park, S. H., et al. (2017). "Type I interferons and the cytokine TNF cooperatively reprogram the macrophage epigenome to promote inflammatory activation." Nat Immunol **18**(10): 1104-1116.

Patel, M. N., et al. (2017). "Inflammasome Priming in Sterile Inflammatory Disease." Trends Mol Med **23**(2): 165-180.

Petnicki-Ocwieja, T., et al. (2009). "Nod2 is required for the regulation of commensal microbiota in the intestine." Proc Natl Acad Sci U S A **106**(37): 15813-15818.

Peyrin-Biroulet, L. (2010). "Anti-TNF therapy in inflammatory bowel diseases: a huge review." Minerva Gastroenterol Dietol **56**(2): 233-243.

Plovier, H., et al. (2017). "A purified membrane protein from Akkermansia muciniphila or the pasteurized bacterium improves metabolism in obese and diabetic mice." Nat Med **23**(1): 107-113.

Qin, J., et al. (2010). "A human gut microbial gene catalogue established by metagenomic sequencing." Nature **464**(7285): 59-65.

Qin, J., et al. (2012). "A metagenome-wide association study of gut microbiota in type 2 diabetes." Nature **490**(7418): 55-60.

Qin, Y., et al. (2017). "NLRP11 disrupts MAVS signalosome to inhibit type I interferon signaling and virus-induced apoptosis." EMBO Rep **18**(12): 2160-2171.

Qu, Y., et al. (2012). "Phosphorylation of NLRC4 is critical for inflammasome activation." Nature **490**(7421): 539-542.

Ramanan, D., et al. (2014). "Bacterial sensor Nod2 prevents inflammation of the small intestine by restricting the expansion of the commensal Bacteroides vulgatus." Immunity **41**(2): 311-324.

Rauch, I., et al. (2016). "NAIP proteins are required for cytosolic detection of specific bacterial ligands in vivo." J Exp Med **213**(5): 657-665.

Rayamajhi, M., et al. (2013). "Cutting edge: Mouse NAIP1 detects the type III secretion system needle protein." J Immunol **191**(8): 3986-3989.

Reeves, A. E., et al. (2012). "Suppression of Clostridium difficile in the gastrointestinal tracts of germfree mice inoculated with a murine isolate from the family Lachnospiraceae." Infect Immun **80**(11): 3786-3794.

Reichardt, N., et al. (2014). "Phylogenetic distribution of three pathways for propionate production within the human gut microbiota." ISME J **8**(6): 1323-1335.

Ridaura, V. K., et al. (2013). "Gut microbiota from twins discordant for obesity modulate metabolism in mice." Science **341**(6150): 1241214.

Rivollier, A., et al. (2012). "Inflammation switches the differentiation program of Ly6Chi monocytes from antiinflammatory macrophages to inflammatory dendritic cells in the colon." J Exp Med **209**(1): 139-155.

Sabat, A. J., et al. (2017). "Targeted next-generation sequencing of the 16S-23S rRNA region for culture-independent bacterial identification - increased discrimination of closely related species." Sci Rep **7**(1): 3434.

Saltiel, A. R. and J. M. Olefsky (2017). "Inflammatory mechanisms linking obesity and metabolic disease." J Clin Invest **127**(1): 1-4.

Sartor, R. B. and G. D. Wu (2017). "Roles for Intestinal Bacteria, Viruses, and Fungi in Pathogenesis of Inflammatory Bowel Diseases and Therapeutic Approaches." Gastroenterology **152**(2): 327-339 e324.

Schauber, J., et al. (2006). "Heterogeneous expression of human cathelicidin hCAP18/LL-37 in inflammatory bowel diseases." Eur J Gastroenterol Hepatol **18**(6): 615-621.

Schmidt, R., et al. (2014). "Effects of bacterial inoculants on the indigenous microbiome and secondary metabolites of chamomile plants." Front Microbiol **5**: 64.

Schneider, M., et al. (2012). "The innate immune sensor NLRC3 attenuates Toll-like receptor signaling via modification of the signaling adaptor TRAF6 and transcription factor NF-kappaB." Nat Immunol **13**(9): 823-831.

Schubert, A. M., et al. (2014). "Microbiome data distinguish patients with Clostridium difficile infection and non-C. difficile-associated diarrhea from healthy controls." MBio **5**(3): e01021-01014.

Sender, R., et al. (2016). "Revised Estimates for the Number of Human and Bacteria Cells in the Body." PLoS Biol **14**(8): e1002533.

Seo, S. U., et al. (2015). "Distinct Commensals Induce Interleukin-1beta via NLRP3 Inflammasome in Inflammatory Monocytes to Promote Intestinal Inflammation in Response to Injury." Immunity **42**(4): 744-755.

Sepehri, S., et al. (2007). "Microbial diversity of inflamed and noninflamed gut biopsy tissues in inflammatory bowel disease." Inflamm Bowel Dis **13**(6): 675-683.

Shanahan, M. T., et al. (2014). "Mouse Paneth cell antimicrobial function is independent of Nod2." Gut **63**(6): 903-910.

Sharpton, T. J. (2014). "An introduction to the analysis of shotgun metagenomic data." Front Plant Sci **5**: 209.

Shaw, P. J., et al. (2010). "Cutting edge: critical role for PYCARD/ASC in the development of experimental autoimmune encephalomyelitis." J Immunol **184**(9): 4610-4614.

Shen, M., et al. (2017). "NLRP12 autoinflammatory disease: a Chinese case series and literature review." Clin Rheumatol **36**(7): 1661-1667.

Shi, F. D., et al. (2000). "IL-18 directs autoreactive T cells and promotes autodestruction in the central nervous system via induction of IFN-gamma by NK cells." J Immunol **165**(6): 3099-3104.

Shoelson, S. E., et al. (2003). "Inflammation and the IKK beta/I kappa B/NF-kappa B axis in obesity- and diet-induced insulin resistance." Int J Obes Relat Metab Disord **27 Suppl 3**: S49-52.

Smith, P. M., et al. (2013). "The microbial metabolites, short-chain fatty acids, regulate colonic Treg cell homeostasis." Science **341**(6145): 569-573.

Soares, F., et al. (2014). "The mitochondrial protein NLRX1 controls the balance between extrinsic and intrinsic apoptosis." J Biol Chem **289**(28): 19317-19330.

Soares, F., et al. (2013). "NLRX1 does not inhibit MAVS-dependent antiviral signalling." Innate Immun **19**(4): 438-448.

Song, L., et al. (2017). "NLRP3 Inflammasome in Neurological Diseases, from Functions to Therapies." Front Cell Neurosci **11**: 63.

Sonnenburg, E. D., et al. (2016). "Diet-induced extinctions in the gut microbiota compound over generations." Nature **529**(7585): 212-215.

Stevenson, B. S., et al. (2004). "New strategies for cultivation and detection of previously uncultured microbes." Appl Environ Microbiol **70**(8): 4748-4755.

Stienstra, R., et al. (2010). "The inflammasome-mediated caspase-1 activation controls adipocyte differentiation and insulin sensitivity." Cell Metab **12**(6): 593-605.

Stienstra, R., et al. (2012). "The inflammasome puts obesity in the danger zone." Cell Metab **15**(1): 10-18.

Stienstra, R., et al. (2011). "Inflammasome is a central player in the induction of obesity and insulin resistance." Proc Natl Acad Sci U S A **108**(37): 15324-15329.

Stokman, G., et al. (2017). "NLRX1 dampens oxidative stress and apoptosis in tissue injury via control of mitochondrial activity." J Exp Med **214**(8): 2405-2420.

Strowig, T., et al. (2012). "Inflammasomes in health and disease." Nature **481**(7381): 278-286.

Sutterwala, F. S., et al. (2006). "Critical role for NALP3/CIAS1/Cryopyrin in innate and adaptive immunity through its regulation of caspase-1." Immunity **24**(3): 317-327.

Tanaka, T., et al. (2011). "Anti-interleukin-6 receptor antibody, tocilizumab, for the treatment of autoimmune diseases." FEBS Lett **585**(23): 3699-3709.

Tattoli, I., et al. (2008). "NLRX1 is a mitochondrial NOD-like receptor that amplifies NF-kappaB and JNK pathways by inducing reactive oxygen species production." EMBO Rep **9**(3): 293-300.

Tattoli, I., et al. (2016). "NLRX1 Acts as an Epithelial-Intrinsic Tumor Suppressor through the

Modulation of TNF-Mediated Proliferation." Cell Rep **14**(11): 2576-2586.

Ting, J. P. and B. K. Davis (2005). "CATERPILLER: a novel gene family important in immunity, cell death, and diseases." Annu Rev Immunol **23**: 387-414.

Ting, J. P., et al. (2010). "How the noninflammasome NLRs function in the innate immune system." Science **327**(5963): 286-290.

Ting, J. P., et al. (2008). "The NLR gene family: a standard nomenclature." Immunity **28**(3): 285-287.

Tong, Y., et al. (2012). "Enhanced TLR-induced NF-kappaB signaling and type I interferon responses in NLRC5 deficient mice." Cell Res **22**(5): 822-835.

Triantafilou, K., et al. (2013). "Rhinovirus-induced calcium flux triggers NLRP3 and NLRC5 activation in bronchial cells." Am J Respir Cell Mol Biol **49**(6): 923-934.

Turnbaugh, P. J., et al. (2008). "Diet-induced obesity is linked to marked but reversible alterations in the mouse distal gut microbiome." Cell Host Microbe **3**(4): 213-223.

Turnbaugh, P. J., et al. (2009). "A core gut microbiome in obese and lean twins." Nature **457**(7228): 480-484.

Tzanavari, T., et al. (2010). "TNF-alpha and obesity." Curr Dir Autoimmun **11**: 145-156.

Ubeda, C., et al. (2012). "Familial transmission rather than defective innate immunity shapes the distinct intestinal microbiota of TLR-deficient mice." J Exp Med **209**(8): 1445-1456.

Vandanmagsar, B., et al. (2011). "The NLRP3 inflammasome instigates obesity-induced inflammation and insulin resistance." Nat Med **17**(2): 179-188.

Vijay-Kumar, M., et al. (2010). "Metabolic syndrome and altered gut microbiota in mice lacking Toll-like receptor 5." Science **328**(5975): 228-231.

Viladomiu, M., et al. (2017). "IgA-coated E. coli enriched in Crohn's disease spondyloarthritis promote TH17-dependent inflammation." Sci Transl Med **9**(376).

Vitale, A., et al. (2013). "Rare NLRP12 variants associated with the NLRP12-autoinflammatory disorder phenotype: an Italian case series." Clin Exp Rheumatol **31**(3

Suppl 77): 155-156.

Vladimer, G. I., et al. (2012). "The NLRP12 inflammasome recognizes Yersinia pestis." Immunity **37**(1): 96-107.

Wang, P., et al. (2015). "Nlrp6 regulates intestinal antiviral innate immunity." Science **350**(6262): 826-830.

Wang, Q., et al. (2007). "Naive Bayesian classifier for rapid assignment of rRNA sequences into the new bacterial taxonomy." Appl Environ Microbiol **73**(16): 5261-5267.

Wang, X., et al. (2015). "Sodium butyrate alleviates adipocyte inflammation by inhibiting NLRP3 pathway." Sci Rep **5**: 12676.

Weisberg, S. P., et al. (2003). "Obesity is associated with macrophage accumulation in adipose tissue." J Clin Invest **112**(12): 1796-1808.

Wen, H., et al. (2011). "Fatty acid-induced NLRP3-ASC inflammasome activation interferes with insulin signaling." Nat Immunol **12**(5): 408-415.

Williams, K. L., et al. (2005). "The CATERPILLER protein monarch-1 is an antagonist of toll-like receptor-, tumor necrosis factor alpha-, and Mycobacterium tuberculosis-induced pro-inflammatory signals." The Journal of biological chemistry **280**(48): 39914-39924.

Wilson, J. E., et al. (2015). "Inflammasome-independent role of AIM2 in suppressing colon tumorigenesis via DNA-PK and Akt." Nat Med **21**(8): 906-913.

Wlodarska, M., et al. (2014). "NLRP6 inflammasome orchestrates the colonic host-microbial interface by regulating goblet cell mucus secretion." Cell **156**(5): 1045-1059.

Wu, C., et al. (2016). "BioGPS: building your own mash-up of gene annotations and expression profiles." Nucleic Acids Res **44**(D1): D313-316.

Wu, C., et al. (2017). "NLRP11 attenuates Toll-like receptor signalling by targeting TRAF6 for degradation via the ubiquitin ligase RNF19A." Nat Commun **8**(1): 1977.

Xia, X., et al. (2011). "NLRX1 negatively regulates TLR-induced NF-kappaB signaling by targeting TRAF6 and IKK." Immunity **34**(6): 843-853.

Xia, X., et al. (2016). "Identification of a Novel NLRP12 Nonsense Mutation (Trp408X) in the Extremely Rare Disease FCAS by Exome Sequencing." PLoS One **11**(6): e0156981.

Xu, H., et al. (2003). "Chronic inflammation in fat plays a crucial role in the development of obesity-related insulin resistance." J Clin Invest **112**(12): 1821-1830.

Xu, X., et al. (2013). "Obesity activates a program of lysosomal-dependent lipid metabolism in adipose tissue macrophages independently of classic activation." Cell Metab **18**(6): 816-830.

Yang, J., et al. (2013). "Human NAIP and mouse NAIP1 recognize bacterial type III secretion needle protein for inflammasome activation." Proc Natl Acad Sci U S A **110**(35): 14408-14413.

Yin, H., et al. (2017). "NLRX1 accelerates cisplatin-induced ototoxity in HEI-OC1 cells via promoting generation of ROS and activation of JNK signaling pathway." Sci Rep **7**: 44311.

Youm, Y. H., et al. (2011). "Elimination of the NLRP3-ASC Inflammasome Protects against Chronic Obesity-Induced Pancreatic Damage." Endocrinology **152**(11): 4039-4045.

Yudkin, J. S., et al. (1999). "C-reactive protein in healthy subjects: associations with obesity, insulin resistance, and endothelial dysfunction: a potential role for cytokines originating from adipose tissue?" Arterioscler Thromb Vasc Biol **19**(4): 972-978.

Zaki, M. H., et al. (2010). "The NLRP3 inflammasome protects against loss of epithelial integrity and mortality during experimental colitis." Immunity **32**(3): 379-391.

Zaki, M. H., et al. (2014). "Salmonella exploits NLRP12-dependent innate immune signaling to suppress host defenses during infection." Proc Natl Acad Sci U S A **111**(1): 385-390.

Zaki, M. H., et al. (2011). "The NOD-like receptor NLRP12 attenuates colon inflammation and tumorigenesis." Cancer cell **20**(5): 649-660.

Zhang, C., et al. (2010). "Interactions between gut microbiota, host genetics and diet relevant to development of metabolic syndromes in mice." ISME J **4**(2): 232-241.

Zhang, H., et al. (2009). "Human gut microbiota in obesity and after gastric bypass." Proc Natl Acad Sci U S A **106**(7): 2365-2370.

Zhang, L., et al. (2014). "NLRC3, a member of the NLR family of proteins, is a negative regulator of innate immune signaling induced by the DNA sensor STING." Immunity **40**(3): 329-341.

Zhang, W., et al. (2016). "Deletion of the Toll-Like Receptor 5 Gene Per Se Does Not Determine the Gut Microbiome Profile That Induces Metabolic Syndrome: Environment Trumps Genotype." PLoS One **11**(3): e0150943.

Zhao, Y., et al. (2011). "The NLRC4 inflammasome receptors for bacterial flagellin and type III secretion apparatus." Nature **477**(7366): 596-600.

Zilbauer, M., et al. (2005). "Intestinal innate immunity to Campylobacter jejuni results in induction of bactericidal human beta-defensins 2 and 3." Infect Immun **73**(11): 7281-7289.